INFORMATION TO USERS

This manuscript has been reproduced from the microfilm master. UMI films the text directly from the original or copy submitted. Thus, some thesis and dissertation copies are in typewriter face, while others may be from any type of computer printer.

The quality of this reproduction is dependent upon the quality of the copy submitted. Broken or indistinct print, colored or poor quality illustrations and photographs, print bleedthrough, substandard margins, and improper alignment can adversely affect reproduction.

In the unlikely event that the author did not send UMI a complete manuscript and there are missing pages, these will be noted. Also, if unauthorized copyright material had to be removed, a note will indicate the deletion.

Oversize materials (e.g., maps, drawings, charts) are reproduced by sectioning the original, beginning at the upper left-hand corner and continuing from left to right in equal sections with small overlaps.

Photographs included in the original manuscript have been reproduced xerographically in this copy. Higher quality 6" x 9" black and white photographic prints are available for any photographs or illustrations appearing in this copy for an additional charge. Contact UMI directly to order.

ProQuest Information and Learning
300 North Zeeb Road, Ann Arbor, MI 48106-1346 USA
800-521-0600

Université d'Ottawa · University of Ottawa

Temperature dependence of the electrical resistivity in amorphous metallic alloys.

by

Khalid Al-Qadi

M.Sc. Thesis

Thesis submitted to the school of Graduate Studies and Research

of the University of Ottawa

in partial fulfillment of the requirements for the degree of

Master of Science

Department of physics

University of Ottawa

Ottawa, Ontario

Canada

Abstract

The purpose of this study is to investigate the conduction electrons' interaction mechanisms over the wide temperature range in order to find possible deviations from the existing theories. The temperature dependence of the electrical resistivity of two scattering systems, the crystalline and the amorphous, in the range of 1.7–300 K is studied. In the pure crystalline metals, the nearly-free-electron model can qualitatively and quantitatively account for the temperature dependence of the electrical resistivity. In the low-temperature range, the electron-electron scattering is the dominant scattering mechanism. Above the Debye temperature, the phonon-electron scattering is the dominant scattering mechanism.

The temperature dependence of the electrical resistivity for the amorphous metallic alloys can be described qualitatively by the Ziman model. The scattering mechanism of the conduction electrons of the samples can be categorized in the weak scattering limit regime. A small, but significant correction must be added to the Ziman model in order to account for the additional scattering contributions that exist in the wide temperature range.

In the very-low-temperature range the electron-electron interaction effect is the major correction to the temperature dependence of the electrical resistivity. In the low-temperature range, the weak localization effect is the major correction to the temperature dependence of the electrical resistivity.

In the high-temperature range, the temperature dependence of the electrical resistivity is linear with a small but significant correction. For some samples the magnetic contribution is the major correction, for others the multiphonon scattering is the major correction. For the resistivity minima at temperatures below 20 K could be due to the Kondo effect. A more plausible explanation, however, is the electron-electron interaction effect. The Ziman model with the proper corrections is found to be an adequate and successful model in accounting for the temperature dependence of the electrical resistivity of all of the studied amorphous metallic alloys.

Acknowledgement

I would like to acknowledge the support of my professor and thesis supervisor, Dr. Z.M. Stadnik. I will always be grateful for his tremendous support and inspiration for this project. I would also like to acknowledge Dr. G. Lamarche for his invaluable advice and contribution to the experimental part of this work. I would also like to thank Dr. B. Blanchard for assisting me in some of the complex mathematical areas of the thesis. Dr. E. Fortin and Dr. A. Song must also be thanked for their kind words of encouragement and wisdom throughout the past years.

Many heartfelt thanks go to Ms. H. Laccasse who has been extremely helpful and generous to me over the past year. I would also like to thank the kind staff in the machine and electronic workshops.

A special acknowledgement is due to the Ministry of Education of the State of Kuwait. This thesis is, in part, a result of the many years of support from the Ministry during my undergraduate studies.

Finally, a deep and most loving acknowledgement to my family. I thank my parents for their continuous support and affection. I thank my wife who has most patiently endured and has done a wonderful job in raising our beautiful children, Mustafa, Khalil, Amenah, and Ahmad.

Contents

4. Results and discussion

1. Introduction

An amorphous solid, often referred to as glass, is a non-crystalline solid obtained by supercooling the liquid. The cooling rate has to be extremely small in comparison to the time of crystallization. An amorphous material has higher energy than a crystalline one. The structure of an amorphous material is a liquid-like structure and the density of an amorphous solid is less than that of a crystalline solid. We can, to some approximation, treat an amorphous solid as a nearly-free-electron liquid. In such a liquid, the density of states at the Fermi level, DOS, has a minimum value when twice the Fermi wave vector, $2k_F$, equals the first peak in the structure factor of the liquid, k_{pl}

The glass structure is not completely random; it lacks the long-range structure only. As a result of the chemical bonds and forces between the atoms, there exists a certain type of short-range order and an average nearest neighbour configuration. Unlike the crystalline structure, the short-range order does not repeat itself periodically and it also has different orientations. The X-ray diffraction technique does not determine the structure of the glass. The only information that can be obtained from the X-ray diffraction is the radial distribution function, which gives the average distance between two atoms [1].

Since the discovery of the first amorphous metallic alloy in 1959, different models were constructed to try to account for the anomalous temperature dependence of the electrical resistivity. The first successful model was the Ziman model in 1961, which originally was put forth for liquid simple metals. However, many of the amorphous metallic alloys which contain transition metals deviate from the Ziman model because of the *s-d* strong scattering process. Evans, in 1971, modified the Ziman model to include the *s-d* scattering in the calculation of the electrical resistivity. In the following year, Mott suggested another model for the temperature dependence of the electrical

resistivity in the amorphous metallic alloys containing transition metals. Another modification to the Ziman model came in the form of the generalized Faber-Ziman model, which solved the anomalous scattering in the *sp* amorphous metallic alloys [2,3].

All of the above theories were based on the nearly-free-electron approximation. However, they failed to explain the resistivity minima and the anomalous negative temperature coefficient of the resistivity over the wide temperature range. These two anomalies were explained by quantum interference effect theory [2–4]. This theory describes two major effects, namely, the weak localization effect and the electron-electron interaction effect. These effects explain the existence of the resistivity minima and the anomalous negative temperature coefficient.

Amorphous metallic alloys have properties that are very interesting to researchers. The most important, and the easiest to measure, is that of electrical resistivity. Amorphous metallic alloys have the following electrical resistivity properties: 1) negative temperature coefficients of resistivity over a wide range of temperatures, 2) electrical resistivity minima, 3) high resistivity values compared to those of crystalline counter alloys, and 4) small changes in values of their electrical resistivity in relation to temperature. Although the amorphous metallic alloys commonly have glass structures, they do have completely different temperature dependence of the electrical resistivity depending on the amorphous alloy composition. The amorphous metallic alloys can be divided into five groups according to their magnetic status: 1) the ferromagnetic amorphous metallic alloys, 2) the weak ferromagnetic amorphous metallic alloys, 3) the spin glasses, 4) the paramagnetic and diamagnetic, and 5) the weak paramagnetic [5].

1.1 Purpose of the thesis

In this experimental study, the temperature dependence of the electrical resistivity of two scattering systems in the range of 1.7–300 K is studied. The first system is the crystalline system, which is used as a tool to verify the accuracy of the experimental setup. It is also used to compare the scattering mechanisms of the conduction electrons of the well-defined structure with the scattering mechanisms of the amorphous structure. The second system is the amorphous system where no long-range structure exists. The purpose of this study is to investigate the conduction electron interaction mechanisms over the wide temperature range in order to find possible deviations from the existing theories.

1.2 Scope of the work

The temperature dependence of the electrical resistivity in the temperature range of 1.7–300 K is discussed within the framework of the classical theories and the quantum interference theories. The samples used included two crystalline pure metals, seven ferromagnetic amorphous metallic alloys, and four weak paramagnetic amorphous metallic alloys.

2. Theoretical review

2.1) Introduction

The theory of electrical resistivity of the crystalline metals is based on the Boltzmann equation of transportation [6] using the nearly free electron model. This equation is valid for amorphous metallic alloys, even though these alloys do not have a long-range structure. The Boltzmann equation does not hold, however, for amorphous metallic alloys in the strong scattering limits. In order to better understand the temperature dependence of resistivity for amorphous metallic alloys, it is useful to have a short review of the temperature dependence of resistivity in the crystalline metals.

2.2) Temperature dependence of the electrical resistivity in pure crystalline metals

2.2.1) General relation

According to the free electron Fermi gas model, the valence electron of a metal becomes a conduction electron and moves freely through the metal. The free electron model assumes that all electrons at the Fermi surface are *s*-like electrons. This will lead to a spherical Fermi surface. Let us assume that there is a constant applied electric field to the metal. The Fermi surface, under the applied electric field, will move as a whole sphere. The sphere will move with a constant speed, assuming that all the different scattering processes in the metal are steady. The electrical resistivity is then given by the Drude formula [7]

$$\rho = \frac{m}{ne^2\tau}, \tag{2-1}$$

where n is the number of electrons per unit volume of mass m, and charge e, and τ is the time between two collisions. Eq. (2-1) illustrates the relation between the different scattering processes and the electrical resistivity. The Drude formula is reasonable and gives a very good insight into electrical resistivity in the case of simple monovalent metals where the Fermi surface lies entirely in the first Brillouin zone. The assumptions of free electrons and a uniform scattering rate over a perfect Fermi sphere are clearly severe restrictions on its applicability [7].

2.2.2) Different contributions to the electrical resistivity of pure crystalline metals

The temperature dependence of electrical resistivity varies over a wide range of temperatures. There are four major contributions to the electrical resistivity in crystalline pure metals.

2.2.3) Lattice resistivity

For temperatures larger than the Debye temperature, Θ_D, the temperature dependence of the electrical resistivity in most metals is proportional to the number of conduction electron collisions with the thermal phonons. The number of thermal phonons is, in turn, proportional to the temperature. As a result, there is a linear relationship between the electrical resistivity and the temperature [6]

$$\rho = a + bT, \quad T > \Theta_D, \tag{2-2}$$

where a and b are constants. At liquid helium temperatures, the contributions from other types of scattering are much stronger than the contributions from the scattering with the thermal phonons. For

example, the electron elastic scattering leads to a contribution proportional to T^2. The resistivity can be written as [6]

$$\rho = d + cT^2, \quad T \approx 4K, \tag{2-3}$$

where d is a constant.

2.2.4) Residual resistivity

The electrical resistivity dependence at low temperatures is caused mainly by the scattering of conduction electrons with the defects in the crystal and the impurity atoms [6]. This residual resistivity is the extrapolated resistivity to 0 K because the lattice resistivity, ρ_L, vanishes as temperature goes to 0 K. The residual resistivity is an indication of the amount of impurity in the pure metal. Matthiessen's rule can be written as [6]

$$\rho_T = \rho_L + \rho_0, \tag{2-4}$$

where ρ_T is the total resistivity. Matthiessen's rule gives an empirical equation which is only valid if: the impurity scattering and phonon scattering are independent and if the relaxation time is isotopic [7]. Matthiessen's rule shows that the total electrical resistivity of a metal is the sum of ρ_L and ρ_0.

2.2.5) Umklapp scattering

Umklapp scattering is a large-angle scattering of the conduction electrons by the lattice phonons at low enough temperatures. The angle of the scattering, θ_U, is close to π [fig. (2-1)]. At low temperatures, umklapp scattering is the largest contribution to the electrical resistivity. In this

scattering the electron momentum change is much larger than in the normal scattering process. A reciprocal vector Q is involved in this collision between the electron and the phonon. This process makes the electron momentum change much larger than under the normal scattering process. The normal electron phonon scattering process in k-space is [6]

$$k' = k + l, \tag{2-5}$$

while the umklapp scattering process is

$$k' = k + l + Q, \tag{2-6}$$

where k, k', l and Q are vectors in the k-space [fig. (2-1)]. The Umklapp scattering process is a scattering involving the same phonon but ending in another Brillouin zone at a point exactly equivalent to the same point where the electron was before the collision. Figure (2-1) shows both the normal and the umklapp scattering. When the Fermi surface lies totally inside the Brillouin zone there is a minimum phonon vector q for umklapp scattering to take place. At low enough temperatures the number of phonons available for umklapp scattering falls as [6]

$$U_s \propto -\exp(\frac{\Theta_U}{T}), \tag{2-7}$$

where Θ_U is the umklapp temperature. The umklapp temperature is a characteristic temperature for a metal and is calculated from the geometry of the Fermi surface inside the Brillouin zone. The umklapp scattering process vanishes as the temperature goes far below Θ_U. The electrical resistivity then is caused by normal small-angle scattering processes.

2.2.6) Kondo effect

In some pure metals with ferromagnetic impurities, the temperature dependence of the electrical resistivity curve has a minimum. The reason for a resistance minimum is the existence of a localized magnetic moment on the impurity atoms. Kondo showed that the minimum electrical resistivity at very low temperatures is due to the presence of unfilled *d* shell ferromagnetic impurities in the pure metal. This leads to a net spin in the host metal at very low temperatures. A spin dependence contribution to the electrical resistivity is [6]

$$\rho_{spin} = c\rho_d\left[1+\frac{3zJ}{E_F}\ln T\right] = c\rho_0 - c\rho_1 \ln T, \tag{2-8}$$

where J represents the exchange energy, z is the number of nearest neighbors, c is the concentration, ρ_d is a measure of the strength of the exchange scattering, and E_F is the Fermi energy. One can see from the above equation that for negative J at low temperatures an increase in the electrical resistivity occurs when the temperature decreases. In the case of unfilled *d* shell magnetic impurity atoms which produce a net spin in the host metal, J is negative [8]. To find the temperature at which the Kondo effect has a minimum in the resistivity, we use the results from Bloch analytic equation. This equation suggests that the contribution from the scattering by phonons to electrical resistivity at very low temperatures is proportional to [7]

$$\rho \propto \frac{T^5}{\theta^6}. \tag{2-9}$$

Because the electrical resistivity is additive, then the total electrical resistivity is [6,8]

$$\rho_{total} = aT^5 + c\rho_0 - c\rho_1 \ln T. \tag{2-10}$$

Differentiating eq. (2-10) gives us the following

$$\frac{d\rho_{total}}{dT} = 5aT^4 - \frac{c\rho_i}{T}. \tag{2-11}$$

The minimum temperature from eq. (2-11) is

$$T_{min} = \left[\frac{c\rho_i}{5a}\right]^{1/5}. \tag{2-12}$$

2.3) Temperature dependence of the electrical resistivity in amorphous metallic alloys

2.3.1) Amorphous metallic alloys

Amorphous metallic alloys generally have very high electrical resistivity, typically more than 100 μΩ·cm, compared with the electrical resistivity of crystalline metals or crystalline metallic alloys [9]. The temperature dependence of resistivity changes very little from room temperature down to liquid helium temperature [10]. They have also high residual resistivity [11]. Amorphous metallic alloys have been classified into five groups according to their magnetic status [5,12,13].

2.3.2.1) Group I

This group contains the ferromagnetic amorphous metallic alloys. The amorphous alloys in this group have two main features. First, the Curie temperature, T_c, is above room temperature. Second, the electronic specific heat coefficient, γ_s, is usually between 5 and 7 mJ/mol·K^2. Usually, γ_s is used as a very good approximation of the DOS at E_F, provided that the electron phonon

enhancement effect factor is between 0.2–0.6. In general, γ_s depends on the composition of the alloy but not on the alloy's structure.

The Fermi level lies within the *d* band, and the dominant electrons at the Fermi level are *d* electrons. These amorphous alloys have a positive temperature coefficient of resistivity, TCR, near the room temperature. They often have a negative TCR at very low temperatures. The change of the sign of TCR leads to a resistivity minimum. The resistivity minimum does not depend on any external magnetic fields and does not exist in the crystalline counterpart.

2.3.2.2) Group II

This group includes the weak ferromagnetic amorphous metallic alloys. These alloys have two main features. T_c is below room temperature and the alloys have spontaneous magnetization. The Fermi level also lies within the *d* band. A resistivity minimum or maximum is usually observed in the region around T_c. This minimum or maximum shows a marked magnetic field dependence.

2.3.2.3) Group III

This group contains amorphous metallic alloys which have magnetic moments. However, they do not show spontaneous magnetization even at low temperatures. This group usually is prepared by adding magnetic atoms in diluted concentrations to a non-magnetic alloy. The resulting amorphous alloy will experience an effect similar to the Kondo effect in the crystalline materials. If the number of magnetic atoms increases, they will start to interact with the host amorphous alloy via the conduction electrons. The conduction electron, one which has a spin parallel to the magnetic atom

moment, will be under the influence of a repulsion force. The conduction electron motion will change from a parallel spin to an oscillatory spin and this oscillatory spin will decay as the electron moves farther from the magnetic atom.

Similarly, the anti-parallel spin conduction electron will be under an attraction force and the motion will change from anti-parallel spin to oscillatory spin distribution, which also decays over distance. The overall effect [fig. (2-2)] is to have an oscillatory spin density, which decays with distance [6]. These amorphous metallic alloys are known as spin glasses. This group can have minimum or maximum resistivity values. The Fermi level also lies within the *d* band.

2.3.2.4) Group IV and V

These two groups include the paramagnetic and diamagnetic (group IV) and the weak paramagnetic (group V). The Fermi level for group IV either lies in the *d* or the *sp* band. The Fermi level for group V lies completely in the *sp* band. For a given amorphous alloy system, in these two groups, the temperature dependence of the electrical resistivity can be described well by one of five curves of resistivity, [fig. (2-3)]. Curve (a) is characterized by a positive TCR with no minimum. The curve has a quadratic temperature dependence at low temperatures and a linear one at higher temperatures. As the residual resistivity increases, the temperature dependence of resistivity is represented by curve (b). This curve has a positive TCR at low temperatures, which changes to a negative TCR at high temperatures, resulting in wide maximum value of the resistivity at intermediate temperature values. When the residual resistivity increases [curve (c)], a dominant negative TCR can be seen with no maximum values. At low temperatures, a negative quadratic dependence is seen. A further increase in the residual resistivity will result in curve (d), where the curve loses its negative

quadratic dependence to a linear dependence. At the highest values of residual resistivity, we have curve (e) where the curve has convex curvature.

2.3.3) Ziman theory

In 1961 Ziman put forth a theory for the temperature dependence of electrical resistivity for liquid metals. In his model he relates the temperature dependence of electrical resistivity to the static structure factor determined from the experimental X-ray diffraction data. As mentioned in section 1.1, in a nearly free electron liquid there is a minimum value in the DOS when $2k_F$ equals k_{pl} [fig. (2-5)]. Ziman predicted [2,11] that the electrical resistivity will be high and have a negative TCR when $2k_F$ is near or equal to k_{pl}, and if $2k_F$ is well above or well below k_{pl} then the electrical resistivity will be low and have a positive TCR.

In Ziman theory, there are several assumptions made in order for the theory to be valid [5,12]. The electrons are scattered elastically by each single individual atom. The multiple scattering of electrons is neglected. The electron mean free path is well defined and it is longer than the inter-atomic distances. The conduction electrons are treated as plane waves, i.e., the concept of Fermi surface is well defined. The Born approximation is valid, which means that scattered electrons can be treated by the first-order perturbation theory by using an appropriate, but not unique, weak pseudo-potential. Ziman used the Boltzmann equation to derive the resistivity formula [2]

$$\rho = \frac{3\pi e^2}{\hbar m v_F} \frac{\Omega}{N} \int_0^1 |V(q)|^2 S(q) 4(q/2k_F)^3 d(q/2k_F), \qquad (2\text{-}13)$$

where $V(q)$ is the pseudopotential, N/Ω is the number of atoms per unit volume, v_F is the Fermi velocity, and $S(q)$ is the structure factor. The temperature dependence of the structure factor is the

reason for the temperature dependence of the electrical resistivity in this model. For a monovalent metal [fig. (2-5)], $2k_F$ is located away from k_{pl}; this will lead to an increase in the value of $S(q)$ with the increase of temperature. A positive TCR is predicted. For a divalent metal, $2k_F$ is near the k_{pl} and $S(q)$ value will decrease with the increase of temperature, leading to a negative TCR [2].

The structure factor is a dynamical quantity, $S(q,\omega)$, with elastic and inelastic contributions. The correct resistivity structure factor $S_c(q)$ should contain an appropriate correcting function given by [2,14]

$$S_c(q) = \int_{-\infty}^{\infty} S(q,\omega)\frac{x}{e^x - 1}d\omega, \tag{2-14}$$

where $x = \frac{\hbar\omega}{k_B T}$. At high enough temperatures $\frac{x}{e^x - 1} \to 1$, which means that $S_c(q)$ is the same as $S(q)$. At low enough temperatures, the temperature dependence of resistivity is the sum of two opposite effects. The first effect is a decrease in the resistivity due to a decrease in the elastic scattering, which can be written as [2]

$$\rho_{elastic} = \rho(0)(1 - aT^2). \tag{2-15}$$

The second effect is a resistivity increase due to the inelastic scattering. The second effect can be written as [2]

$$\rho_{inelastic} = \rho(0)(1 + aT^2). \tag{2-16}$$

The resistivity increase is more by a factor of two. This will lead to a total resistivity dependent on $+T^2$. The T^2 dependence is a characteristic phenomenon of phonon scattering in disordered systems.

Ziman model is considered to be an adequate and a successful model when dealing with the amorphous metallic alloys in the weak scattering limit [2,15,16]. In the weak scattering limit the electrons mean free path is long compared to the inter-atomic distances. The electron motion is along

a classical trajectory and the electrons do not suffer multiple scattering. However, the Ziman model fails to explain why do most of metallic glasses have minimum values in their resistivity at low temperatures, usually below 20 K.

2.3.4) Extended Ziman theory for transition metals

Transition metals (scandium through zinc) have the *3d* orbital filled before the *4p* one. The *3d* and the *4s* levels overlap in energy. This will cause some electrons to fill the *N* shell before the *M* shell is completely filled. This effect gives the transition metals a fairly similar chemical properties. Iron, cobalt, and nickel have stronger ferromagnetic properties due to the partially filled *3d* sub-shell. These properties are a result of the Pauli exclusion principle. This principle allows several electrons of the same parallel spin to exist in the *3d* and *4s* sub-shells [17].

Because of the strong interaction between the *3d* and the *4s*, it is not possible to introduce a weak ion-electron pseudopotential to calculate the resistivity. Even in crystalline transition metals the interaction, or hybridization, between the *3d* and *4s* sub-shells usually leads to a lower DOS for free electrons at the Fermi Energy.

In 1971, Evans extended the Ziman theory to amorphous transition metals by using the muffin-tin model [18]. In this model each ion is considered as a sphere center. The potential of this sphere is considered to be spherically symmetrical. The ion spheres are not allowed to overlap [18].

For transition metals we need to consider the *d*-phase shift η because the *s*- and *p*-phase shift are zero. In this model we still assume that the *d* band does not modify the free electron *s* band. We also assume the scattering is weak, and the Boltzmann equation is valid. Because of these assumptions, Evans' approach to extend the Ziman theory is only valid for the case of weak scattering

amorphous metallic transition alloys [19]. The resistivity formula for this model can be written as [17]:

$$\rho \approx \frac{30\pi^3\hbar^3}{me^2k_F^2E_F\Omega}\sin^2[\eta(eE_F)]S_T(2k_F), \tag{2-17}$$

where Ω is the atomic volume, $\eta(E_F)$ is the d partial wave phase shift, $S_T(2k_F)$ is the temperature dependent structure factor. $S_T(k)$ can be estimated as

$$S_T(k) \cong 1 + [S_E(k) - 1]e^{-2W_k(T)}, \tag{2-18}$$

where $S_E(k)$ is the equilibrium structure factor and exp[-2W$_k$(T)] is the Debye-Waller factor. The $W_k(T)$ of the exponent is equal to

$$W_k(T) = W_k(0) + \left[\frac{T}{\Theta_D}\right]^2 \int_0^{\Theta_D/T} \frac{zdz}{e^z - 1}, \tag{2-19}$$

where

$$W_k(0) = \frac{3(\hbar k)^2}{8Mk_B\Theta_D}. \tag{2-20}$$

For k=2k$_F$,

$$W_k(0) = \frac{3(\hbar k_F)^2}{2Mk_B\Theta_D}. \tag{2-21}$$

In low and high temperature limits, eq. (2-19) reduces to

$$W_k(T) = W_k(0) + 4W_k(0)\frac{\pi^2}{6}\left(\frac{T}{\Theta_D}\right)^2, \quad T << \Theta_D, \tag{2-22}$$

$$W_k(T) = 4W_k(0)\frac{T}{\Theta_D}, \quad T \geq \Theta_D. \tag{2-23}$$

For the amorphous metallic alloys that contain ferromagnetic transition metals and have resistivity minimum, the resistivity formula can be written as [20,21]

$$\rho(T) = \alpha_0 + \alpha \ln T, \quad 4 \le T \le 12\,K \quad (T < T_{\min}), \tag{2-24}$$

$$\rho(T) = \beta_0 + \beta T^2, \quad 50 \le T \le 100\,K \quad (T > T_{\min}), \tag{2-25}$$

$$\rho(T) = \gamma_0 + \gamma_1 T + \gamma T^2, \quad 200 \le T \le 300\,K, \tag{2-26}$$

where α_0, α, β, β_0, γ_0, γ_1, and γ are constants. We can estimate the Debye temperature as

$$\Theta_D \cong \frac{\pi^2 \gamma_1}{6(\beta - \gamma)}. \tag{2-27}$$

2.3.5) The Mott model

In the Mott model, the scattering of conduction electrons is due to what is called the fluctuation in the local environment due to the structure disorder. The resistivity is caused by the existence of large number of empty *d* states which the *s* electrons can scatter into. Mott assumes that the *s* electron mean free path is large compared to the average inter-atomic distance and the *d* electron mean free path is close to the average inter-atomic distances. The conduction is caused by unmodified free electron band. The resistivity equation can be written as [2]

$$\rho = \rho_0 \{1 - \frac{1}{6}(\pi k_B T)^2 [3(\frac{d}{dE} \ln N_d)^2 - \frac{d^2}{dE^2} \ln N_d]\Big|_{E=E_F}\}, \tag{2-28}$$

where N_d is the number of *d* electrons at the Fermi energy. The broadening of the Fermi function with increasing temperature can, in principle, lead to the temperature dependence in resistivity. However, the temperature dependence according to eq. (2-28) is extremely small, leading to an almost temperature independence of resistivity [2].

The Mott model gives another important relationship between the resistivity and the g-value. The g-value is defined as the ratio of the DOS at E_F over the corresponding free electron value [5]

$$g = \frac{N(E_F)}{N(E_F^{free})}, \tag{2-29}$$

or

$$g = \frac{v_F}{v_F^{free}}. \tag{2-30}$$

The conductivity, according to Mott model, can be written as [5]

$$\sigma = \frac{1}{3} e^2 g^2 \Lambda_F v_F^{free} N(E_F)^{free}, \tag{2-31}$$

where Λ_F is the elastic mean free path and v_F is the average Fermi velocity. The g-value can give an indication of the behavior of resistivity for a given amorphous alloy. If g ≅1, then we are in the weak scattering limit [5,22] because the mean free path is long and the speed of the conduction electrons equal approximately the speed of the free Fermi electrons (~10^6 m/s). We have the ordinary dependence of $+T^2$. If g ≅ 0.2–0.3, then we are in the strong scattering limit. In this limit, Λ_F is constant and equals the average inter-atomic distances. Eq. (2-31) can be written as [5]

$$\sigma = Cg^2, \tag{2-32}$$

where $C = \frac{1}{3} e^2 \Lambda_F v_F^{free} N(E_F)^{free} = consant$. The g^2 dependence of conductivity agrees with the experimental data for some of the strong scattering alloys [5]. We can write the resistivity in the strong scattering limit as

$$\rho = C_1 g^{-2}, \tag{2-33}$$

where $C_1 = C^{-1}$. The resistivity in Mott model is related to the g-value and not to T, which is in agreement with the conclusion taken from eq. (2-28).

In the Mott model, like in the Ziman model, the unmodified free electron band is responsible for carrying the current. However, the electrons in the Mott model are considered to be more tightly

bounded to the ions of the alloy. The scattering is caused by the fluctuations in the potential of those ions, while in the Ziman model the scattering is caused by the ionic potential wells. Finally, the Mott model does not depend directly on the structure as the Ziman model does [2].

2.3.6) The generalized Faber-Ziman theory

The electrons in the Ziman model are considered to be scattered elastically. In some *sp* amorphous metallic alloys, TCR changes sign when ρ_0 is about 40–60 μΩ·cm and it has no relation to $2k_F$ and k_{pl} [5]. This theory includes the electron-phonon interaction factor into the original Ziman model [23]. The resistivity can be written as [23]

$$\rho = (\rho_0 + \Delta\rho)e^{-2W(T)},$$

where ρ_0 is the residual resistivity, $\Delta\rho$ is the contribution due the inelastic electron-phonon scattering, and the exponential term is the Debye-Waller factor. The Debye-Waller factor is the combination of inelastic and elastic scattering. When temperature increases, $\Delta\rho$ contributes to an increase in the resistivity while the Debye-Waller factor results in a decrease in the resistivity [5]. The total temperature dependence of resistivity is the sum of these two contributions. At very low temperatures, the contribution from the inelastic scattering is very small and can be neglected. At low temperatures the Debye-Waller factor leads to [23]

$$\frac{\rho}{\rho_0} = 1 - bT^2, \quad \Theta_D >> T \geq 20K, \tag{2-34}$$

where b is a constant. This temperature dependence is characteristic of *sp* amorphous metallic alloys [23]. At temperatures higher that Θ_D, the Debye-Waller factor can be expanded as [24]

$$e^{-2W} \approx 1 - 2W \approx 1 - \beta T, \; T > \Theta_D. \tag{2-35}$$

The resistivity is equal to [24]

$$\rho = (1 - \beta T)(\rho_0 + \alpha T) = \rho_0 + \gamma T - \alpha\beta T^2, \quad T > \Theta_D, \tag{2-36}$$

where α and β are the parameters describing the electron-phonon interaction and the phonon-phonon coupling, respectively, and $\gamma = \alpha - \rho_0\beta$.

2.3.7) Mooij correlation

In 1973 Mooij collected data for amorphous and thin films alloys and found that there exists a similar correlation between TCR and ρ_0. TCR will change sign from positive to negative when ρ_0~100–150 μΩ·cm [7]. The value 150 μΩ·cm is considered to be a universal boundary that divides the negative and the positive TCR. However, experimental evidence shows that this is not a universal boundary. The relation between TCR and ρ_0 is more complex. It has been reported for some amorphous alloys that TCR can change sign when ρ_0~30–400 μΩ·cm [25]. In some *sp* electron amorphous alloys TCR reverses its sign when ρ_0~40–60 μΩ·cm [5]. The 150 μΩ·cm value holds only for *d* electron systems or the strong scattering limit [5]. The negative TCR in this case is a result of the short mean free path relative to inter-atomic distances. As speculated by Mooij, this negative TCR is related to the quantum interference contributions [2].

2.3.8) Beyond the nearly free electron model

The above theories, which are based on the nearly free electron Boltzmann transport equation, cannot explain two anomalous features. The first is the existence of high values of negative TCR over

a wide range of temperatures [2,4,26]. The second is the existence of a low temperature resistivity minimum [2].

When the mean free path of an electron becomes short relative to inter atomic distances, the electron's motion becomes diffusive rather than along free trajectory [3]. In this case, the nearly free electron assumptions are not valid and we need a new theory to deal with the multiple scattering of electrons. As a result of this diffusive motion, two important effects occur: weak localization, WL, and electron-electron interaction, EEI. Both of these effects occur in an environment of a multiple-scattering elastic process. The WL effect involves a single conduction electron while the EEI effect involves two conduction electrons [3].

2.3.8) Weak localization

When the electron mean free path becomes close to the inter-atomic distances, a multiple elastic scattering process with a short scattering time will occur. This will enhance the probability for the electron to return to its origin and this will cause the back-scattering process. The motion of the electrons is diffusive. The diffusion coefficient D can be determined from Einstein relation of conductivity [3]

$$\sigma = e^2 DN(E_F). \tag{2-37}$$

The back-scattering process is a result of the interference of two waves of the same electron traversing the same path but in opposite directions [fig. (2-5)] [3]. Let us assume the current to be the movement of electrons from lead point A to lead point B through any path. If there exists a point C where the electron leaves it clockwise and returns back to it anti-clockwise, or vice-versa, then the probability of the electron which traverses the closed path can be written as [3,27]

$$W = |\Psi_1|^2 + |\Psi_2|^2 + \Psi_1^*\Psi_2 + \Psi_1\Psi_2^*, \tag{2-38}$$

where Ψ_1 is the probability amplitude of the clockwise path and Ψ_2 is the probability amplitude of the anti-clockwise path. Ψ_1 and Ψ_2 have the same path but traverse in the opposite direction. Because Ψ_1 and Ψ_2 are coherent, the second interference term in eq. (2-38) cannot be neglected. The total probability of the electron returning to point C is twice the probability of going from A to B. This is the source of back-scattering and, consequently, of the WL effect. In other words, WL arises from the probability decrease of electrons to diffuse from A to B and this is due to the higher probability for electrons to localize at C. Any process that changes either the energy state or the spin state of the electron will destroy this quantum coherence [27]. Inelastic scattering, spin-orbit scattering, and the presence of a magnetic field are important effects that can destroy WL [3].

The probability of finding an electron at a distance between r and $r+dr$ at a time between t and $t+dt$ can be given by [3]

$$p(r,t)drdt = \frac{1}{(4\pi Dt)^{3/2}}\exp(\frac{-r^2}{4Dt})drdt. \tag{2-39}$$

The probability of the electron returning to a small fixed volume around $r = 0$ is proportional to $t^{-3/2}$. To calculate the probability of back scattering, we integrate eq. (2-39) from the minimum elastic scattering time, t_o, to the maximum time for the elastic scattering to occur, t_i, i.e., the time when we have inelastic scattering. The probability of back scattering will then be proportional to $(t_o)^{-1/2} - (t_i)^{-1/2}$. When t_o equals t_i, the WL effect disappears completely. Because $(t_o)^{-1/2}$ is a constant, the term $(t_i)^{-1/2}$ is responsible for the temperature dependence of WL. In three dimension amorphous systems, t_i is proportional to T^2. This will lead to a linear temperature dependence of WL [3,28]. The formula for the conductivity correction at low temperatures in three dimension amorphous systems is given by [4]

$$\Delta\sigma_{WL}(T) = \frac{e^2}{\pi^2 \hbar a} T, \tag{2-40}$$

where a is a constant.

2.3.8.2 Magnetic field effect on WL

A magnetic field of a magnetic flux ϕ will change the two counter-propagating waves of the weak localized electron by the amount $\frac{2e\phi}{\hbar}$ [3]. This will lead to a dephase between the two waves, which is proportional to the magnetic flux. The WL effect therefore diminishes with the increase of the magnetic flux and this effect leads to a negative magnetoresistance. The increase in the conductivity of non-magnetic metallic glasses due to the magnetic field is proportional to $B^{1/2}$ [2].

2.3.8.3 Spin-orbit coupling effect on WL

The resistivity of an amorphous metallic glass can be increased by the WL effect and decreased by the spin-orbit scattering effect. In WL, if the two counter-propagating waves have the same spin and there is no spin-orbit scattering, they recombine to enhance the probability of localization. If the two counter-propagating waves have opposite spins, they recombine to reduce the probability of localization. For single state waves, which have opposite anti-parallel spins, the effect of spin-orbit is the same for both waves in each scattering event. When the two waves return to their starting point, they will be in phase.

In the case of triple state waves, if the two waves have parallel spins, they will suffer changes in the spin direction which are equal in magnitude but opposite in sign. The two waves will randomize

rapidly and they will have the tendency to cancel each other. Usually, the ions of high atomic number, such as gold, have strong spin orbit coupling. The spin-orbit scattering time, t_{so}, for this process to happen depends on the scattering number and the strength of the spin-orbit coupling. This scattering time is usually independent of temperature. If the inelastic time, t_i, is longer than t_{so} then the spin-orbit effect will destroy the constructive interface of the triple state. The total contribution from the spin-orbit effect will be a negative contribution and the probability will be half of the classical value. This will result in a decrease of conductivity as temperature increases. The correction to the conductivity due to the spin-orbit effect is given by [29]

$$\Delta\sigma_{so} = \sigma_o + a\left(\sqrt{1+y} - \sqrt{y}\right) \tag{2-41}$$

where $a = \left(\frac{\sqrt{3}e^2}{2\pi^2 l_e \hbar}\right)\left(\frac{\tau_o}{\tau_{so}}\right)^{1/2}$, $y = \frac{\tau_{so}}{4\tau_i}$, and $\sigma_o = \left(\frac{4e^2}{3\pi^2 l_e}\right)\left(E_F \tau_o\right)^2$.

2.3.8.4 Electron-electron interaction

The electron-electron interaction or the Coulomb anomaly is a result of the interaction between two conduction electrons in the presence of a multiple scattering process [3]. In order for EEI to occur, the electrons have to move diffusively and the elastic scattering has to be strong. EEI is due to the interference of two electrons which traverse the same path in the same direction. The two electrons may have different frequencies due to their different energies. The frequency difference could be of the order of $\frac{k_B T}{\hbar}$. The time between the two electron waves to be out of phase after being in phase is called the thermal coherence time, which is equal to [3]

$$t_t = \frac{\hbar}{2\pi k_B T}. \tag{2-42}$$

The EEI will occur only when the elastic scattering time of the electrons by the ions is significantly smaller than t_t. The EEI, therefore, can be seen only at temperatures less than 20 K. Given the fact that these electrons move diffusively, eq. (2-39) can be applied. In order to calculate the probability of all the paths that can be crossed in a time less than t_t we need to integrate eq. (2-39) from t_o up to $t_t = \frac{\hbar}{2\pi k_B T}$. The result will be proportional to $T^{1/2}$ provided there is no inelastic scattering. This behaviour has been frequently reported [30-35]. The correction to the conductivity equation of the temperature dependence of EEI at low temperatures can be written as [4,18,33]

$$\Delta\delta_{EEI} = \frac{1.3e^2}{4\pi^2\hbar}\left(\frac{4}{3} - \frac{3}{2}F_\delta\right)\sqrt{\frac{k_B T}{\hbar D}}, \tag{2-43}$$

where F_δ is screen factor for the Coulomb interaction.

2.3.9 Summary

The temperature dependence of the electrical resistivity in amorphous metallic alloys can be divided into two main regimes. These are the weak scattering and strong scattering regimes. In the weak scattering limit, the mean free path of the conduction electrons is much larger than the average inter-atomic distances. In this case, the electron can be described as moving in a free trajectory in a classical way, i.e., they do not suffer multiple scattering during the scattering process.

The amorphous system can be treated as a nearly free electron system and the Boltzmann transport equation can thus be used. The first successful model to describe the weak scattering limit was the Ziman model. This model predicts a T^2 dependence at low temperatures and a T dependence

at high temperatures. This model is adequate for most amorphous metallic alloys in the weak scattering limit. This model, however, fails to justify the resistivity minima and the negative TCR in some low-resistivity amorphous metallic alloys.

The Evans model is an attempt to extend the Ziman model to include alloys with transition metals. These transition metals normally cause the strong scattering process in the alloy system.

The Mott model uses another approach to predict the resistivity dependence of temperature for amorphous metallic alloys having transition metals. This model almost predicts the temperature independence of resistivity.

The generalized Ziman-Faber theory modifies the original Ziman model to include the electron-phonon interaction factor in the calculations of the temperature dependence of resistivity.

All of the above models are based on the nearly free electron assumptions and on the Boltzmann transport equation. These models, however, fail to answer two important questions: why do some amorphous metallic alloys have high negative TCR over a wide range of temperatures and why do some of the other alloys have a resistivity minima.

When the electron mean free path is comparable to the inter-atomic distances and the electron motion is diffusive rather than along a free trajectory, the multiple scattering process starts to appear. The Boltzmann equation is not valid. We have to include these multiple scattering processes in the new theories. The WL and the EEI effects deal with the multiple scattering of the conduction electrons. Both the WL theory and the EEI theory provide answers to the above two questions. First, the high negative TCR is due to weakly localized electrons and, second, the resistivity minimum is due to the EEI which disappears completely as a result of inelastic scattering.

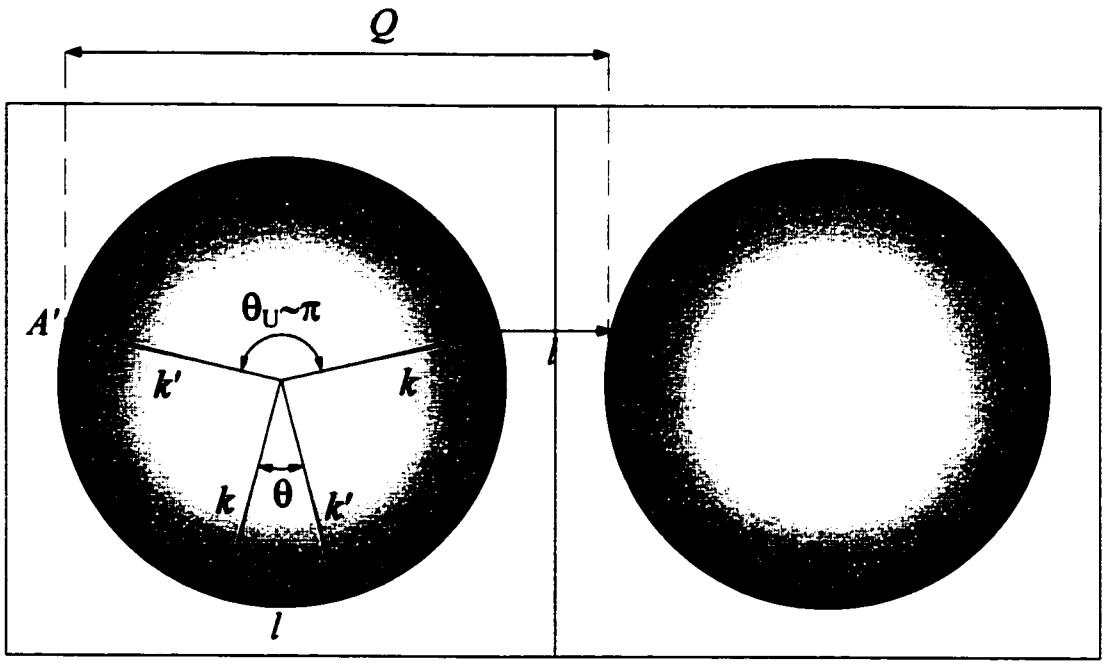

Fig. (2-1) Two Fermi sphere in adjacent Brillouin zones. A' is in the first zone, while A is in the second zone where the umklapp scattering ends.

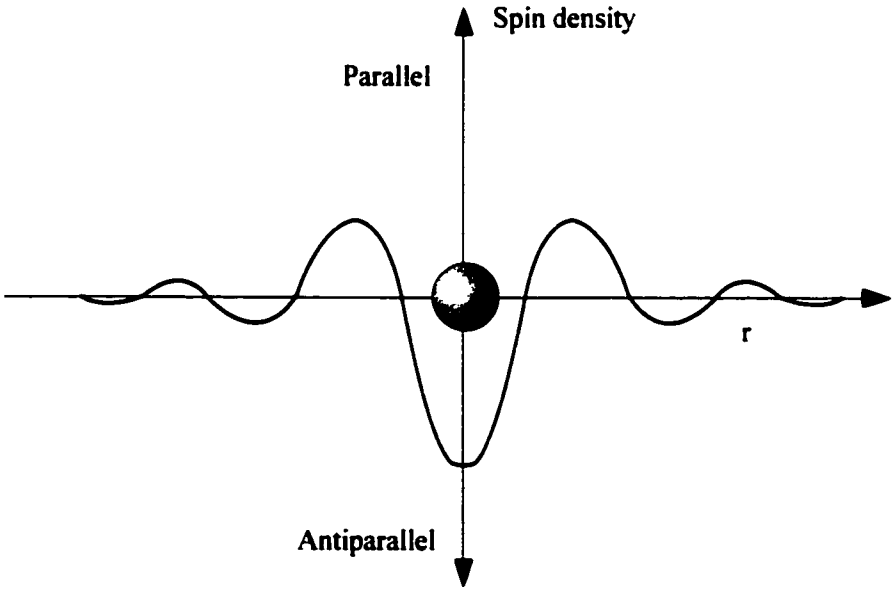

Fig. (2-2) Schematic representaion of conduction electron spin densityaround an isolated magnetic impurity.

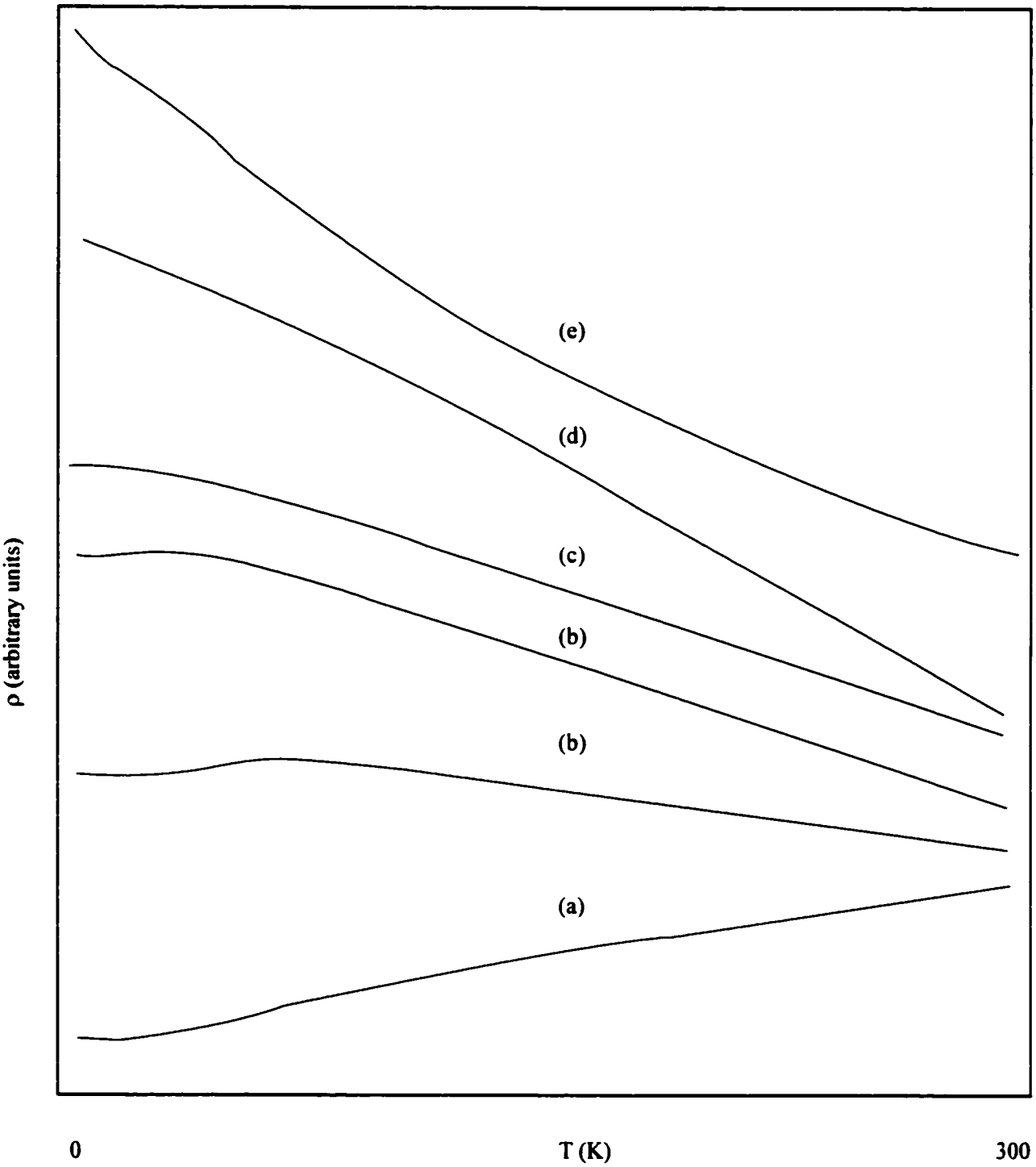

Fig. (2-3) Schematic illustration of the resitivity dependence curves observed for amorphous metallic alloys

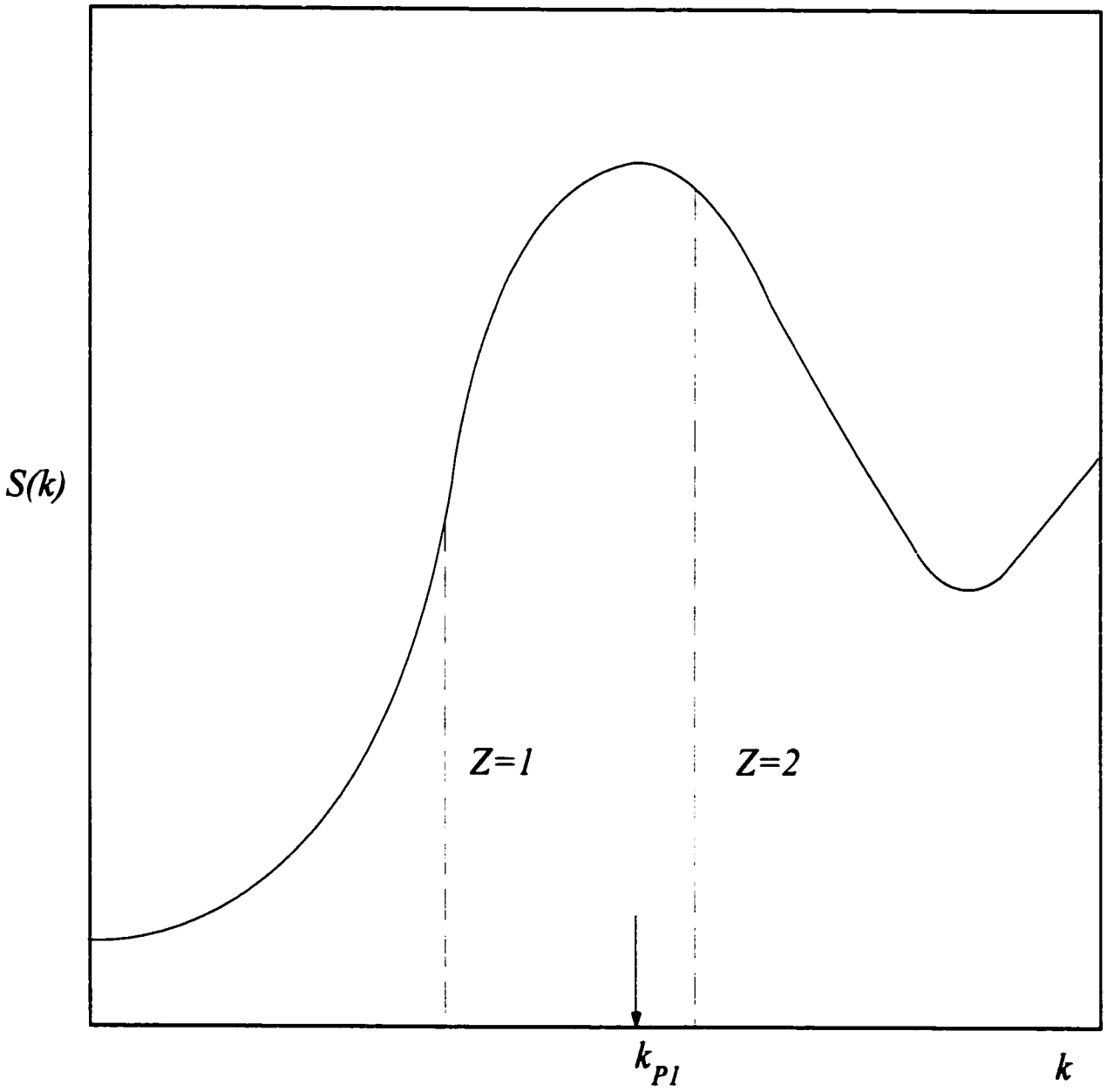

Fig. (2-4) A typical structure factor for an amorphous metal. The two dashed lines show the position of $2k_F$ for monovalent and divalent metals.

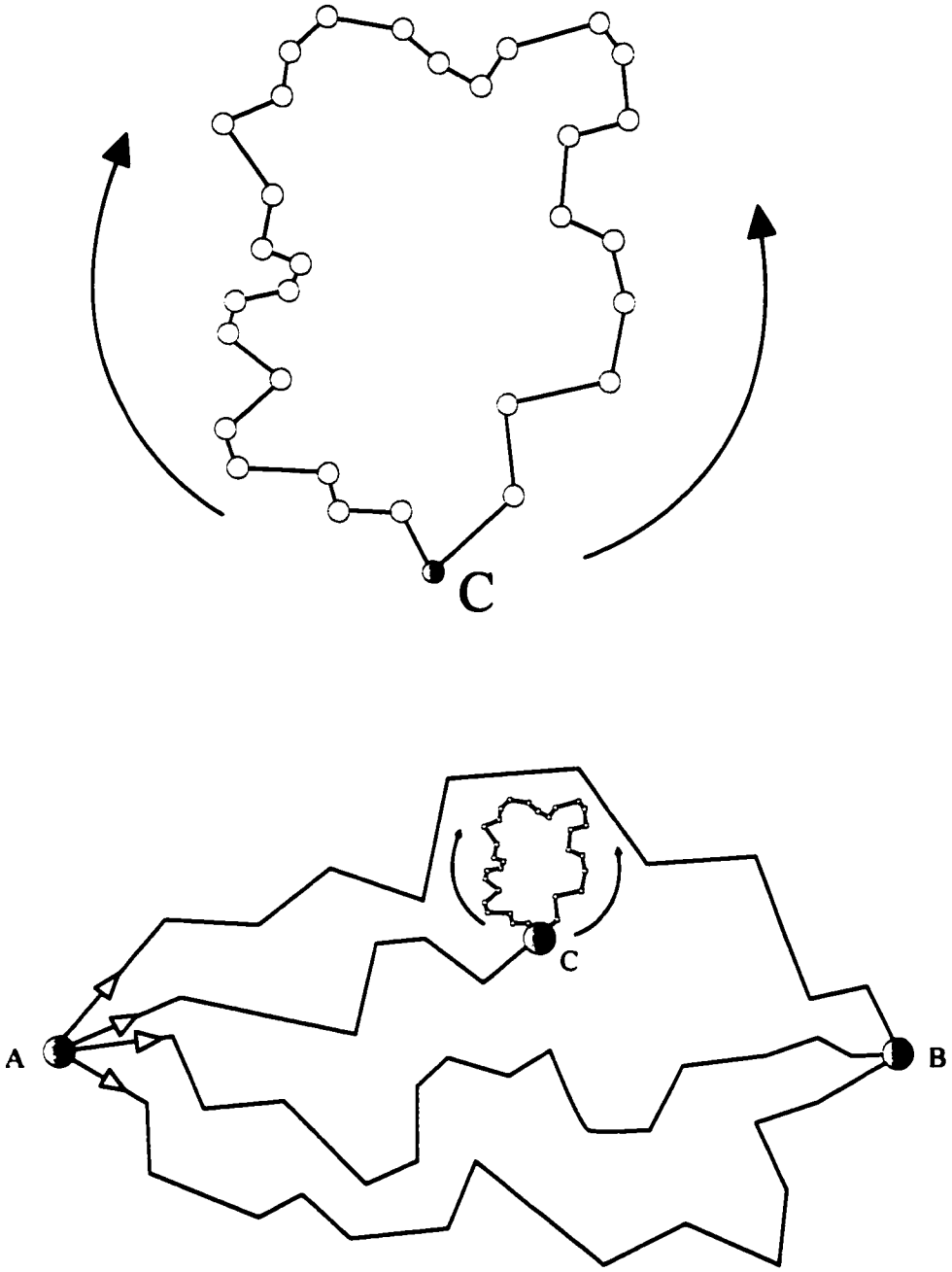

Fig. (2-5) The current going from A to B and being localized at C

3. Experimental procedure

3.1) Introduction

The resistivity measurement system consists of a cryostat, a hardware, and a software. The cryostat is used to cool the sample to the desired temperature. The hardware consists of a computer, an IEEE card, a digital temperature controller, and a digital multimeter. The software is a program written in Qbasic language to control the hardware and accumulate the data in the American standard code for information interchange, ASCII, format.

3.2) System design.

Designing an experiment to measure resistance values of 1 Ω or less, which is considered to be a low-level measurement, involves some fundamental difficulties. By definition, low-level measurements are measurements close to theoretical limits [36]. Theoretical limits are due to the thermal noise or Johnson noise in the device internal resistance [37]. For any resistance, the movement of charges due to thermal energy in the resistance material results in noise. The power available from this motion is given by

$$p = 4k_B T\Delta f, \tag{3-1}$$

where k_B is Boltzmann's constant, T is the absolute temperature, and Δf is the noise bandwidth. The Johnson voltage noise root-mean-square, V_{rms}, developed in a resistance R is

$$V_{rms} = (4k_B T\Delta f R)^{1/2}. \tag{3-2}$$

The Johnson current noise root-mean-square, I_{rms}, developed in a resistance R is

$$I_{rms} = (4k_B T\Delta f / R)^{1/2}. \tag{3-3}$$

At room temperature, the above equations become

$$V_{rms} = 4.6\times10^{-10}(\Delta f R)^{1/2}, \tag{3-4}$$

and

$$I_{rms} = 4.6\times10^{-10}(\Delta f / R)^{1/2}. \tag{3-5}$$

Since all voltage and current sources contain internal resistance, they exhibit Johnson noise and have theoretical limits.

Other difficulties are errors caused by other factors related to the electrical connections such as lead resistance. Lead resistance is typically in the range of 0.01–1 Ω. Thermoelectric voltages or thermal electro-motive forces, EMF, are another major source of error. Thermal EMF arises when different parts of a circuit are at different temperatures, or when conductors made of dissimilar materials are joined together, as in ordinary solder joint. For example, the thermal EMF resulting from a lead-tin solder joint of two copper wires at different temperatures is 3μV/C° [38].

A measuring system can also pick up interference from any electromagnetic field. Even the earth's weak magnetic field can generate nV noise levels in dangling leads.

3.3) Electronics

In any low-level electrical resistivity measurements the lead resistance is the largest error source and the easiest to solve. In the typical two-wire connection method, a testing current, I_{test} , of the order of 10 mA is forced through the leads and through the resistance being measured. The testing current will result in small voltage drop across the leads. Although this voltage drop is small, it is significant to the measurements. A four-wire connection method or the Kelvin connection method is

the solution to remove the lead resistance [36]. In the four-wire connection method, two wires are used to force a testing current, through the resistance and the other two-wires are used to measure the voltage drop by a sensing current, I_{sen} . This sensing current is in the order of pA. Because I_{sen} is very small, the voltage drop across the leads can be neglected. Although four-wire connection method minimizes the effect of the lead resistance, EMF can add a significant amount of error to the measurement.

Thermal EMF results from temperature difference within a measuring circuit at a junction between conductors composed of dissimilar materials [39]. There are several steps which should be taken to minimize EMFs. We must use the same type of material in all wire connections, keep the wires as clean as possible before soldering, use low thermal cadmium-tin solder instead of lead-tin solder to connect Cu-Cu connections, provide good thermal coupling to the sample holder, which is a massive heat sink, by using Apiezon-N grease, and control the temperature increase in the system to 10 mK/s at a maximum. In addition, we must allow the test equipment to warm up and reach thermal equilibrium in a constant ambient temperature. The final step involves the elimination of the remaining effect of the thermal EMF. There are two ways to achieve this goal. The first way is to make the measurements using two opposite currents $I_{sen(-)}$ and $I_{sen(-)}$

$$V_{(+)} = V_{EMF} + I_{sen}R, \tag{3-6}$$

$$V_{(-)} = V_{EMF} - I_{sen}R. \tag{3-7}$$

By subtracting the two values and dividing by two we cancel the V_{EMF} completely. The second way is to do an offset compensating measurement. In this way, I_{sen} is used to measure both the voltage drop across the resistance and the thermal EMF. I_{sen} is then set to zero and the thermal EMF is measured alone. The thermal EMF is subtracted from the total voltage drop to give the offset compensated voltage value.

In any low level resistance measurement, it is important to determine what level of accuracy is

needed. There are three distinct methods for making low-resistance measurements [36].

(1) The DMM (Digital Multi-Meter) with four-terminal. This method is sensitive to 100 μΩ.

(2) The Micro-Ohmmeter with four-terminals. This method is sensitive to 0.1 μΩ.

(3) The separate current source and separate sensitive voltmeter. This method is sensitive to 0.1 nΩ. For our experiments, we chose the DMM method. The specific type of DMM used was the Keithly 2010 $7\frac{1}{2}$ digit digital multimeter. This particular DMM has three distinct advantages: 1) it has a four-wire connection which will eliminate the lead resistance; 2) it has the offset compensating function to cancel the thermal EMF; 3) its accuracy is 90 μΩ. In this experiment the first method of measuring the resistance was used. This is because the uncertainty in measuring the sample resistance is much lower than the systematic error due to the sample dimensions.

The measurement value of the thermal EMF is negligible in the experiment. This is because the value of the offset thermal EMF voltage in the Cu-Cu connection (using lead-tin solder) is 3μV/C°. The magnetic and electric fields interference are also negligible because the magnetic and electric fields produce a nV noise and the length of the connection wires is short. In addition, all of the electronic elements in the experiment are connected to a common ground.

The temperature controller used in this experiment is Lakeshore 330 auto tuning temperature controller. It is a $4\frac{1}{2}$ digit digital device. Its measurement resolution can reach 1.3 mK at 4.2 K. A DT-470-SD-13 silicon diode is used to read the temperature. The range of this sensor is from 1.4 K to 475 K. The accuracy of the sensor is $\pm$1.5 K or $\pm$1.5% of the reading, whichever is greater. The repeatability is $\pm$10 mK.

An IEEE 488.2 interface card is used to control the DMM, the temperature controller, and to accumulate the data. The DMM and the temperature controller are connected to the computer through a general purpose interface bus, GPIB, cable. The data is then stored in a computer hard disk in an

ASCII mode. Fig. (3-1) shows the block diagram of the electronic system.

3.4) Software

A computer program, written in the Qbasic language, controls the devices through the GPIB cable. The program is designed to read up to $3x10^4$ data points for each sample. Fig. (3-2) shows the flow chart of the program. Both the values of temperature and resistance are stored in the computer random access memory, RAM, until the number of data points reaches $1x10^4$. The data are then stored in the hard disk. A universal language interface driver, ULI, had to be added in order for the computer to execute the GIPB commands. The corresponding program in Qbasic language is given in Appendix A.

3.5) Cryostat

The cryostat [fig. (3-3)] consists of an outside liquid nitrogen dewar (A), an inside liquid helium dewar (B), a sample chamber (C), an electrical insert (D), a sample holder (D1), and the internal wiring (D4). The liquid nitrogen dewar has a vacuum jacket (A1) to thermally isolate the dewar. The vacuum jacket has a valve (A2) to control the vacuum. The vacuum inside the exterior liquid nitrogen dewar jacket can reach 10^{-6} Torr at room temperature.

The cryostat originally was designed to reach a minimum temperature of 10 K. A modification was made to the inside liquid helium dewar so that it can be evacuated. A steel ring with a circular hole (B5) was soldered at the top of the liquid helium dewar. The sample chamber (C) passes through the ring hole into the liquid helium dewar and is mounted at a distance of 1 cm from the bottom of the liquid helium dewar. The steel ring and the hole are vacuum-sealed.

The purpose of this modification is to allow pumping out the helium gas to reduce the pressure inside the helium dewar, thus achieving lower temperatures than the liquid helium boiling temperature of 4.2 K at 1 atm. The lowest temperature reached by this new modification is 1.56 K after about 40 min of pumping with two rotary pumps. This modification proved to be very efficient in terms of liquid helium consumption. Three liters of liquid helium per sample were used to reach 1.7 K. Furthermore, the rate of heating can be controlled by controlling the pressure inside the helium dewar. This rate can reach levels of 0.1 mK/s.

The interior of the liquid helium dewar, which is immersed in the liquid nitrogen dewar, has a vacuum jacket (B1) with a vacuum valve (B2). The vacuum inside the liquid helium dewar jacket can reach 10^{-6} Torr at room temperature. The liquid helium dewar is fixed and mounted inside the liquid nitrogen dewar by a mechanical clamp (B3) made of a material of low thermal conductivity. The liquid helium dewar is closed with a steel ring with a circular hole (B6) and there are an inlet valve (B4) and outlet valve (B5). A steel tube (B7), with an adjustable height, carries liquid helium to the bottom of the dewar. After the desired amount of liquid helium is put inside the dewar, the adjustable steel tube is pulled out. To reach the desired temperature, the inlet valve is used together with the outlet valve to pump out the helium gas from the helium dewar using two small rotary pumps. The temperature of 1.7 K is reached after approximately 30 min of pumping out the liquid helium dewar.

The sample chamber (C) is made of a long single layer of steel, which is immersed into liquid helium. The sample chamber has two valves, (C1) and (C2). The first valve is used to fill the sample chamber with helium gas, which is used as a thermal conducting gas. The helium gas is filled after evacuating the sample chamber from any other gases to avoid freezing problems during the experiment. The other valve is connected to a pressure gage (C3).

The electrical insert (D) is the innermost part of the cryostat and holds the cryogenic part of the electrical insert. The cryogenic part of the electrical insert [fig. (3-4)] consists of the sample holder

(D1), the wiring (D4), the temperature sensor (D5), the sample (D6), and a glass substrate (D7). Both the sample and the temperature sensor are connected using the four-terminal method. The sample holder is screwed to the bottom end of the electrical insert and kept very close to the bottom of the chamber. The sample holder is made of copper and its mass is about 70 times as large as the total mass of the sample and the wires. Because of its large mass, the sample holder acts as a heat sink. The top head of the electrical insert (D2) is made up of a light aluminum alloy and contains one vacuum-tight feed-through (D3), which connects the wiring of the sample and the sensor to the out-side outlet connections. The temperature sensor is embedded inside a hole in the sample holder and is kept near the sample glass substrate surface by means of Apiezon-N grease. The glass substrate and the sample are put on the sample holder using also Apiezon-N grease (D8), which is used as a good thermal conductor down to 4 K. The Apiezon-N grease covers the sample.

All the vacuum jackets in the system, the liquid helium container, and the sample chamber were leak detected.

3.6) Sample preparation

Amorphous metallic alloy ribbons can be produced by a technique known as melt spinning [40]. The melt spinning is used for achieving very high rate of cooling needed to form a metallic glass. The metallic alloy first is melted instantly in a quartz tube under high radio frequency. A jet of the hot molten alloy is then propelled against the surface of a high speed-rotating copper wheel at room temperature. The liquid alloy is then converted into a solid in the shape of thin ribbons (20–30 μm thick). The liquid alloy solidifies at a rate of about 10^6 K/s. The solid film is spun off the wheel as a continuous ribbon. Since the film is very thin and it contacts a large heat sink, and since the metals have high thermal conductivity, then the metallic alloy will solidify to an amorphous state. X-ray

scans proved that the ribbons are amorphous [41]. The samples are the same as those studied in Ref. [41].

It requires special care to prepare samples for electrical resistivity measurements. The samples should keep good electrical connection and should be stress- and strain-free at very low temperatures. Ordinary methods of heat soldering will convert the amorphous ribbons into crystalline state. Silver paste is used to make very good electrical connections that will stand even at very low temperatures. It is very important to keep the contact surface between the wire and the sample very clean. A mix of 50% nitric acid with distilled water is used to clean the surfaces. The sample is put in the solution of the nitric acid for two to three minutes and then washed by distilled water. The copper wires are put in the nitric acid solution for several seconds and then washed by distilled water. Immediately after the sample and wires are cleaned, the sample surface from both ends and the wires are painted with silver paste. After the wires and the sample are dry, they are put on a thin glass substrate and fixed mechanically by special commercial glue.

The sample should have a proper curvature to stay stress- and strain-free at very low temperatures. The glue is used as a fixer and is kept away from the silver paste connections. After the sample and the wires are fixed by the glue, another silver paste layer is put to connect the wires and the sample. Typically a period of 48 hours is needed for each sample in order for the glue and the silver paste to reach a hard enough state to withstand very low temperatures. Figs. (3-5) and (3-6) show the connection of the ribbon sample and the pure metal, respectively.

A micrometer of an accuracy of 1/1000 mm and a microscope of the magnification power of 30x were used to measure the dimensions of the ribbons. The average relative error of the volume of the ribbons was about 10%. The error results mainly from the irregularity in the thickness and width of the ribbons. This will lead to a 10% systematic error in the values of the calculated electrical resistivity. The changes in the calculated electrical resistivity due to the thermal expansion of the

ribbons can be neglected.

3.7) Procedure

The sample is put on the sample holder and then the sample copper wires are soldered with the setup wires using a low-heat solder pen to avoid transferring heat to the sample. Next, the sample and the wires are covered with the Apiezon-N grease. The grease is used to hold the sample on the sample holder and as a good thermal conductor.

The sample is put inside the sample chamber. The sample chamber is then evacuated and a desired amount of He gas is placed in the chamber. The sample chamber is evacuated twice in order to eliminate the presence of other gases. Next, liquid nitrogen (LN) is poured into the LN dewar, filling half of the dewar. The LN is then slowly transferred into the liquid helium (LHe) dewar until the temperature reaches about 80 K. Next, all of the LN is pumped out using pressured He gas. After that, LHe is slowly transferred into the LHe dewar until the LHe temperature is reached. Next, two rotary pumps are used to pump out the liquid helium using the inlet and outlet valves of the helium chamber.

After approximately 30 min, the temperature of about 1.7 K is reached. The temperature will stay at this equilibrium point until all the LHe evaporates. After that, the temperature will start to rise up steadily at a rate of 1 mK/s. The computer program is activated when the temperature starts to rise. The computer starts to take data when there is an increase of 10 mK in the temperature. After about 18 hours, the system reaches LN temperature. Then the remaining LN in the LN dewar is pumped away and the system will continue to warm up steadily until it reaches room temperature. The computer program is capable of accumulating 3×10^4 data points. Typically, there are 2.5×10^4 data points for a measurement in the temperature range 1.7–300 K. The average time for accumulating the full data set

is 48 h.

The resistivity system was tested using electrical resistivity standards before accumulating data for the investigated samples. Two standard samples, Au and Pt, were prepared to test the accuracy of the experimental setup. Each sample was about 22 cm long and 0.1 mm in diameter, with a purity of 99.998% . The Au and Pt samples were tested in the temperature range of 1.8–290 K. About 25000 data points for each sample were collected and then compared to the published data. The results were consistent with the published data within an experimental error [figs. (3-7) and (3-8)].

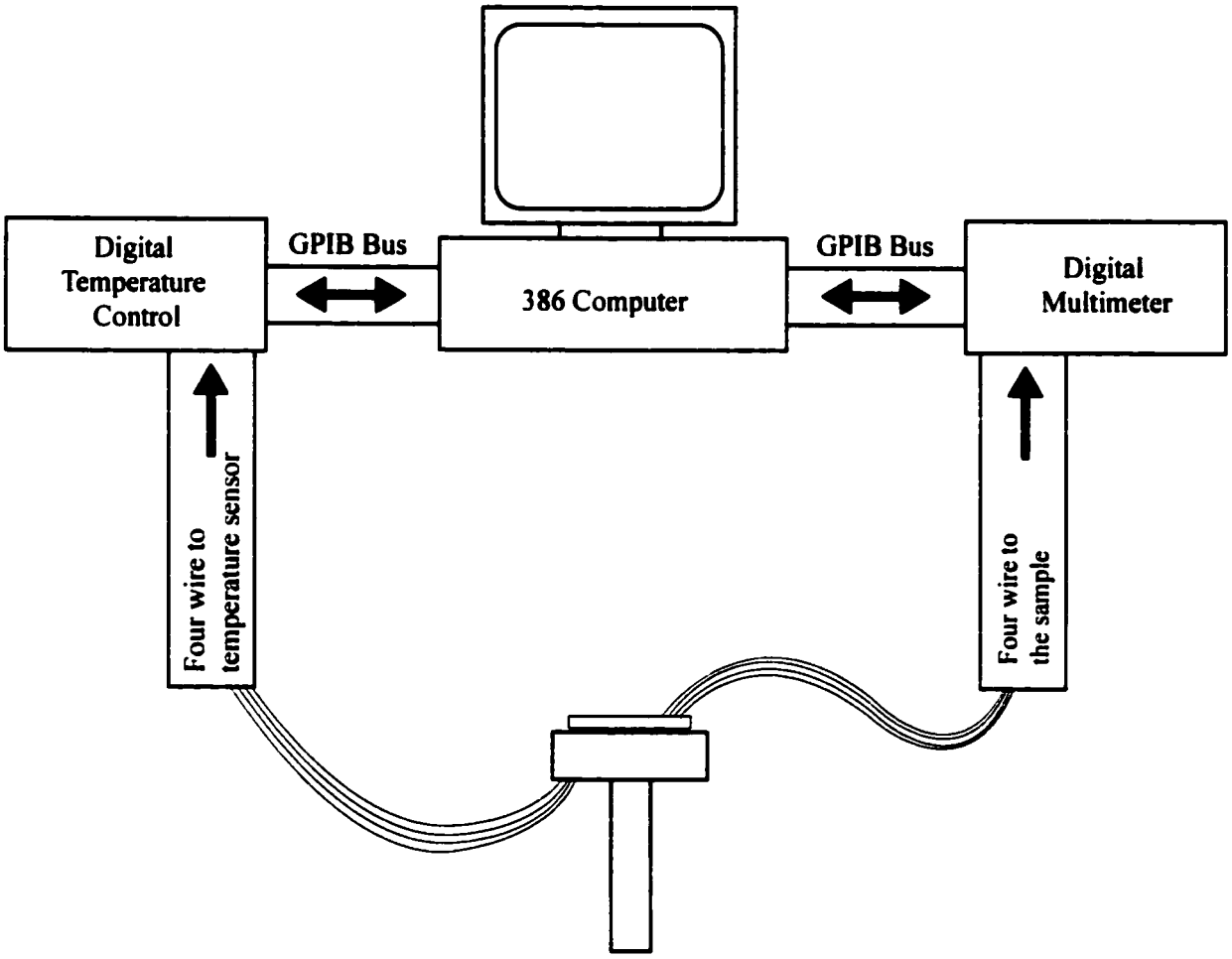

Fig. (3-1) The block diagram of the electronic system

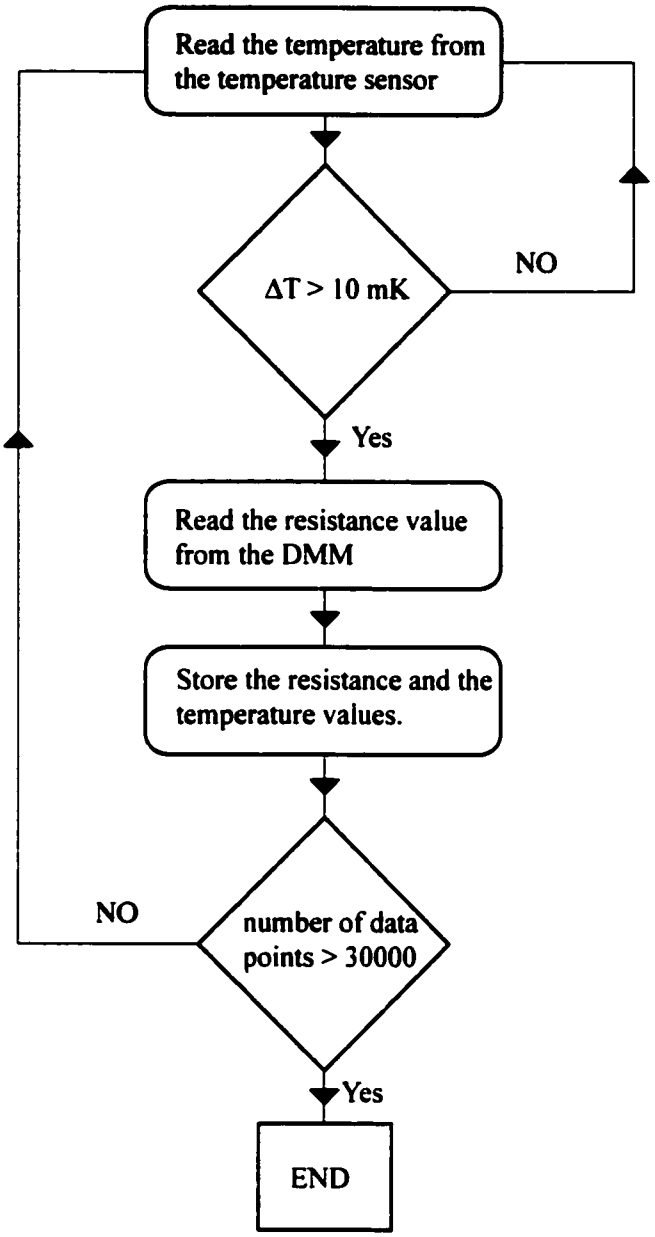

Fig. (3-2) The flow chart of the program used in accumulating the data.

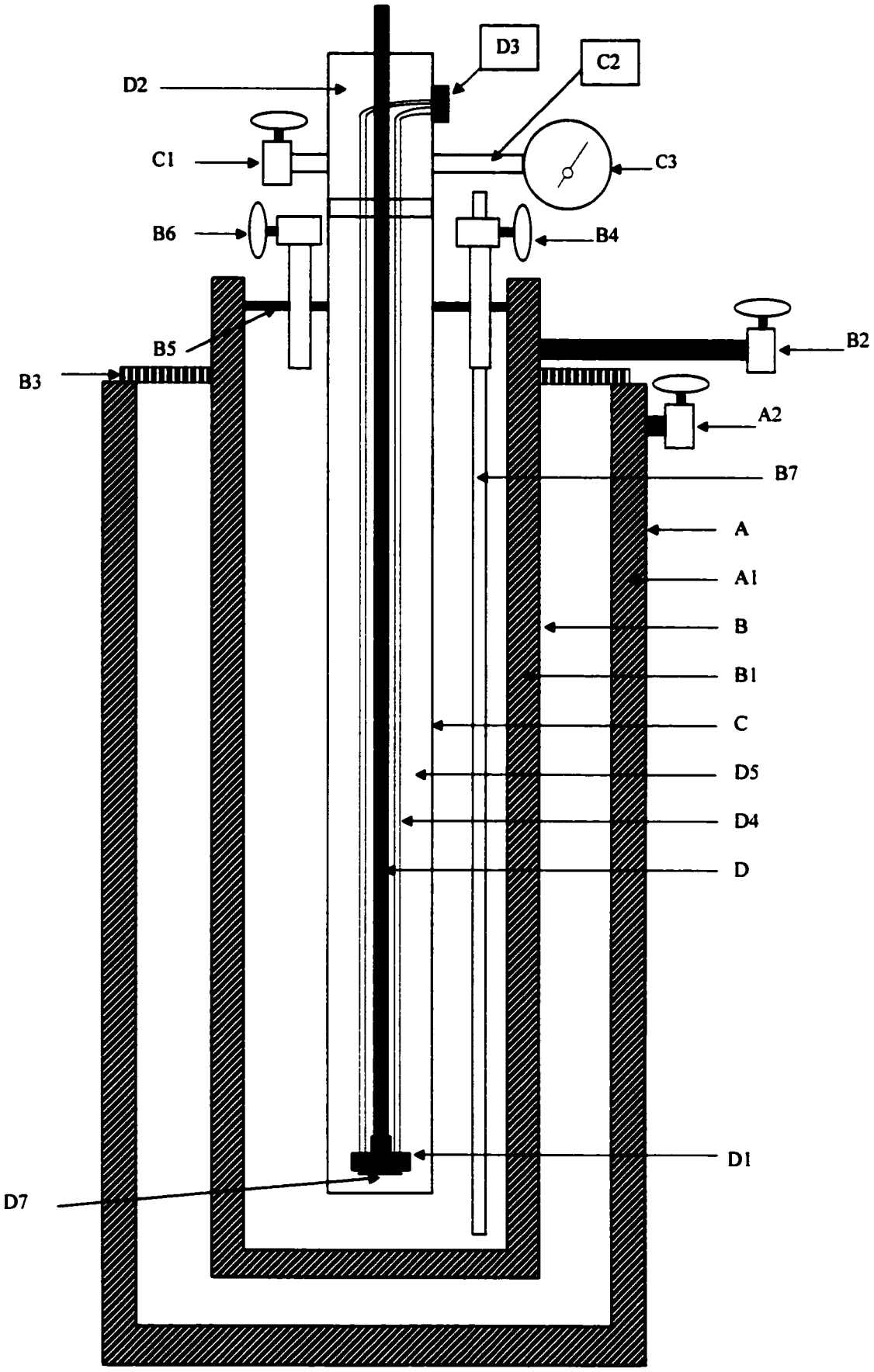

Fig.(3-3) The block diagram of the cryostat.

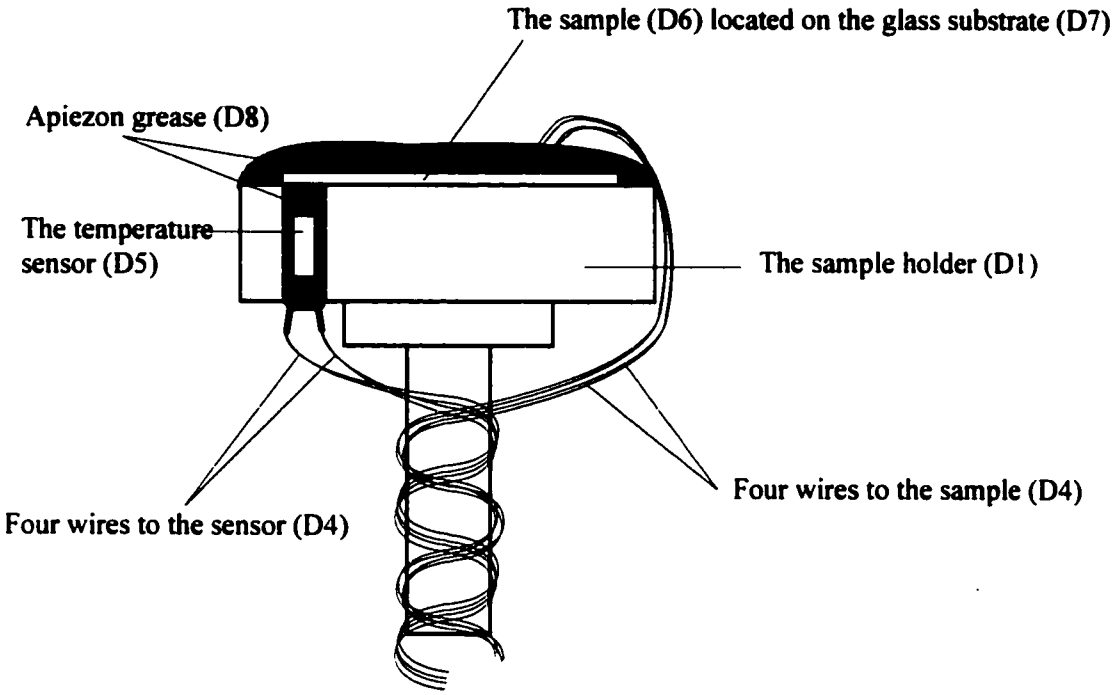

Fig. (3-4) The block diagram of the electronic system

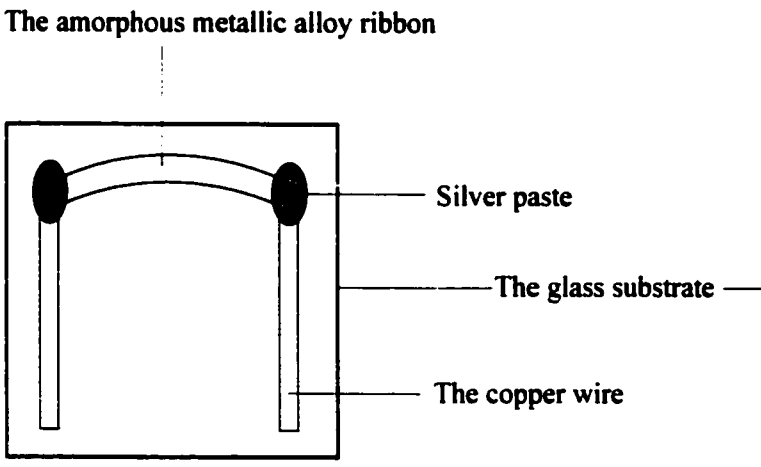

Fig. (3-5) The amorphous metallic alloy sample

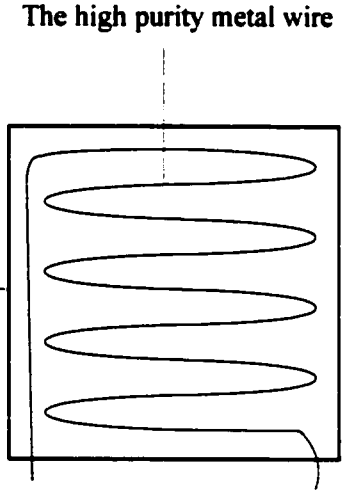

Fig. (3-6) The pure metal sample

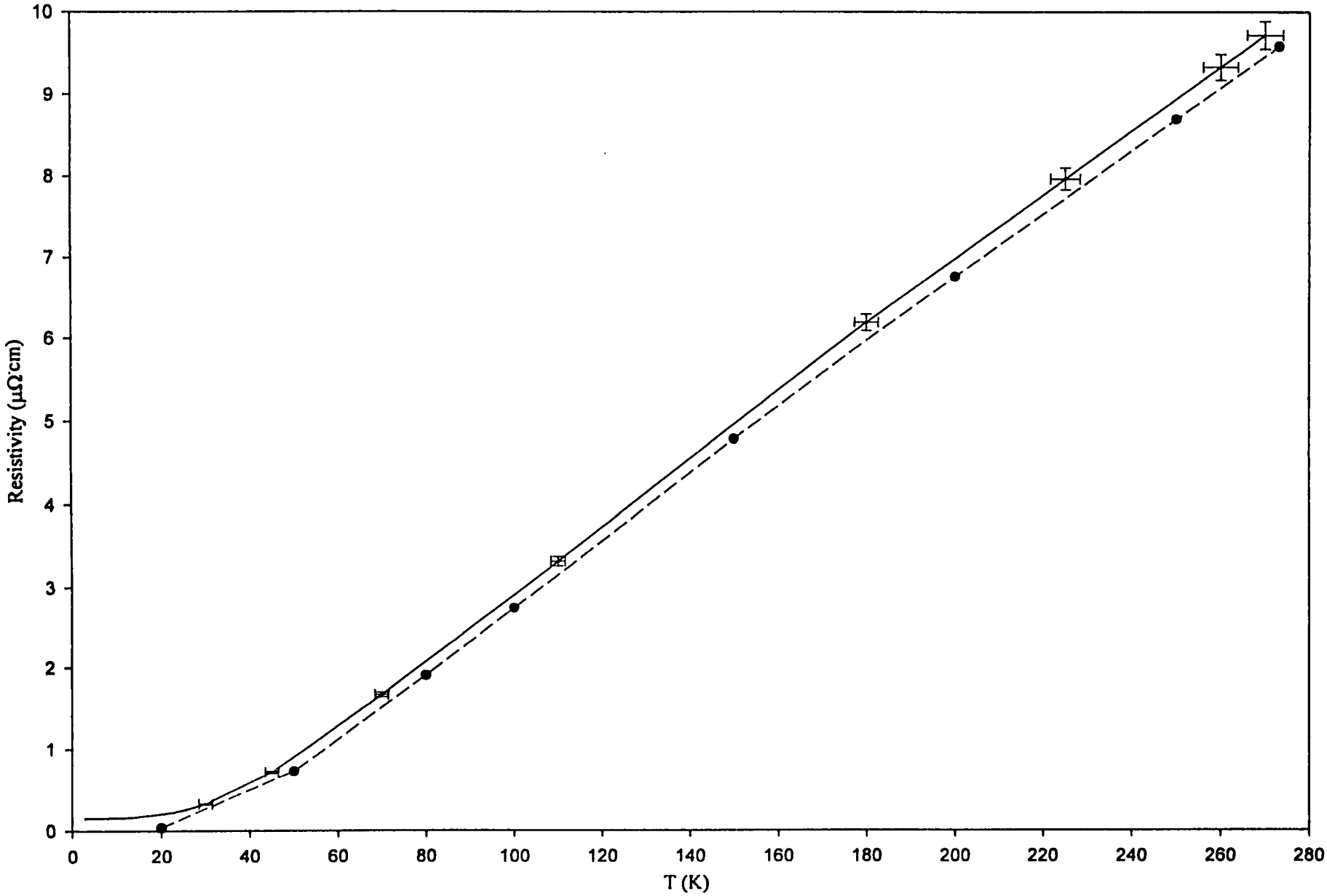

Fig. (3-6) The measured resistivity (solid line) of Pt and the published data (circles).

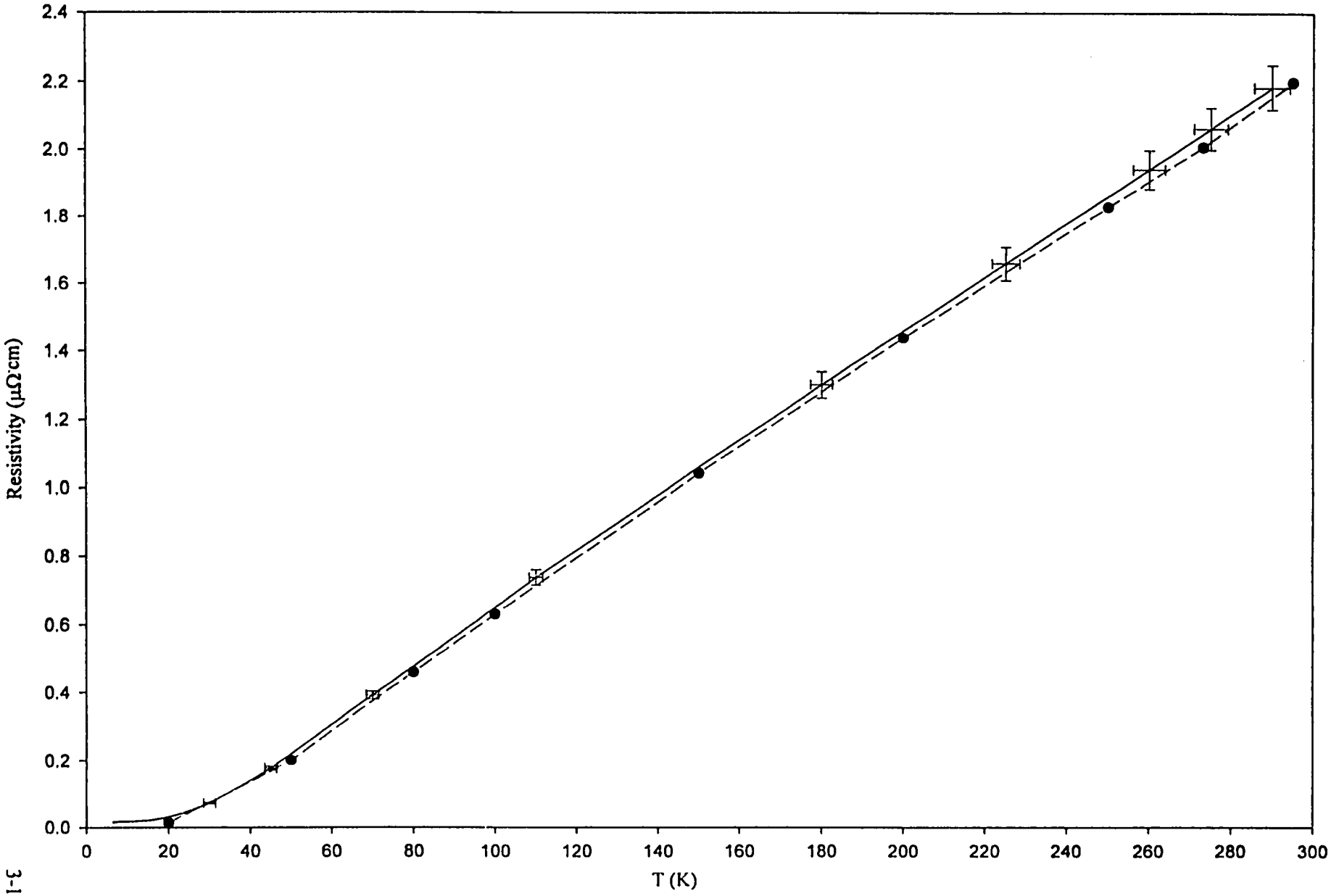

Fig. (3-7) The measured resistivity (solid line) of Au and the published data (circles).

4. Results and discussion

4.1) Introduction

In this chapter, we will discuss the temperature dependence of the electrical resistivity for the following three sets of samples: 1) two samples of pure crystalline metals, 2) seven samples of group I (C1–C7), and 3) four samples of group V (C8–C11). Table (4-1) shows the composition of each of these samples. All of the amorphous samples contained transition metals.

Electrical resistivity is an additive quantity. This means that we can have more than one contribution to the resistivity resulting from different and simultaneous scattering mechanisms. When fitting the experimental data to the theories, the sum of more than one equation is used.

The coefficient of determination, r^2, is the measure of how well the model describes the data. r^2 values near one indicate that the equation is a good description of the relation between the independent and dependent variables. The fits are non-linear least-squares fits based on the Marquardt-Levenberg Algorithm [42]. The r^2 is defined as

$$r^2 = 1 - \frac{\sum_{i=1}^{n} W_i (Y_i - y_i)^2}{\sum_{i=1}^{n} W_i (y_i - \bar{y})^2},$$

where Y_i is the theoretical y value at the ith point, y_i is the experimental y value at the ith point, $\bar{y}$ is the mean of y_i, and W_i is the weight corresponding to the ith point.

4.2) Temperature dependence of the electrical resistivity in pure crystalline metals.

4.2.1) T < 6 K

In this temperature range, the number of phonons will begin to vanish. The scattering of conduction electrons is caused by impurities and lattice defects and this process will eventually lead to the residual resistivity. The residual resistivity is an indication of the amount of impurities and defects present in the sample. Both of the pure metal samples have constant resistivity below 6 K. The value of ρ_0 is determined from the extrapolation of the resistivity data to T = 0 K [fig. (4-1)]. Table (4-2) gives the values of ρ_0 for Au and Pt metals.

4.2.2) T < Θ_D

At low temperatures, i.e., the temperatures lower than the Debye temperature, the two metal samples have a quadratic temperature dependence [eq. (2-3)]. The temperature range of fitting of the electrical resistivity data for platinum is wider than the range for gold. It is possible that this is related to the fact that Θ_D of platinum is higher than Θ_D of gold [2]. The quadratic dependence at low temperatures is a sign of the electron-electron scattering [2]. Figure (4-2) shows the fit of the electrical resistivity of platinum and gold to eq. (2-3) and the values of the fitted parameters are given in Table (4-2). The parameter d for Au in eq. (2-3) should be the value of the residual resistivity, however in this particular case it has no physical meaning because it has a negative value.

4.2.3) $T > \Theta_D$

At temperatures above Θ_D, the temperature dependence of the electrical resistivity of the two samples can be very well fitted with eq. (2-2) [fig. (4-3)]. This linear relationship is the result of the linear dependence of the number of phonons on temperature. Table (4-3) gives the values of the fitted parameters a and b.

4.3) Temperature dependence of electrical resistivity for samples of group I

4.3.1) Introduction

The samples in this group are ferromagnetic amorphous alloys and each of these samples contains both iron and nickel. Iron and nickel are both considered as monovalent metal atoms [10]. Figures (4-4)–(4-6) show the temperature dependence of the electrical resistivity over a wide range of temperatures for the samples of group I.

4.3.2) $T < 6$ K

All the samples in this group have a negative TCR at very low temperatures and a positive TCR at higher temperatures. This change of TCR leads to resistivity minima. The value of a sample's resistivity minimum is sensitive to its ferromagnetic metals composition. No specific relationship could be observed between the change of the composition and the resulting change of the resistivity

minimum. For example, the samples C4 and C5 have almost the same value of the resistivity minimum despite having different compositions.

The cause of the electrical resistivity minimum in the temperature dependence of the electrical resistivity of the amorphous metallic alloys is a controversial issue. Usually the data at very low temperatures can be fitted with eq. (2-24) [43-45] or the reciprocal of eq. (2-43) [30-35]. The first method of fitting can be interpreted as evidence for the existence of the Kondo effect [5,6,42]. However, the dependence of the electrical resistivity of the amorphous metallic alloys, in many cases, is not sensitive to an external magnetic field, which suggests that this phenomenon is not caused by the Kondo effect [5,46]. The second method is to fit the data of the electrical resistivity to $T^{-1/2}$ [eq. (2-43)] as a correction to the electrical resistivity predicted by the Ziman model. The fitting is made using the sum of the classical resistivity at very low temperatures [eq. (2-15)] and the quantum interference correction due to the EEI effect [the reciprocal of eq. (2-43)]. In eq. (2-15), the resistivity is due to the elastic scattering of electrons. In eq. (2-43), the resistivity is a result of the interaction between two electrons due to the multiple elastic scattering process. In this process the electrons move in diffusive motion rather than along a free classical trajectory with a diffusion coefficient D. The fits of the temperature dependence of the electrical resistivity to the sum of eq. (2-15) and the reciprocal of eq. (2-43) are shown in figs (4-7)–(4-9). The diffusion coefficient can be determined from the value of the parameter b, which is the reciprocal of the coefficient of $T^{-1/2}$ in eq. (2-43), and assuming $F_\sigma = 0$ [33] [Table (4-4)].

As the temperature increases from zero, the inelastic scattering starts to appear and this results in the destroying of the EEI. The extra contribution to the electrical resistivity decreases with the increase of temperature, thus resulting in a resistivity minimum. The EEI effects disappear completely at about 20 K. This is the reason why all the resistivity minima values exist at temperatures below 20

K. In all of the samples in this group, the data can be fitted more accurately using the EEI correction to the electrical resistivity than to the $\ln(T)$ dependence. However, the difference in the r^2 values corresponding to the fits is small and it is hard to relate the minima phenomena to one of the two scattering mechanisms without carrying out further magnetoresistance measurements. For example, for sample C4, the quality of the fit with the EEI and the $\ln(T)$ dependencies is almost the same [Table (4-4)].

4.3.3) $T < \Theta_D$

All of the electrical resistivity data can be fitted well to the sum of two equations, i.e., the quadratic dependence predicted by the Ziman model and the quantum interference correction, WL [eq. (2-16) and the reciprocal of eq. (2-40)]. The T^2 dependence at low temperatures is the proof for the existence of phonon inelastic scattering of the conduction electrons. The data cannot be fitted accurately using the quadratic equation (2-16) unless a term T^1 [the reciprocal of eq. (2-40)] is added. The fits of the temperature dependence of the electrical resistivity to the sum of eq. (2-16) and the reciprocal of eq. (2-40) are shown in figs. (4-10)–(4-12). The corresponding fitted parameters are given in Table (4-5). The values of r^2 are very close to 1 [Table (4-5)] which indicates that the theoretical model accounts well for the data.

In the Ziman model, the electrical resistivity is the result of two opposite contributions from eq. (2-15) and eq. (2-16). The total contribution is $+T^2$ because the contribution of eq. (2-16) is two times larger than that of eq. (2-15) [5]. At low temperatures, there exists an elastic scattering which is sufficient to cause the WL effect. For example, in sample C1 at T = 11 K, the contribution from the WL correction is about three times more than the contribution from the phonon inelastic scattering. At

the end of the low temperature fitting range (T = 50 K) the contribution from the phonon inelastic scattering is about 2000 times larger than that due to the WL effect [Table (4-5)]. The WL effect eventually will completely disappear when the inelastic scattering is the dominant scattering mechanism.

4.3.4) $T > \Theta_D$

In the Evans' model for transition metals, the electrical resistivity dependence on temperature in the high-temperature range is considered to be linear. In the high-temperature range, all of the electrical resistivity data can be fitted to a linear relationship. However, the fits are not satisfactory. Equation (2-26) has a quadratic term added to the linear term and is used as a correction to the linear fit. Fitting the data using eq. (2-26) [figs. (4-13)–(4-16)] satisfactorily accounts for the temperature dependence of the electrical resistivity. The fitted parameters are given in Table (4-6).

The contribution to the electrical resistivity at high temperatures is a proof of a magnetic contribution from the ferromagnetic atoms [15,18,47]. All of the samples, except C1, have a small but significant magnetic contribution to the electrical resistivity. For example, for sample C7, the contribution to the electrical resistivity from the ferromagnetic atoms at T = 80 K is about 6% of the contribution from the phonon inelastic scattering. At the high temperature (T = 250 K), the percentage is about 16%. In fact, the percentage of the magnetic contribution divided by the structure contribution, ξ, is the same for C2 and C3. As we increase the amount of iron [fig. (4-17)], ξ increases rapidly, reaches the maximum value for sample C6 and then decreases sharply for sample C7. For sample C6, ξ is 140% at 200 K, which means that the magnetic contribution to the electrical resistivity is much larger than the structure contribution.

For the sample C1, the data can be fitted to Evans' model with a magnetic contribution using eq. (2-26) [fig (4-18)]. However, the coefficient of the quadratic term is extremely small [$\sim 10^{-13}\,K^{-2}$]. The data for the sample C1 can be fitted more accurately using eq. (2-36) which has a phonon-phonon correction instead of a magnetic correction to the Ziman model at high temperatures. Equation (2-36) is usually used to fit the electrical resistivity data of *sp* amorphous alloys. This suggests that, at high temperatures, C1 belongs to group V rather than group I, which means that C1 does not have magnetic contributions at this range of temperatures. However, it has been reported that nickel and iron atoms do carry magnetic moments for this specific alloy composition [48].

The Debye temperature can be determined in the Evans' model by using eq. (2-27) [Table (4-6)]. Equation (2-27) uses the parameters of the fit of the temperature dependence of the electrical resistivity data in the low temperature and the high temperature ranges to eq. (2-25) and eq. (2-26), respectively.

4.4) Temperature dependence of the electrical resistivity for samples of group V.

4.4.1) Introduction

The samples C8–C11 are aluminum-rich amorphous metallic alloys. The temperature dependence of the electrical resistivity can be described well by curve (a) of fig. (2-3). The Fermi level for this group lies completely in the *sp* band. All the samples in this group have a positive TCR with no minima. They have a quadratic temperature dependence at low temperatures and a linear one at higher temperatures [figs. (4-19) and (4-20)].

4.4.2) T < 6 K

For the samples C8–C11 the electrical resistivity data below 6 K can be fitted to the sum of eq. (2-16) and the reciprocal of eq. (2-40). This is an indication that there is a strong elastic scattering at low temperatures and therefore the WL correction to the total electrical resistivity is applied. The residual resistivities of all the samples are less than 150 μΩ·cm, except for the sample C9 for which the residual resistivity is about 163 μΩ·cm [Table (4-7)]. This suggests that the Mooij correlation does not apply to group V.

4.4.3) T < Θ_D

All the electrical resistivity data have the quadratic temperature dependence at low temperatures. The T^2 dependence is a sign of the inelastic phonon scattering. As mentioned in section 4.3.3, the elastic scattering and the inelastic scattering exist simultaneously. As a result, the data cannot be fitted accurately using the T^2 dependence only. The T^{-1} WL effect correction must be introduced to achieve satisfactory fits [figs. (4-21) and (4-22)]. The WL contribution is an evidence for the multiple elastic scattering in these samples at low temperatures. The range of the above fitting can include the very low temperatures below 6 K [Table (4-7)], however, the r^2 values are more close to 1 in the low temperature range. The corresponding fitted parameters are given in Table (4-8).

4.4.4) T > Θ_D

According to the Ziman model, the temperature dependence of the electrical resistivity can be fitted to a linear relationship at high temperatures. However, the fittings are not satisfactory because the electrical resistivity values at high temperatures seem to deviate from the linear relationship. Both the Evans' model and the generalized Faber-Ziman model added a quadratic correction term to the

temperature dependence of the electrical resistivity. The Evans' model quadratic term is a positive T^2 contribution to compensate for the magnetic contribution to the electrical resistivity. In the generalized Faber-Ziman model the quadratic term is a negative T^2 contribution to account for the multiphonon scattering. The temperature dependence of the electrical resistivity can be fitted to both models. However, the values of the quadratic coefficient should have a physical meaning in order to judge what type of correction to consider at different temperature ranges.

In the samples C8–C11 of group V, the data can be fitted well to eq. (2-36) in the range between approximately 50 K and room temperature [figs. (4-23) and (4-24)]. The corresponding fitted parameters are given in Table (4-9). In the high-temperature range, the application of eq. (2-36) indicates that the Fermi level of the samples C8–C11 lies completely in the *sp* band [11,39]. The α parameter was found to be always bigger than the β parameter. This leads to a positive linear slope. The quadratic slope is always negative by definition. The fact that α is always bigger than β implies that the inelastic single-phonon scattering gives more contribution to the electrical resistivity than the multiphonon scattering contribution. The β parameters in the samples of group V have the values in the range $(3.66–4.61)\times10^{-4}$ K^{-1} [Table (4-9)], which are in agreement with the β values of Ag-Cu-Ge amorphous metallic alloy [40].

The Debye temperature can be determined by fitting the data with eq. (2-26). The fitted parameters are given in Table (4-10). The parameter of the quadratic term at high temperatures gives the value of the magnetic contribution to the electrical resistivity. For the samples C8–C11, the magnetic atom is iron. The samples C9 and C11 do not have any magnetic contribution from the iron atoms at high temperatures. However, the samples C8 and C10 do have a small but significant magnetic contribution [fig. (4-25)]. For example, the ξ values at 230 K for the samples C8 and C10 are about 12% and 25%, respectively.

Table (4-1) The composition of the samples and the corresponding groups.

Sample	Composition	Group
C1	$(Fe_{0.1}Ni_{0.9})_{77}Si_{10}B_{13}$	I
C2	$(Fe_{0.2}Ni_{0.8})_{77}Si_{10}B_{13}$	I
C3	$(Fe_{0.3}Ni_{0.7})_{77}Si_{10}B_{13}$	I
C4	$(Fe_{0.4}Ni_{0.6})_{77}Si_{10}B_{13}$	I
C5	$(Fe_{0.5}Ni_{0.5})_{77}Si_{10}B_{13}$	I
C6	$(Fe_{0.6}Ni_{0.4})_{77}Si_{10}B_{13}$	I
C7	$(Fe_{0.7}Ni_{0.3})_{77}Si_{10}B_{13}$	I
C8	$Al_{90}Fe_5Ce_5$	IV
C9	$Al_{87}Fe_{6.7}Ce_{6.3}$	IV
C10	$Al_{87}Fe_{9.3}Ce_{3.7}$	IV
C11	$Al_{87}Fe_{8.7}Ce_{4.3}$	IV
C12	Au	99.998% pure metal
C13	Pt	99.998% pure metal

Table (4-2) The parameters from the fits with eq. (2-3) of the temperature dependence of the electrical resistivity of Au and Pt and the corresponding coefficient of determination r^2. ρ_0 is the residual resistivity.

Metal	ρ_0 ($\mu\Omega$·cm)	T range (K)	d ($\mu\Omega$·cm)	c (K^{-2})	r^2
Au	0.0136	28–49	-0.014	8.47×10^{-5}	0.9999
Pt	0.1456	29–60	0.003	3.48×10^{-4}	0.9998

Table (4-3) The parameters from the fits with eq. (2-2) of the temperature dependence of the electrical resistivity of Au and Pt and the corresponding coefficient of determination r^2.

Metal	Θ_D (K)	T range (K)	a ($\mu\Omega$·cm)	b (K^{-1})	r^2
Au	165	165–290	-0.18	7.99×10^{-3}	0.999997
Pt	240	240–280	-0.76	3.97×10^{-3}	0.99999

Table (4-4) The parameters from the fits with eq. (2-24) and the reciprocal of eq. (2-43) [b is the reciprocal of the coefficient of $T^{-1/2}$ in eq. (2-43)] of the temperature dependence of the electrical resistivity of samples C1–C7 and the corresponding coefficient of determination r^2.

sample	T range (K)	α	r^2	b ($K^{1/2}$)	D (cm^2/s)	r^2
C1	1.7–6	-0.1349	0.9870	0.2991	1.34×10^{-12}	0.9920
C2	1.9–6	-0.0465	0.9890	0.1703	4.33×10^{-13}	0.9928
C4	1.9–6	-0.0752	0.9928	0.1989	5.91×10^{-13}	0.9936
C5	1.8–6	-0.0935	0.9786	0.2282	7.77×10^{-13}	0.9803
C6	1.8–6	-0.0718	0.9733	0.1301	2.53×10^{-13}	0.9779
C7	1.7–6	-0.0488	0.9528	0.0729	7.93×10^{-14}	0.9736

Table (4-5) The parameters from the fits with eq. (2-16) and the reciprocal of eq. (2-40) [e is the reciprocal of the coefficient of T^{-1} in eq. (2-40)] of the temperature dependence of the electrical resistivity of samples C1–C7 and the corresponding coefficient of determination r^2.

Sample	T range (K)	a (K^{-2})	e (K)	r^2
C1	11–50	1.67×10^{-5}	9.64	0.9998
C2	9–49	9.30×10^{-6}	1.84	0.9999
C4	14–50	6.42×10^{-6}	6.78	0.9995
C5	16–53	8.19×10^{-6}	11.29	0.9996
C7	17–44	2.12×10^{-6}	4.06	0.9991

Table (4-6) The parameters from the fits with eq. (2-25) and eq. (2-26) of the temperature dependence of the electrical resistivity of samples C1–C7 and the corresponding coefficient of determination r^2. The Debye temperature is calculated using eq. (2-27).

Sample	T range (K)	β (K^{-2})	γ_1 (K^{-1})	γ (K^{-2})	Θ_D (K)	r^2
C1	115–280	2.11×10^{-3}	0.136	2.26×10^{-13}	106	0.9999
C2	58–220	1.03×10^{-3}	0.094	3.26×10^{-5}	155	0.99996
C3	60–220	1.29×10^{-3}	0.133	4.70×10^{-5}	177	0.9997
C4	50–200	1.03×10^{-3}	0.070	1.48×10^{-4}	129	0.9999
C5	55–200	1.51×10^{-3}	0.086	3.04×10^{-4}	118	0.9992
C6	75–220	-	0.009	6.66×10^{-5}	-	0.9996

C7	80–250	2.69×10^{-4}	0.036	2.56×10^{-5}	243	0.9999

Table (4-7) The parameters from the fits with eq. (2-16) and the reciprocal of eq. (2-40) [b is the reciprocal of the coefficient of T^{-1} in eq. (2-40)] of the temperature dependence of the electrical resistivity of samples C8–C11 and the corresponding coefficient of determination r^2.

Sample	T range (K)	a (K^{-2})	b (K)	ρ_0 ($\mu\Omega$·cm)	r^2
C8	2–47	1.04×10^{-5}	0.475	91	0.9984
C9	1.7–55	6.78×10^{-6}	0.231	164	0.9988
C10	1.7–47	7.92×10^{-6}	0.333	131	0.9988
C11	1.4–49	8.53×10^{-6}	0.093	97	0.9995

Table (4-8) The parameters from the fits with eq. (2-16) and the reciprocal of eq. (2-40) [b is the reciprocal of the coefficient of T^{-1} in eq. (2-40)] of the temperature dependence of the electrical resistivity of samples C8–C11 and the corresponding coefficient of determination r^2.

Sample	T range (K)	a (K^{-2})	b (K)	r^2
C8	11–47	1.11×10^{-5}	2.583	0.9999
C9	14–55	7.28×10^{-6}	4.254	0.9999
C10	9–47	8.33×10^{-6}	1.824	0.9999
C11	8–45	8.91×10^{-6}	0.864	0.9997

Table (4-9) The parameters from the fits with eq. (2-36) of the temperature dependence of the electrical resistivity of samples C1 and C8–C11 and the corresponding coefficient of determination r^2.

Sample	T range (K)	α (K^{-1})	β (K^{-1})	r^2
C1	115–280	0.16	1.44×10^{-4}	0.99996
C8	54–260	0.12	4.61×10^{-4}	0.9999
C9	47–200	0.15	3.94×10^{-4}	0.9999
C10	48–230	0.22	4.05×10^{-4}	0.9999

C11	45–240	0.12	3.61×10^{-4}	0.99996

Table (4-10) The parameters from the fits with eq. (2-25) and eq. (2-26) of the temperature dependence of the electrical resistivity of samples C8–C11 and the corresponding coefficient of determination r^2. The Debye temperature is calculated using eq. (2-27).

Sample	T range (K)	β (K^{-2})	γ_1 (K^{-1})	γ (K^{-2})	r^2	Θ_D (K)
C8	170–260	1.01×10^{-3}	0.059	3.10×10^{-5}	0.9999	99
C9	170–200	1.19×10^{-3}	0.124	9.77×10^{-13}	0.9998	171
C10	170–230	1.09×10^{-3}	0.053	5.76×10^{-5}	0.99995	84
C11	160–240	8.67×10^{-4}	0.055	2.37×10^{-13}	0.9998	105

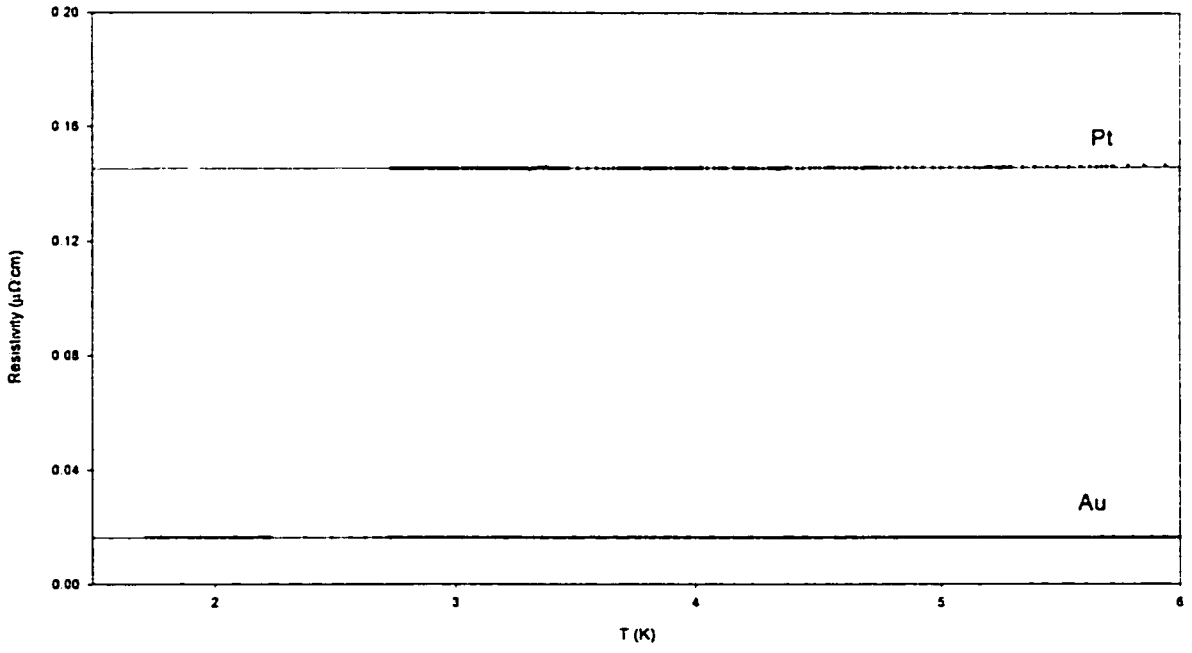

Fig. (4-1) Temperature dependence of the electrical resistivity of Pt and Au (circles) and the extrapolated line for the temperature range 1.7–6 K.

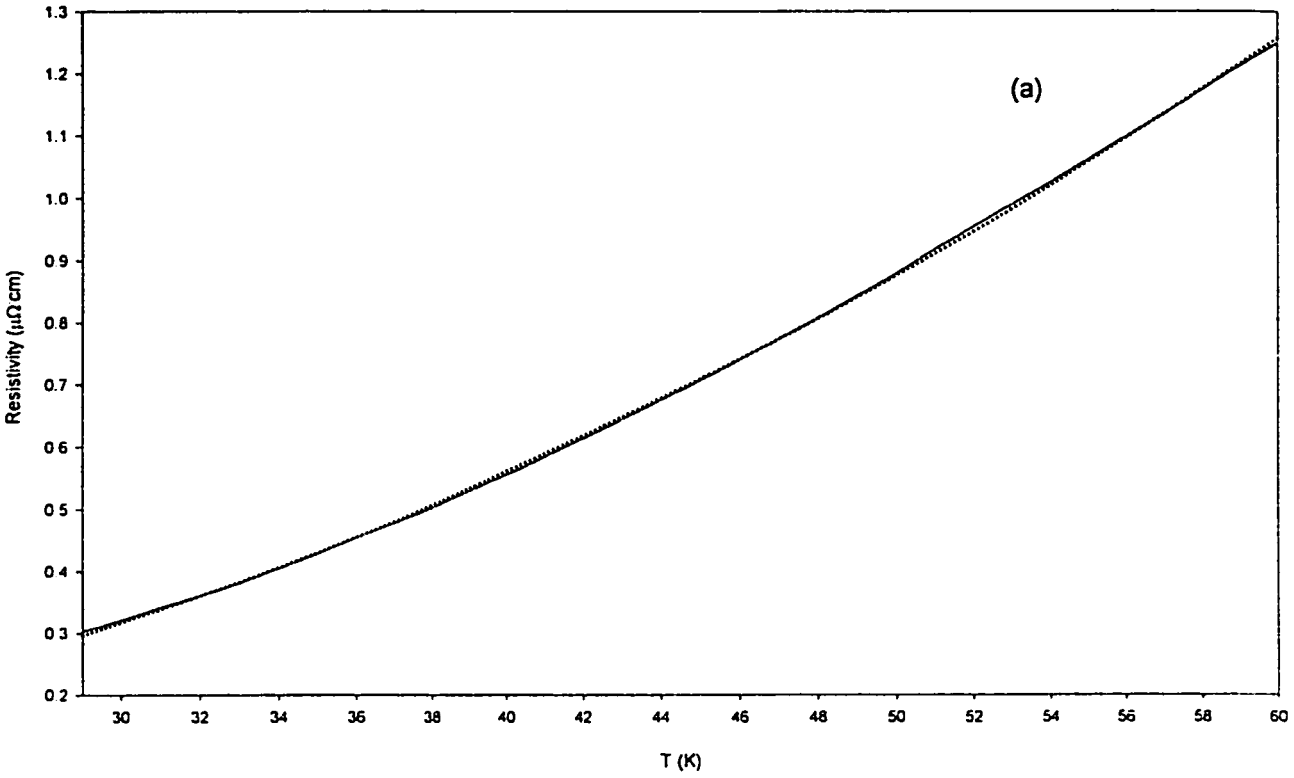

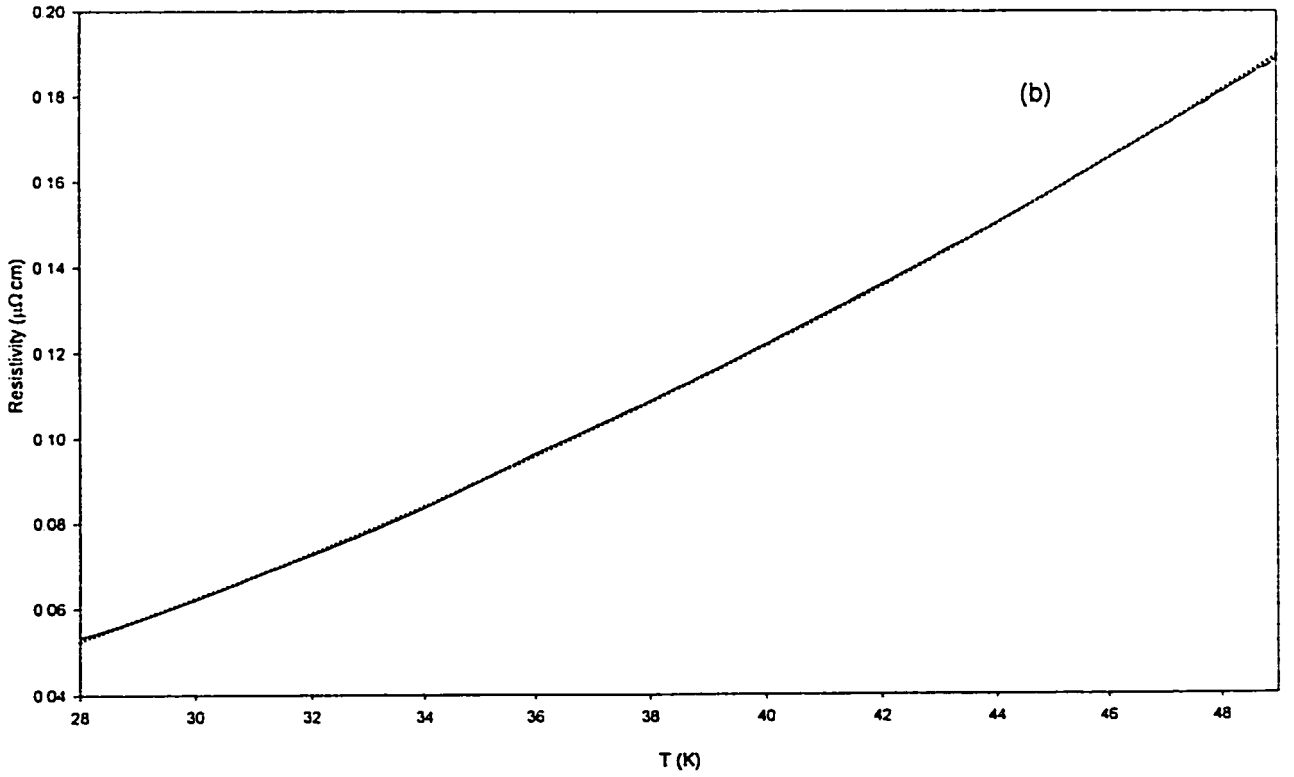

Fig. (4-2) The fit (triangles) of the temperature dependence of the electrical resistivity (solid line) of (a) Pt and (b) Au to eq. (2-3).

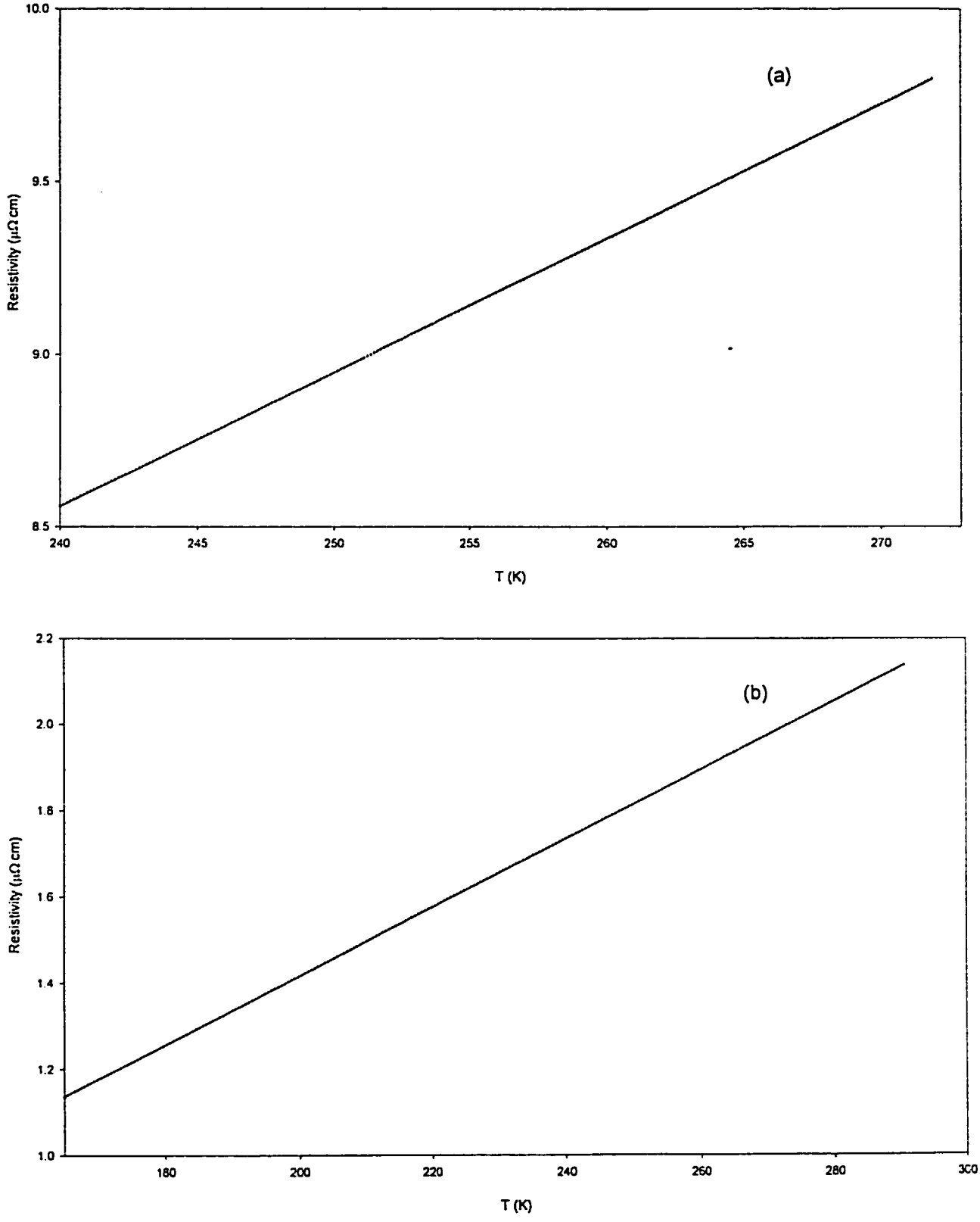

Fig. (4-3) The fit (triangles) of the temperature dependence of the electrical resistivity (solid line) of (a) Pt and (b) Au to eq. (2-2).

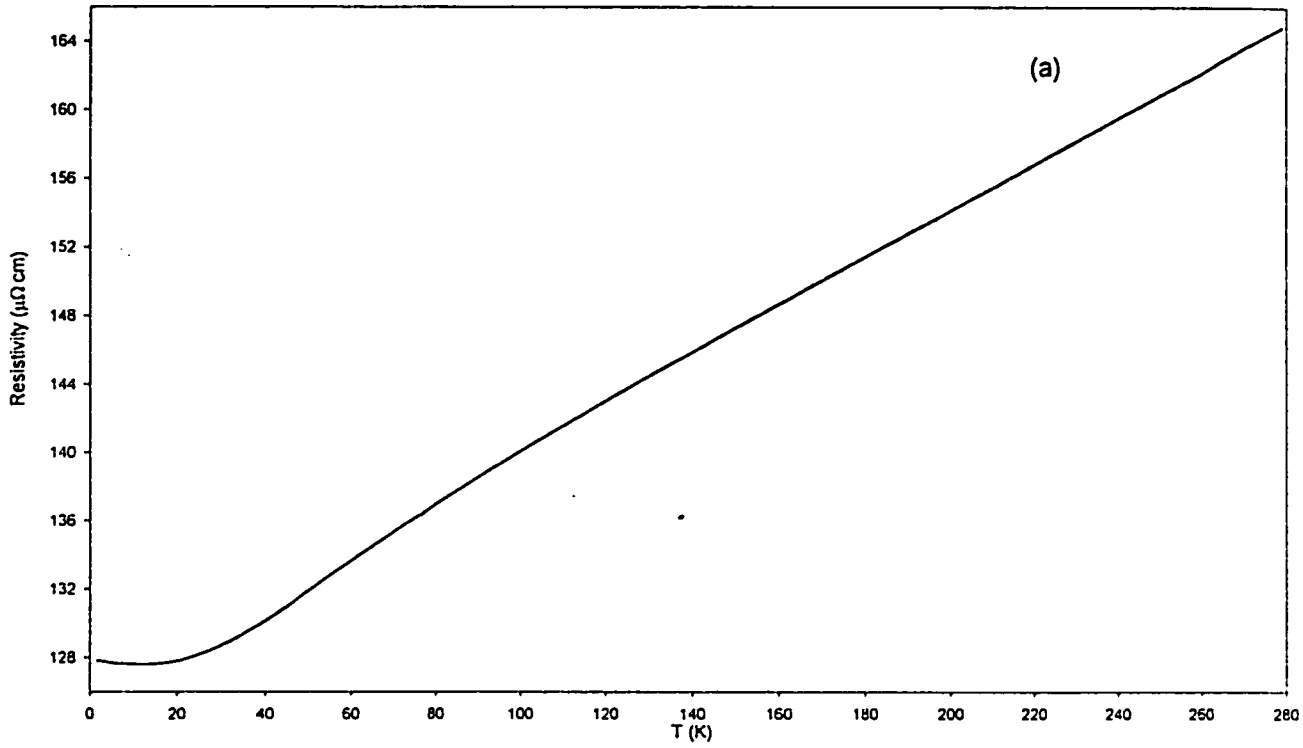

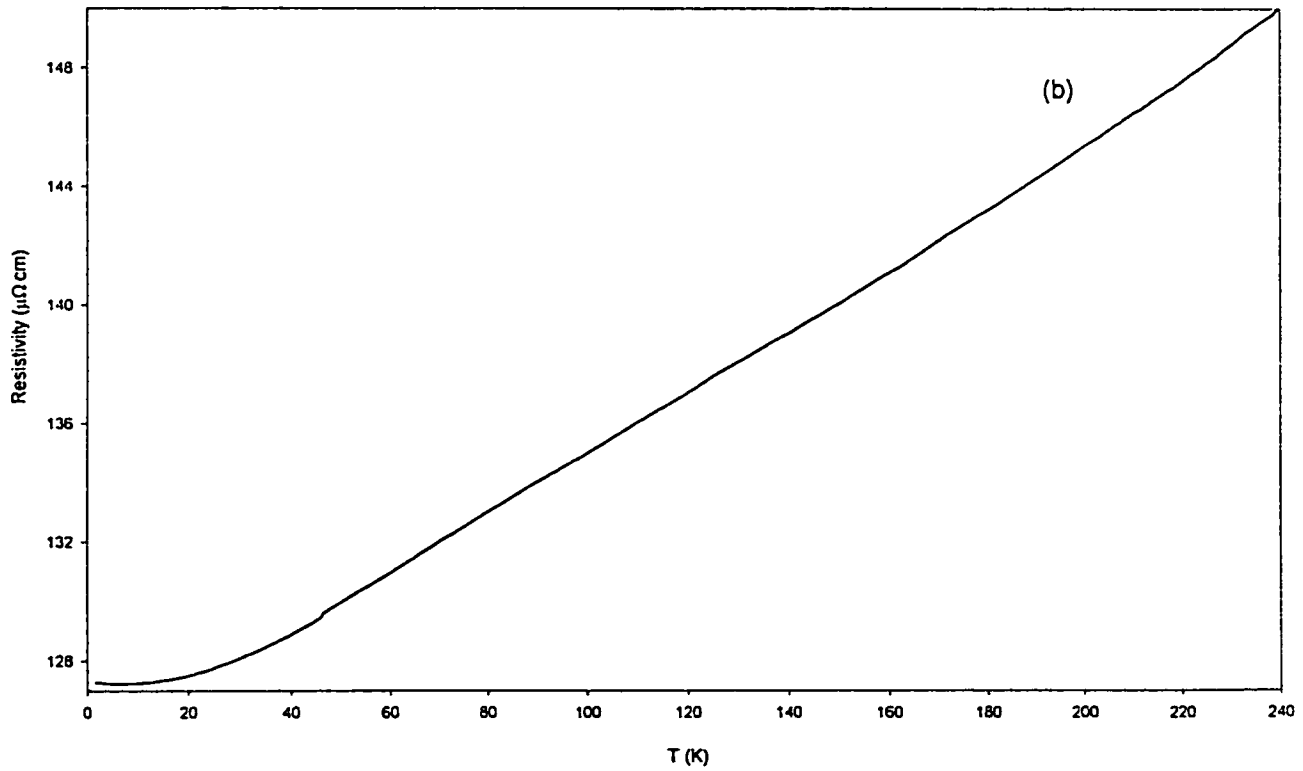

Fig. (4-4) The temperature dependence of the electrical resistivity for (a) sample C1 and (b) sample C2.

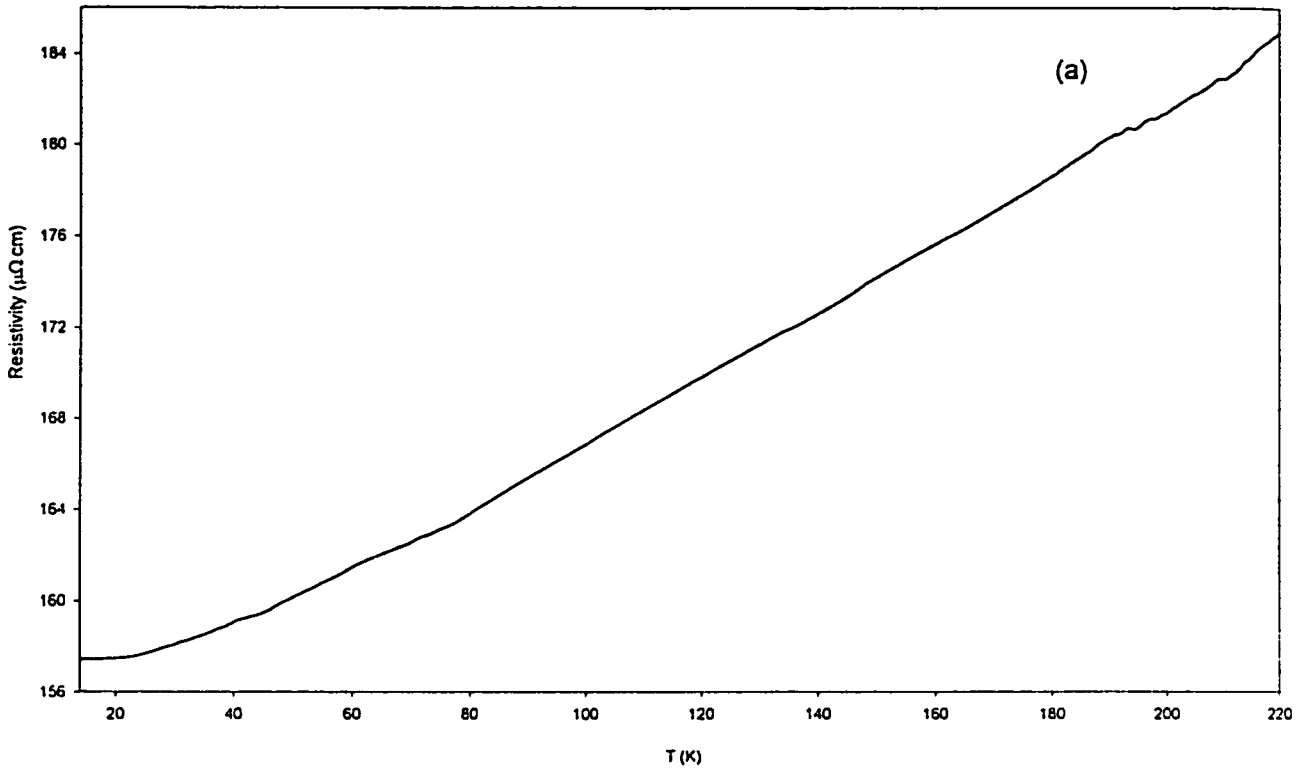

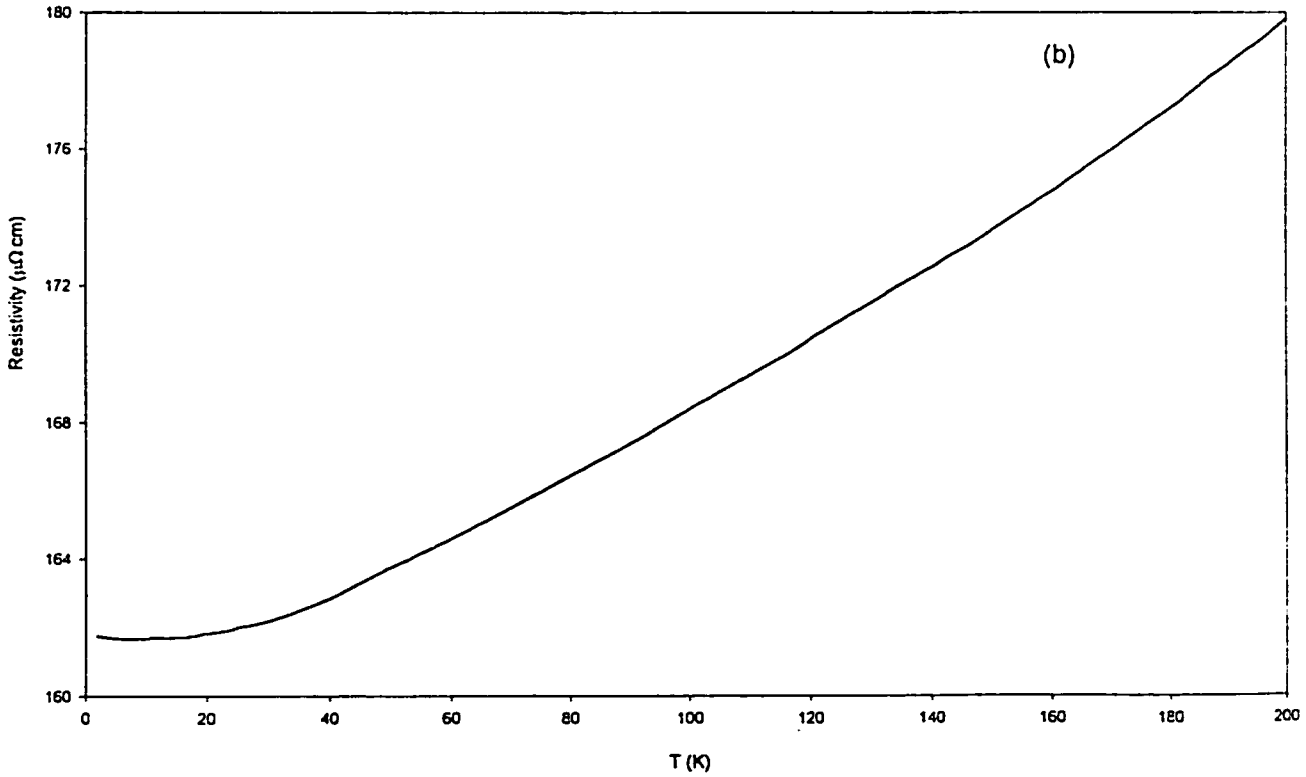

Fig. (4-5) The temperature dependence of the electrical resistivity for (a) sample C3 and (b) sample C4.

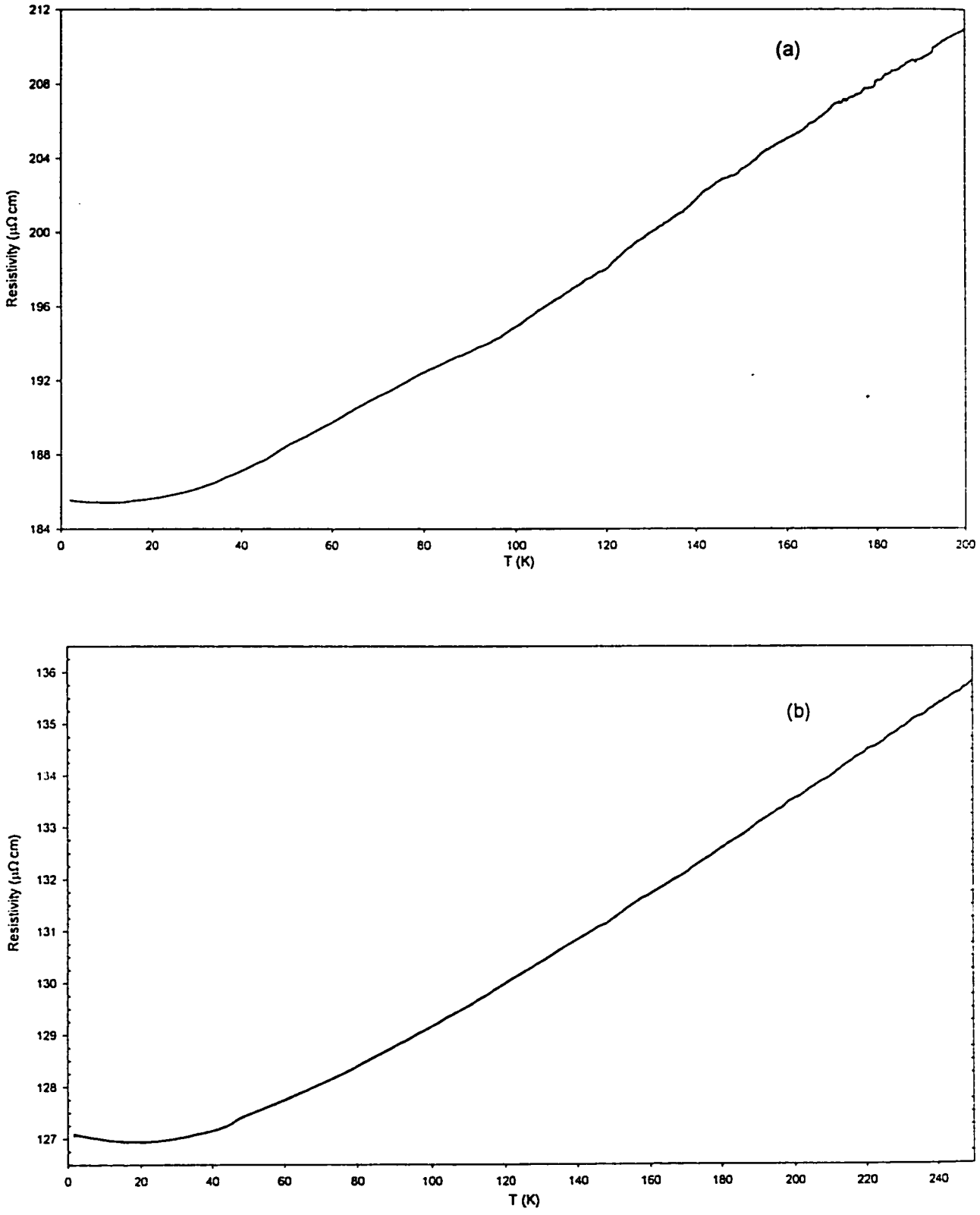

Fig. (4-6) The temperature dependence of the electrical resistivity for (a) sample C5 and (b) sample C7.

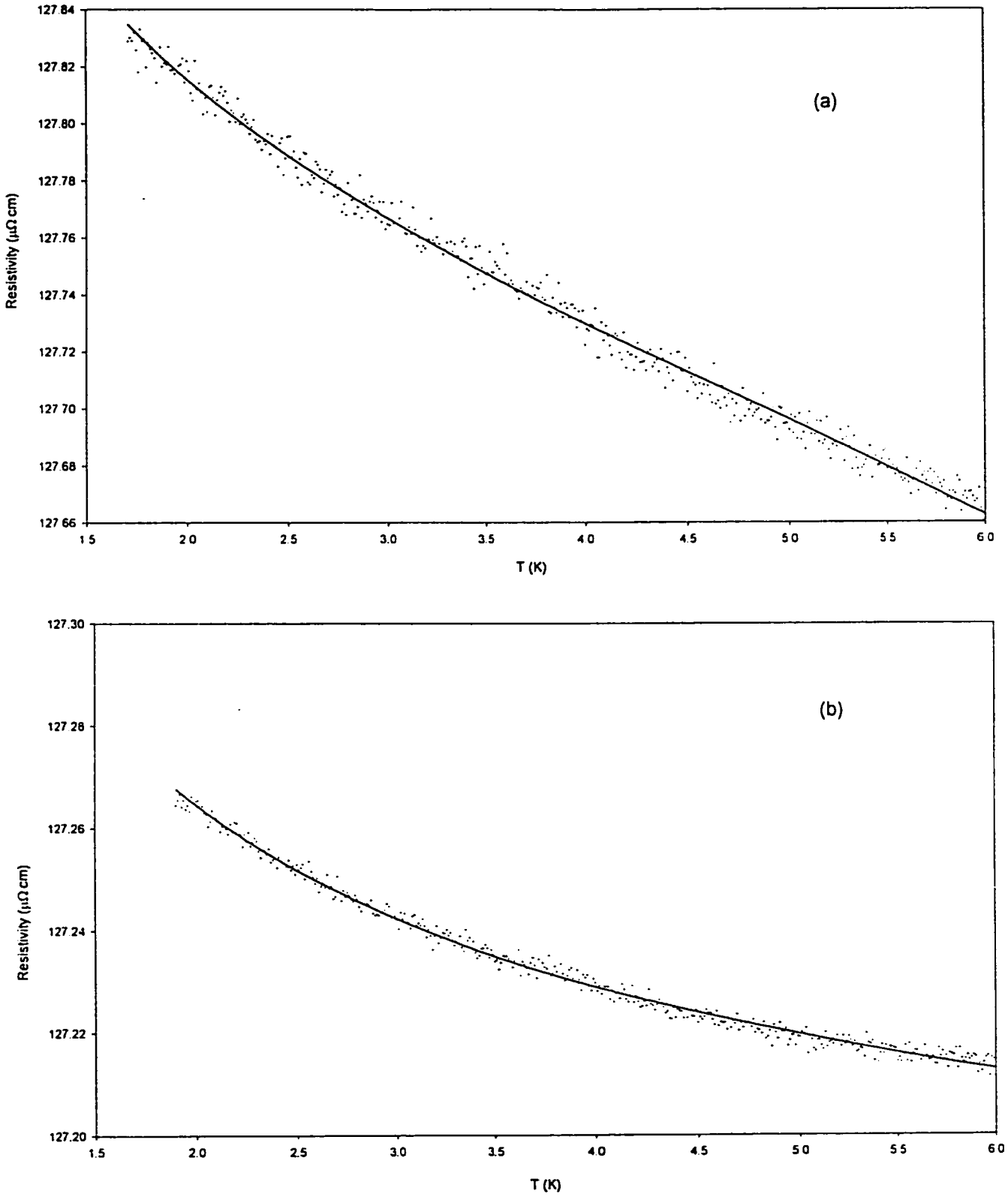

Fig. (4-7) The fit (solid line) of the temperature dependence of the electrical resistivity (dots) of (a) sample C1 and (b) sample C2 to the sum of eq. (2-15) and the reciprocal of eq. (2-43).

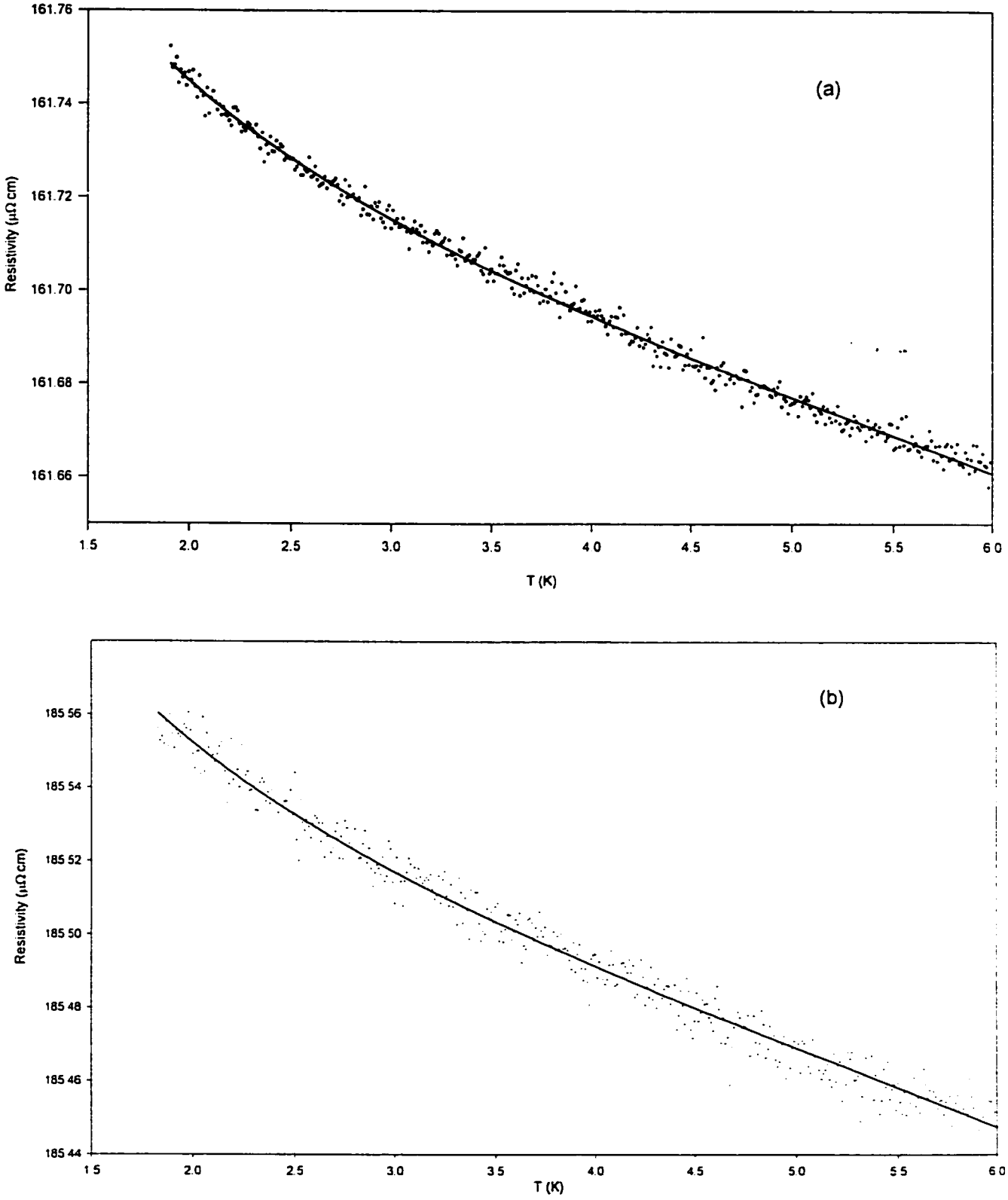

Fig. (4-8) The fit (solid line) of the temperature dependence of the electrical resistivity (dots) of (a) sample C4 and (b) sample C5 to the sum of eq. (2-15) and the reciprocal of eq. (2-43).

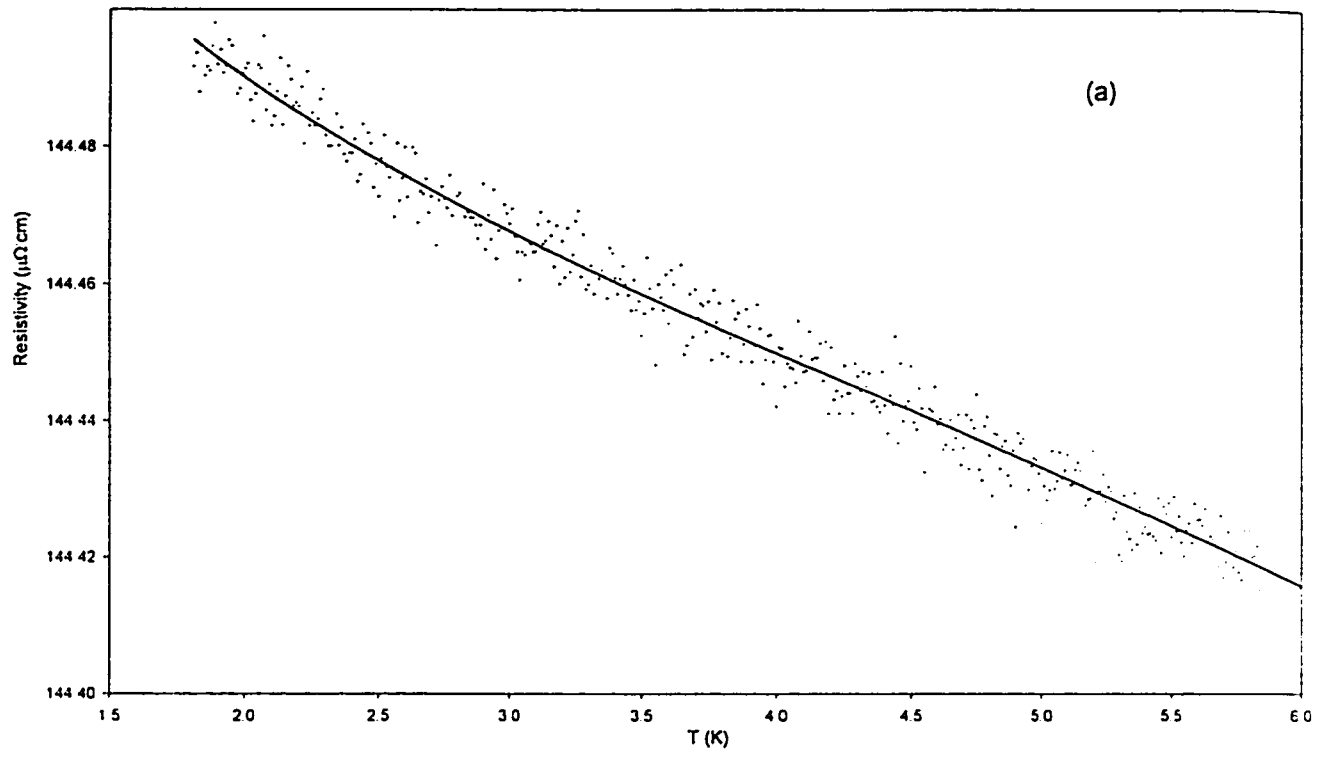

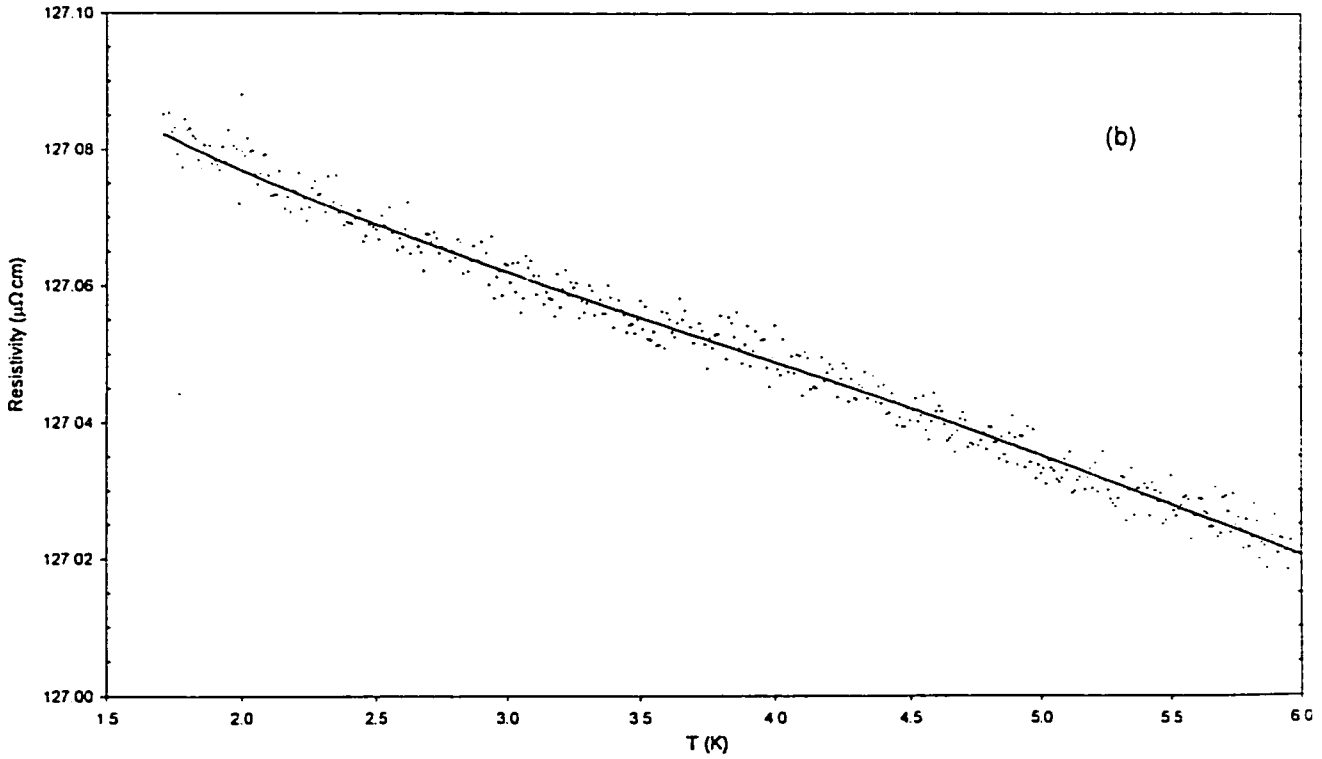

Fig. (4-9) The fit (solid line) of the temperature dependence of the electrical resistivity (dots) of (a) sample C6 and (b) sample C7 to the sum of eq. (2-15) and the reciprocal of eq. (2-43).

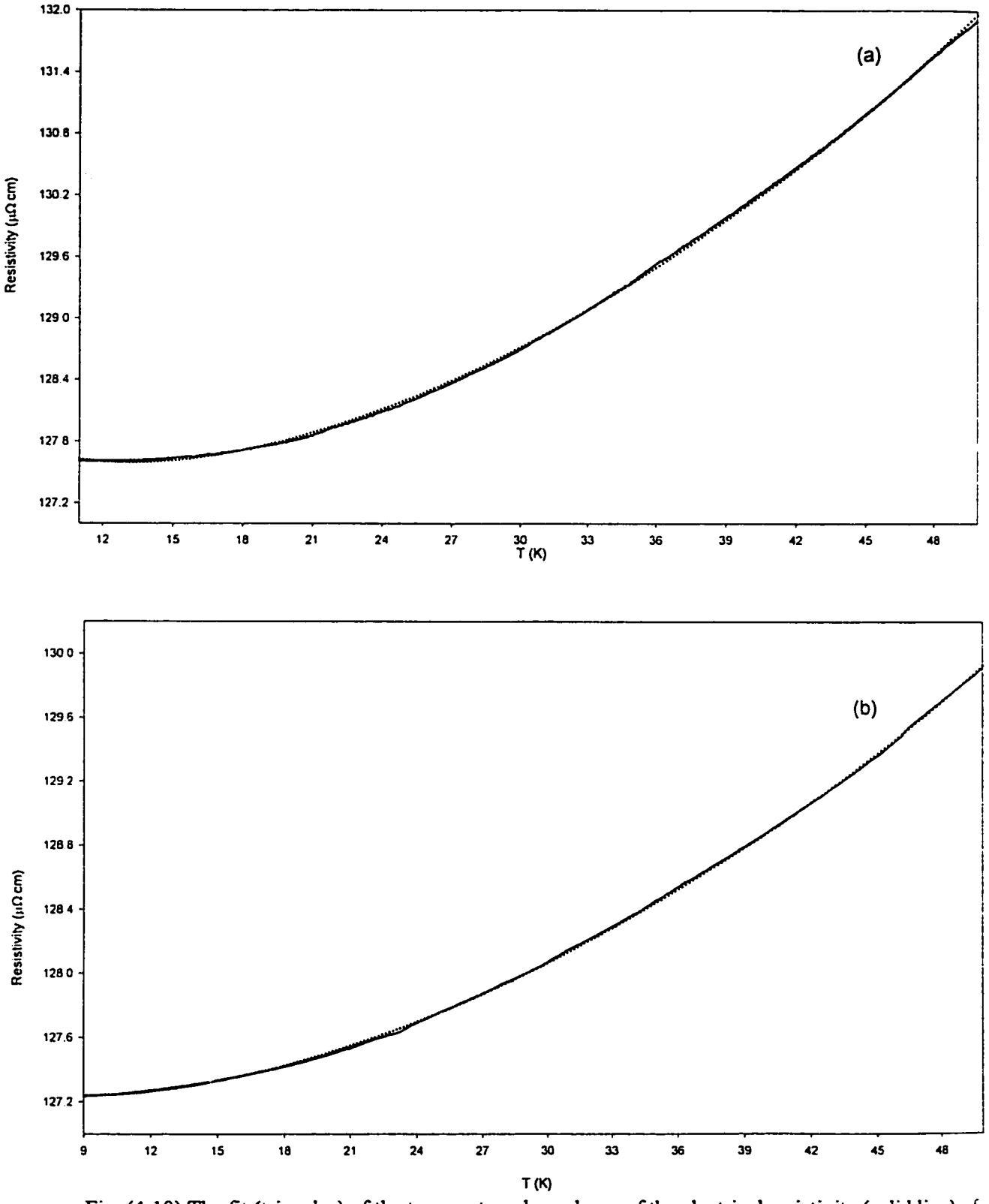

Fig. (4-10) The fit (triangles) of the temperature dependence of the electrical resistivity (solid line) of (a) sample C1 and (b) sample C2 to the sum of eq. (2-16) and the reciprocal of eq. (2-40).

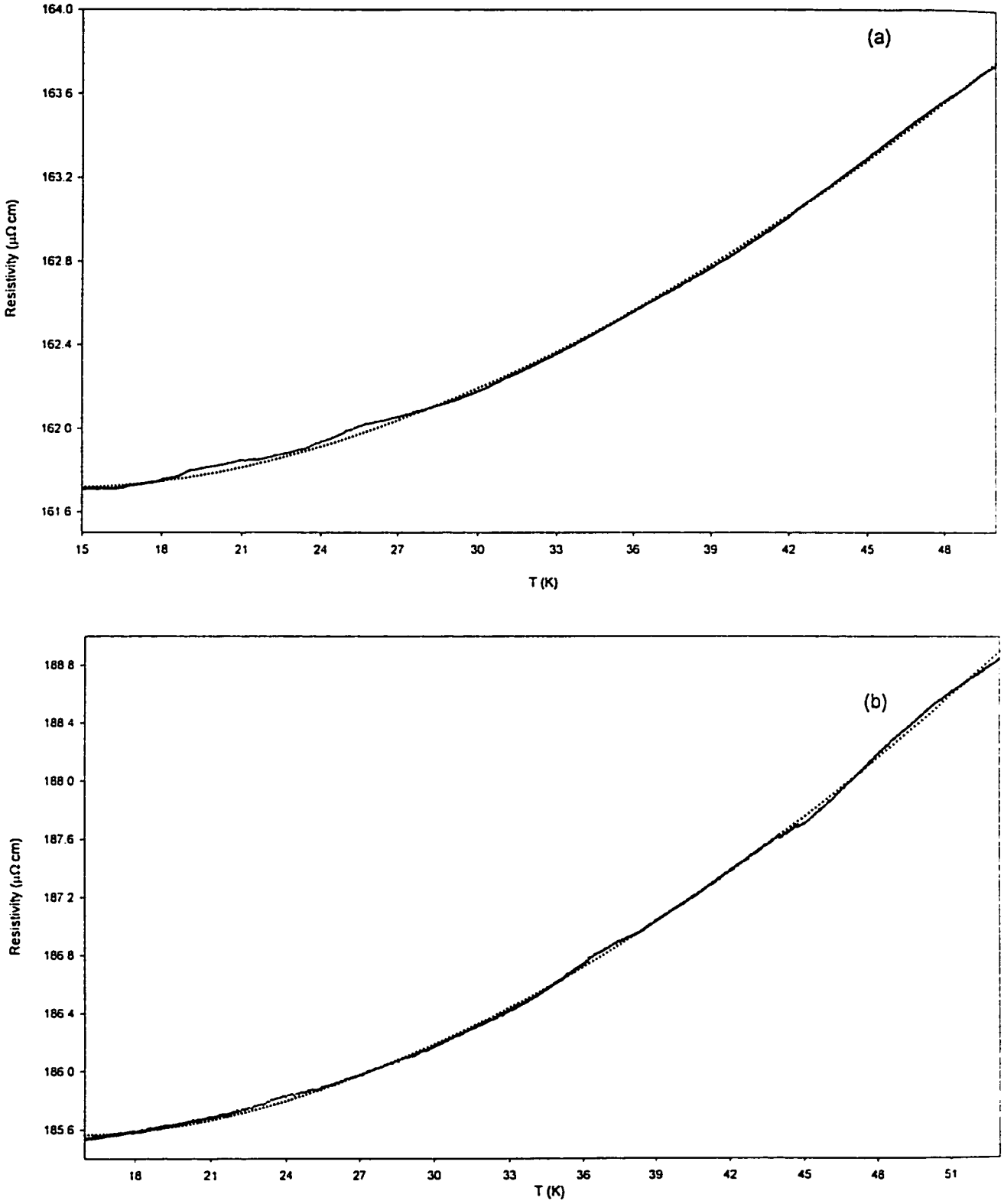

Fig. (4-11) The fit (triangles) of the temperature dependence of the electrical resistivity (solid line) of (a) sample C4 and (b) sample C5 to the sum of eq. (2-16) and the reciprocal of eq. (2-40).

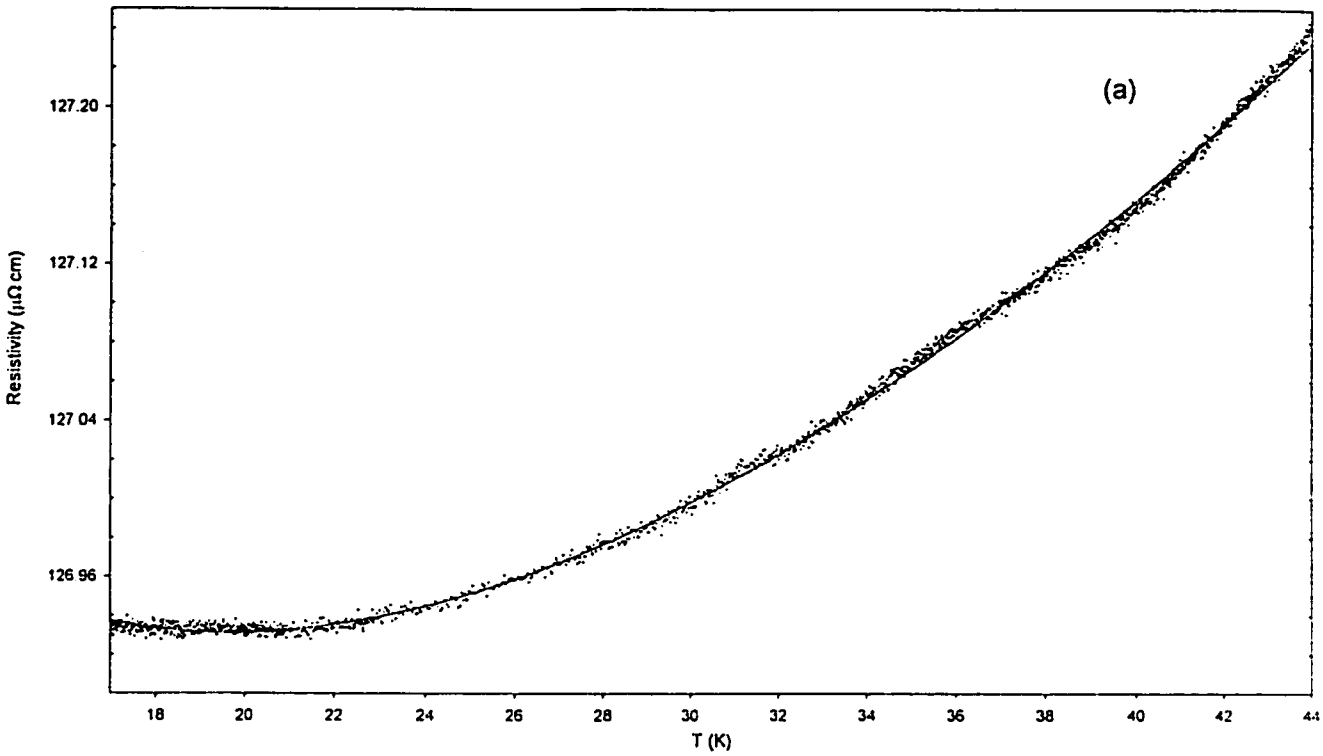

Fig. (4-12) The fit (solid line) of the temperature dependence of the electrical resistivity (dots) of sample C4 to the sum of eq. (2-16) and the reciprocal of eq. (2-40).

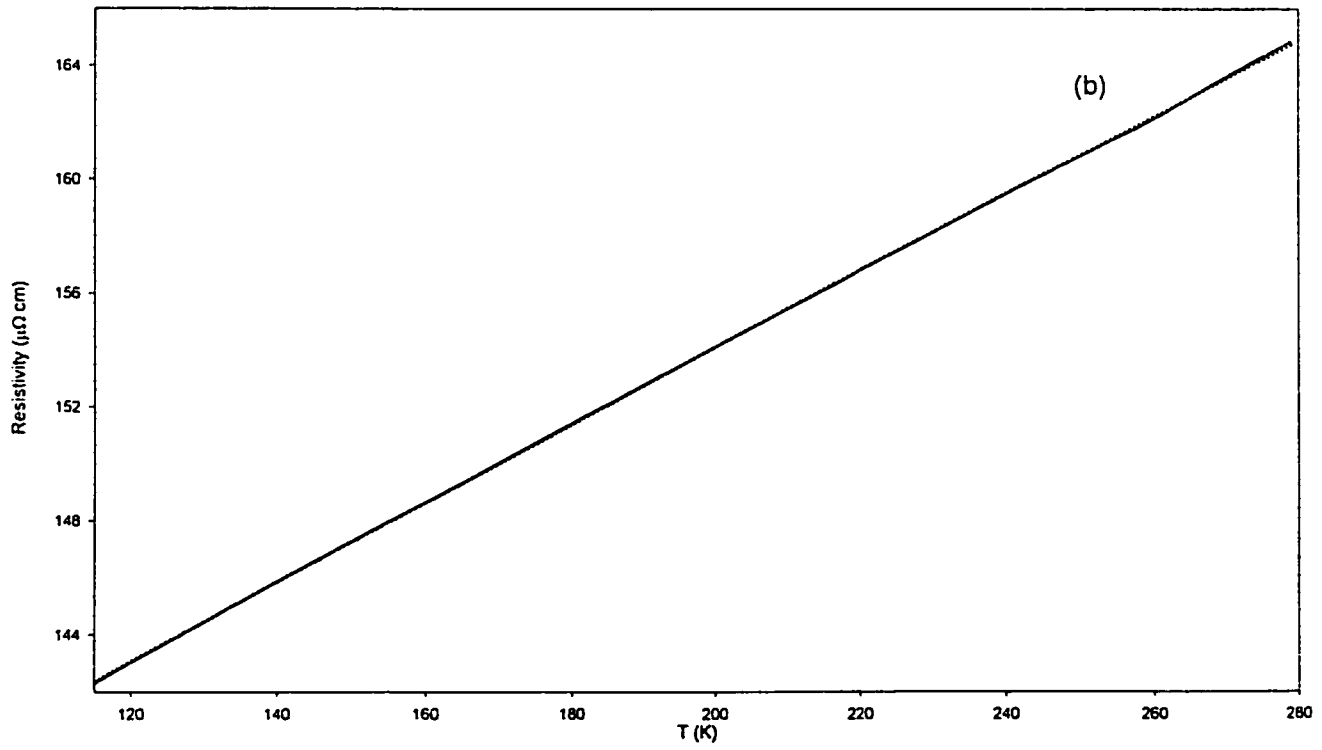

Fig. (4-13) The fit (triangles) of the temperature dependence of the electrical resistivity (solid line) of sample C1 to eq. (2-36).

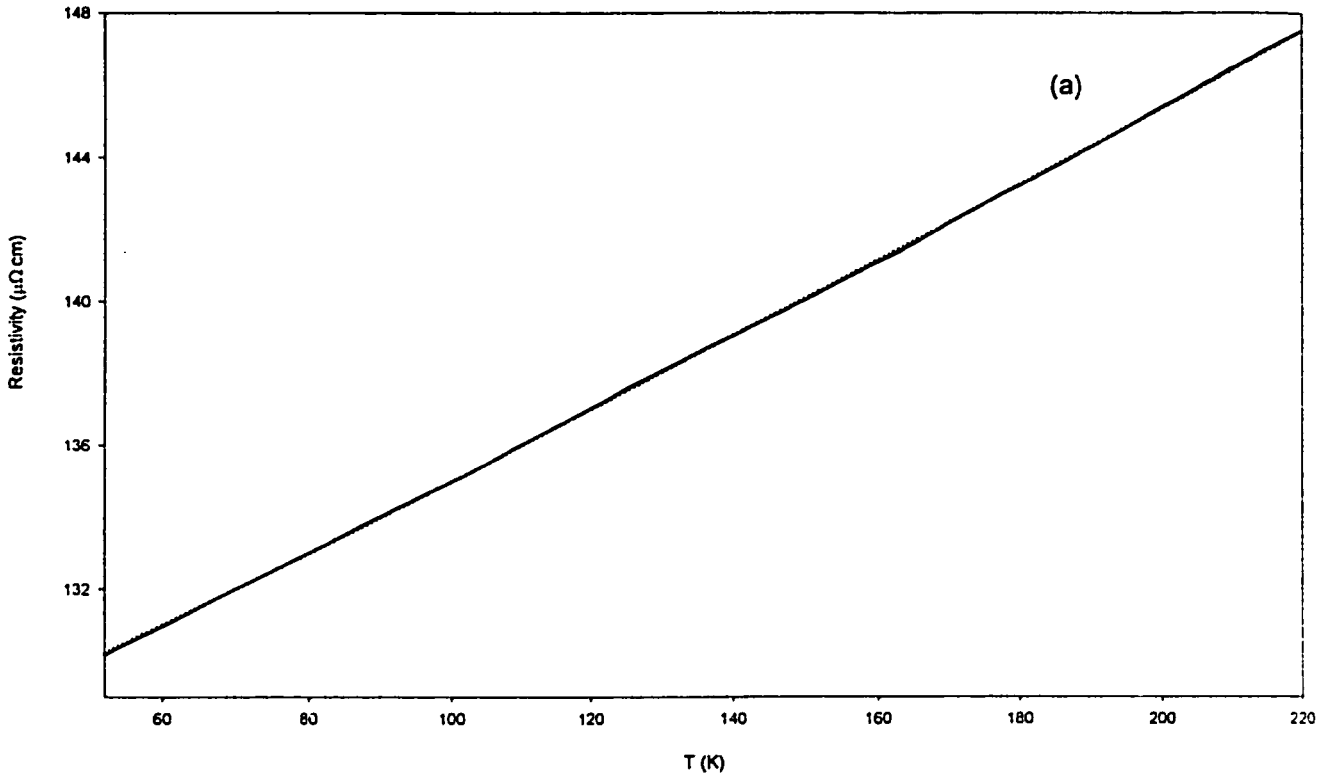

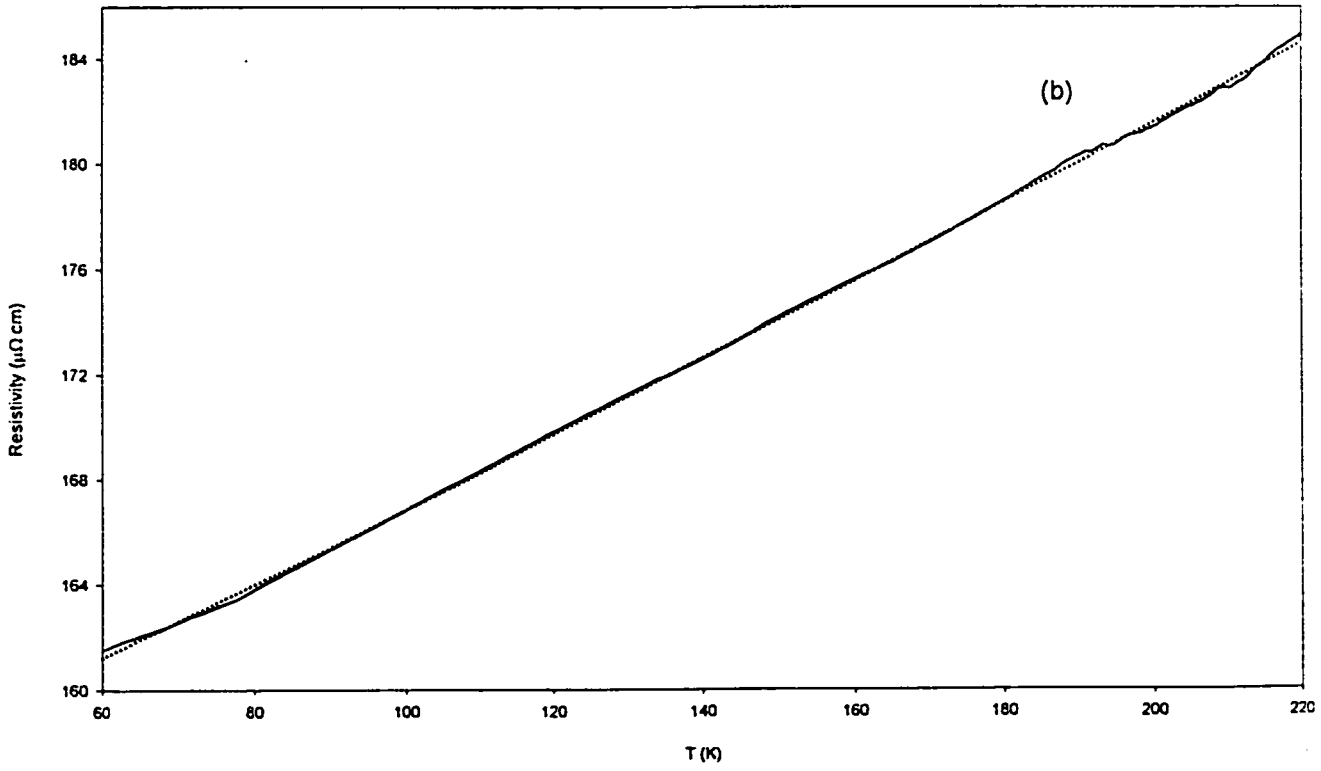

Fig. (4-14) The fit (triangles) of the temperature dependence of the electrical resistivity (solid line) of (a) sample C2 and (b) sample C3 to eq. (2-26).

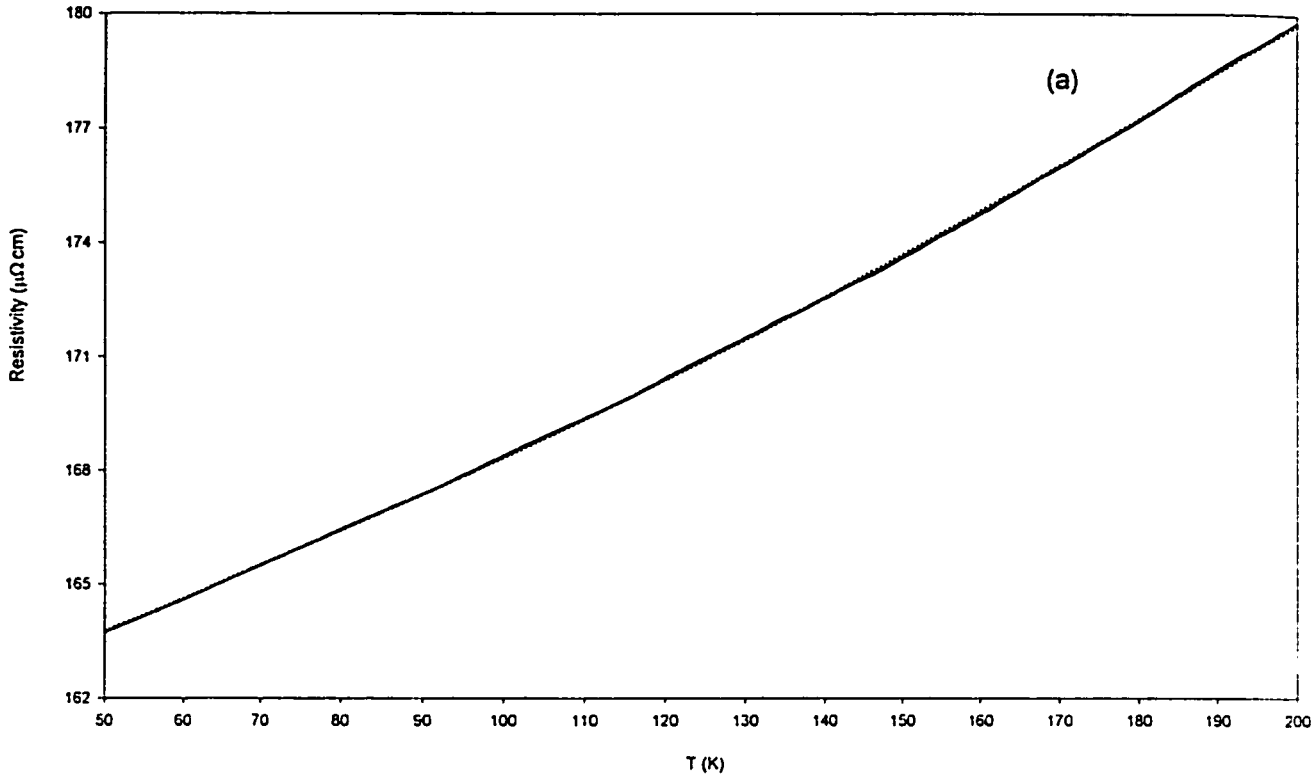

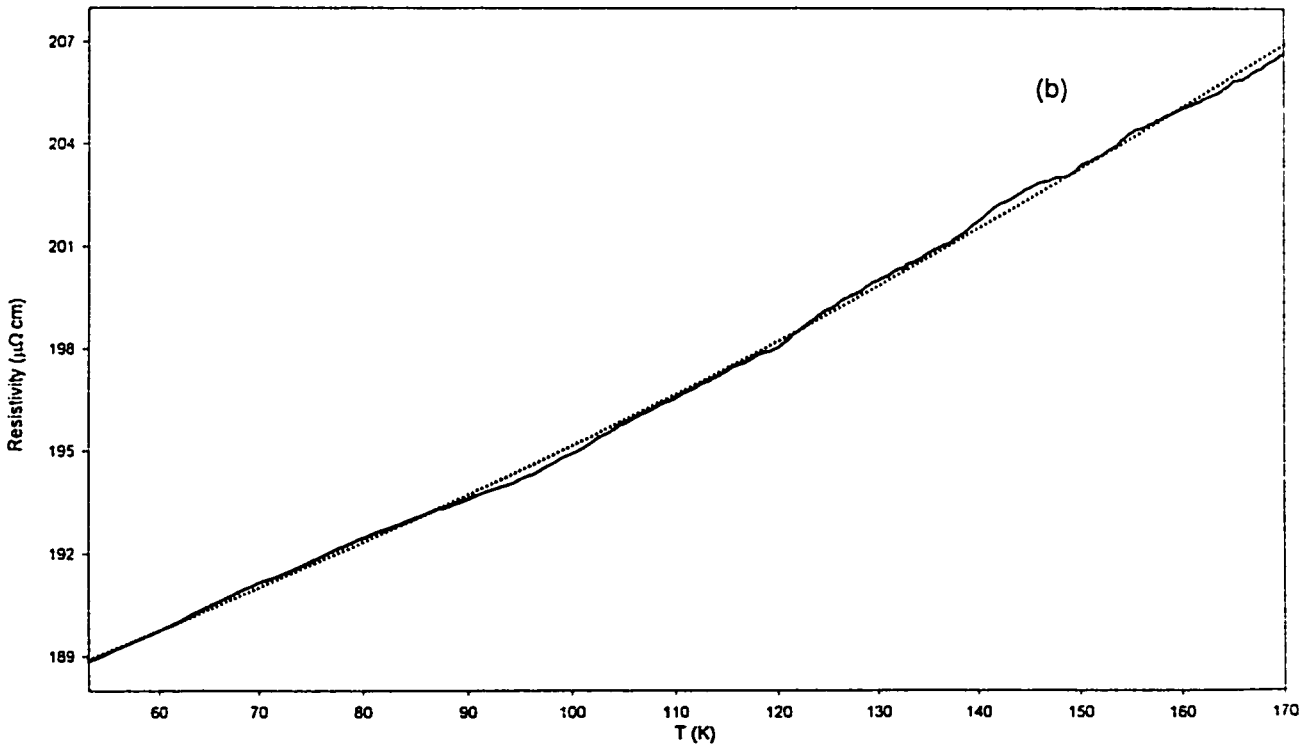

Fig. (4-15) The fit (triangles) of the temperature dependence of the electrical resistivity (solid line) of (a) sample C4 and (b) sample C5 to eq. (2-26).

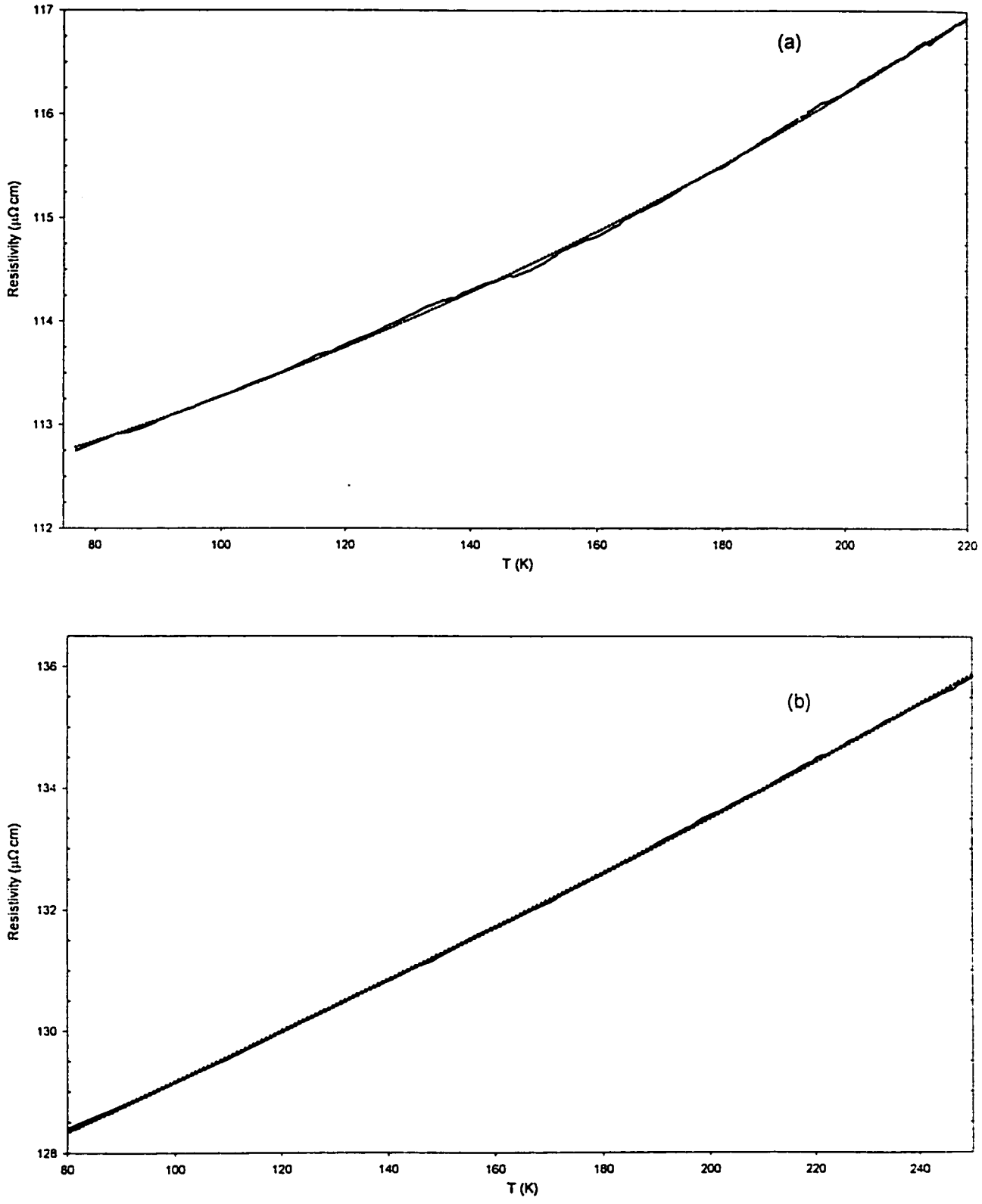

Fig. (4-16) The fit (triangles) of the temperature dependence of the electrical resistivity (solid line) of (a) sample C6 and (b) sample C7 to eq. (2-26).

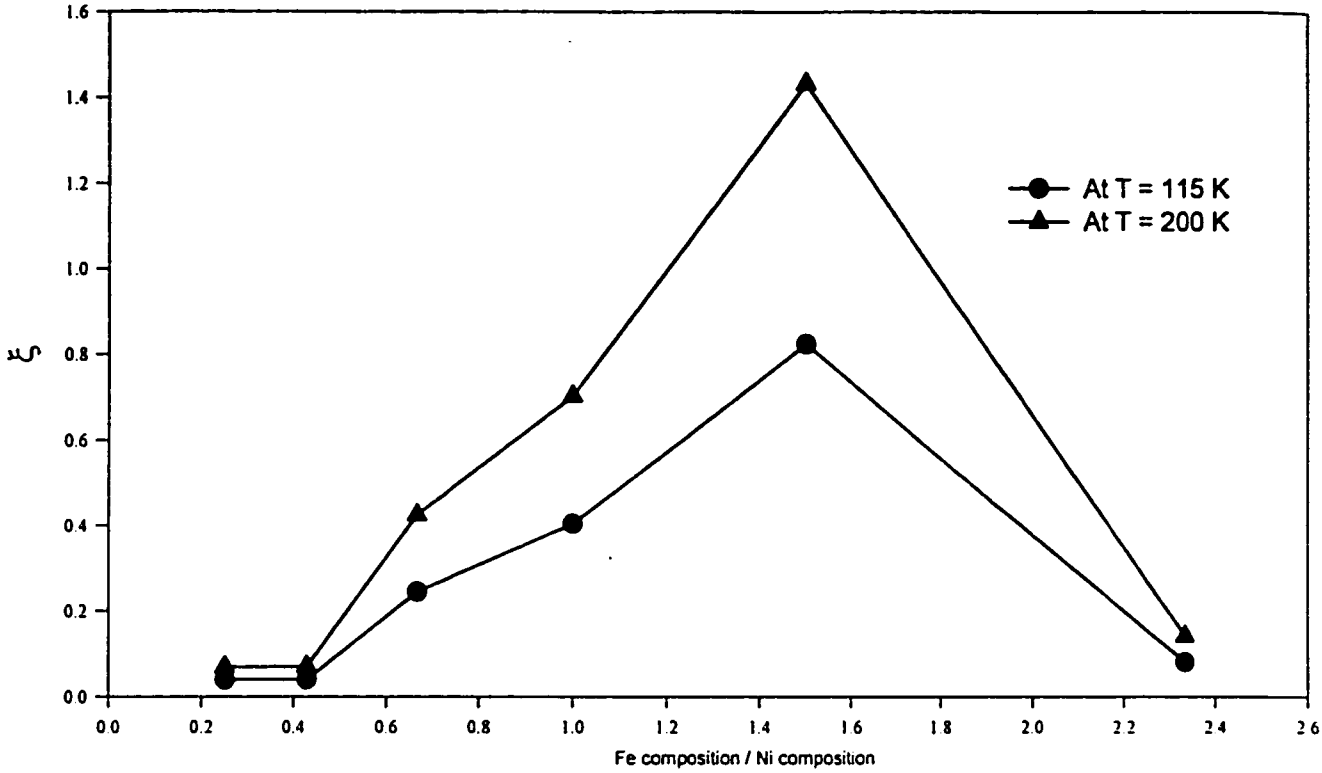

Fig. (4-17) ξ as a function of the ratio of the Fe content to Ni content for the samples of group I.

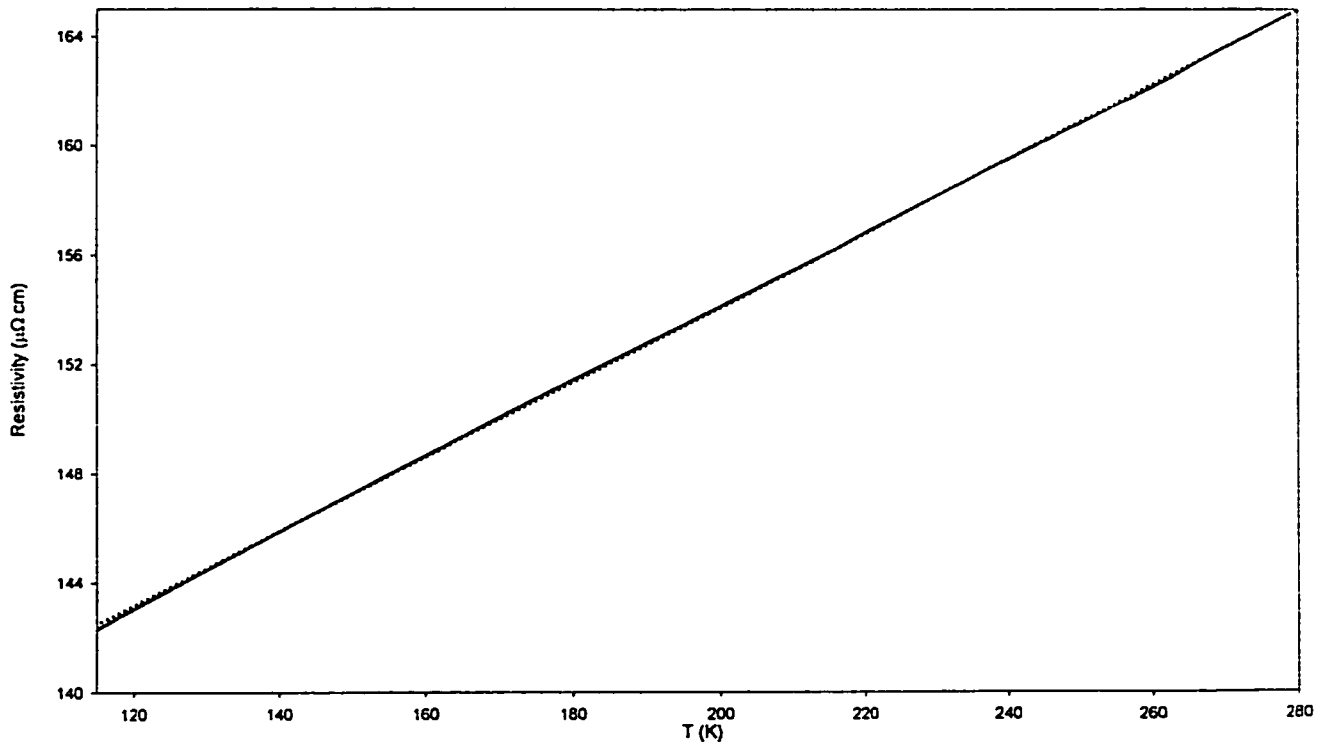

Fig. (4-18) The fit (triangles) of the temperature dependence of the electrical resistivity (solid line) of sample C1 to eq. (2-26).

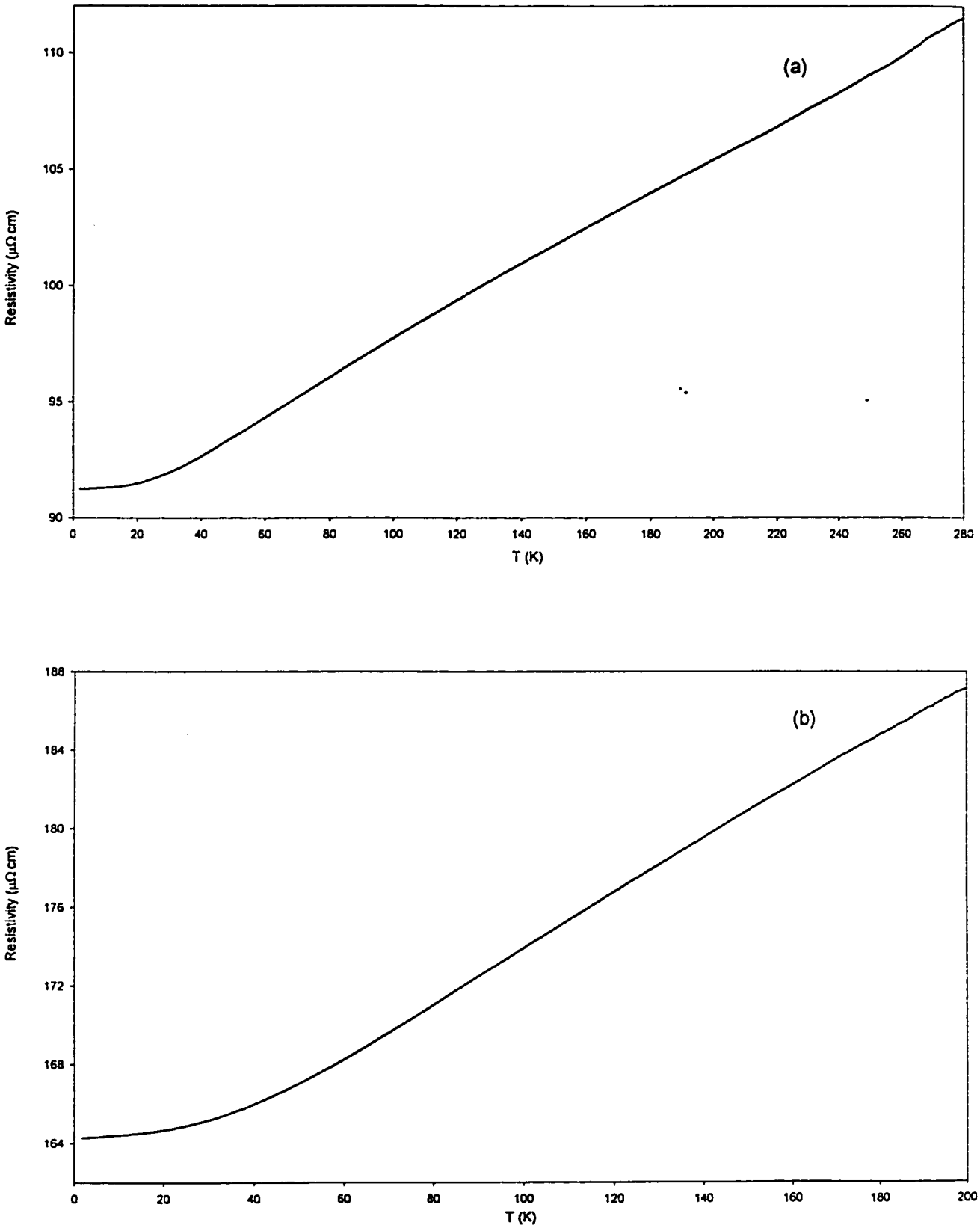

Fig. (4-19) The temperature dependence of the electrical resistivity of (a) sample C8 and (b) sample C9.

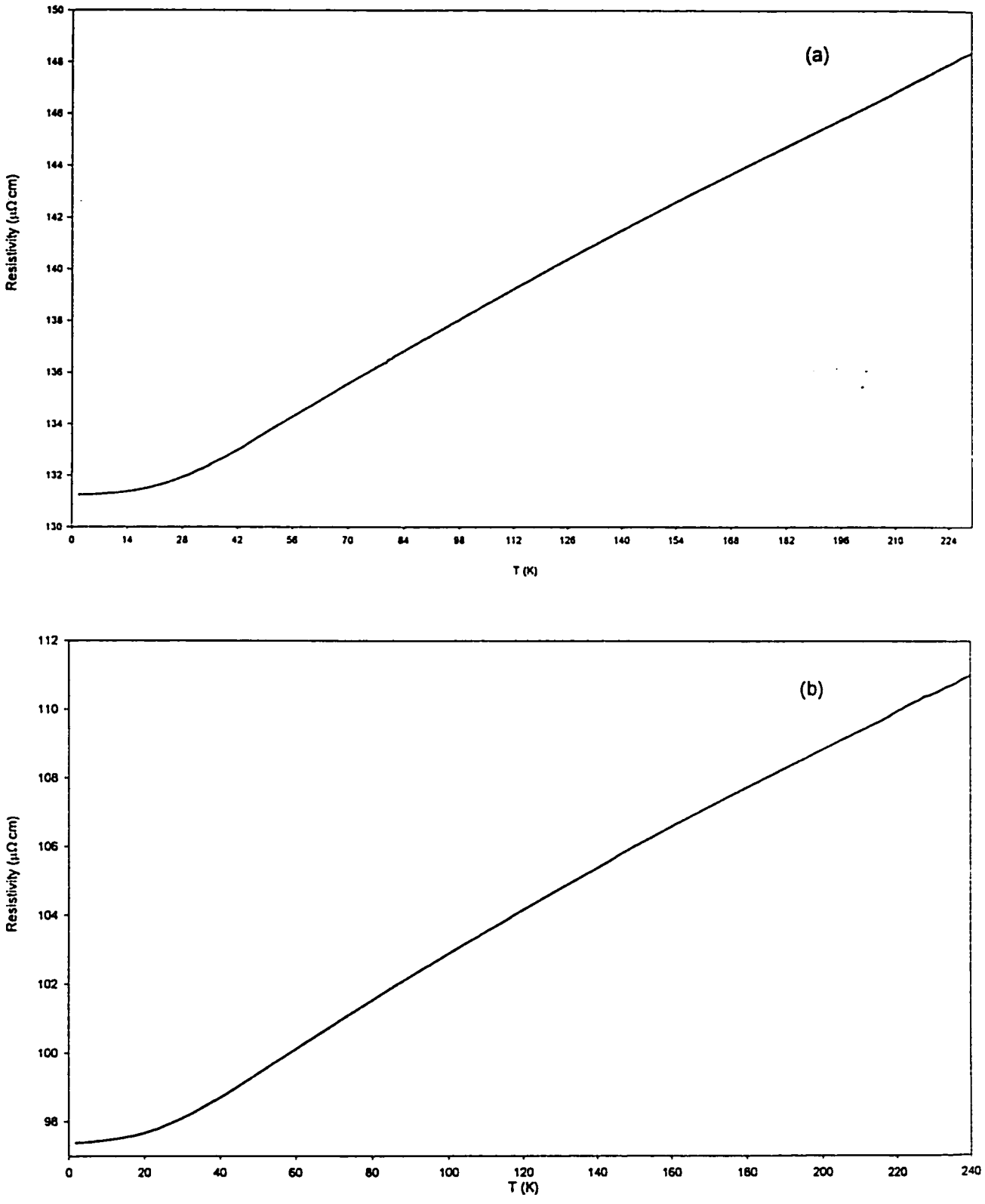

Fig. (4-20) The temperature dependence of the electrical resistivity of (a) sample C10 and (b) sample C11.

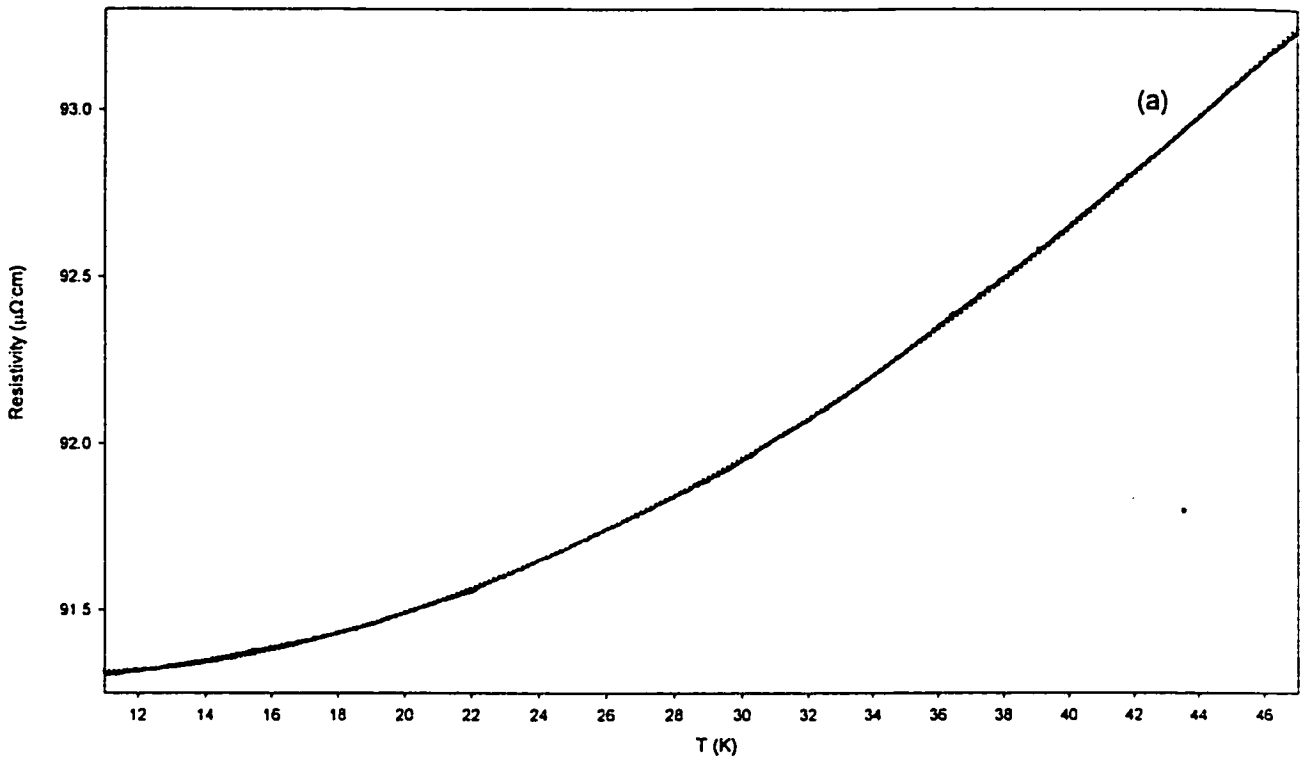

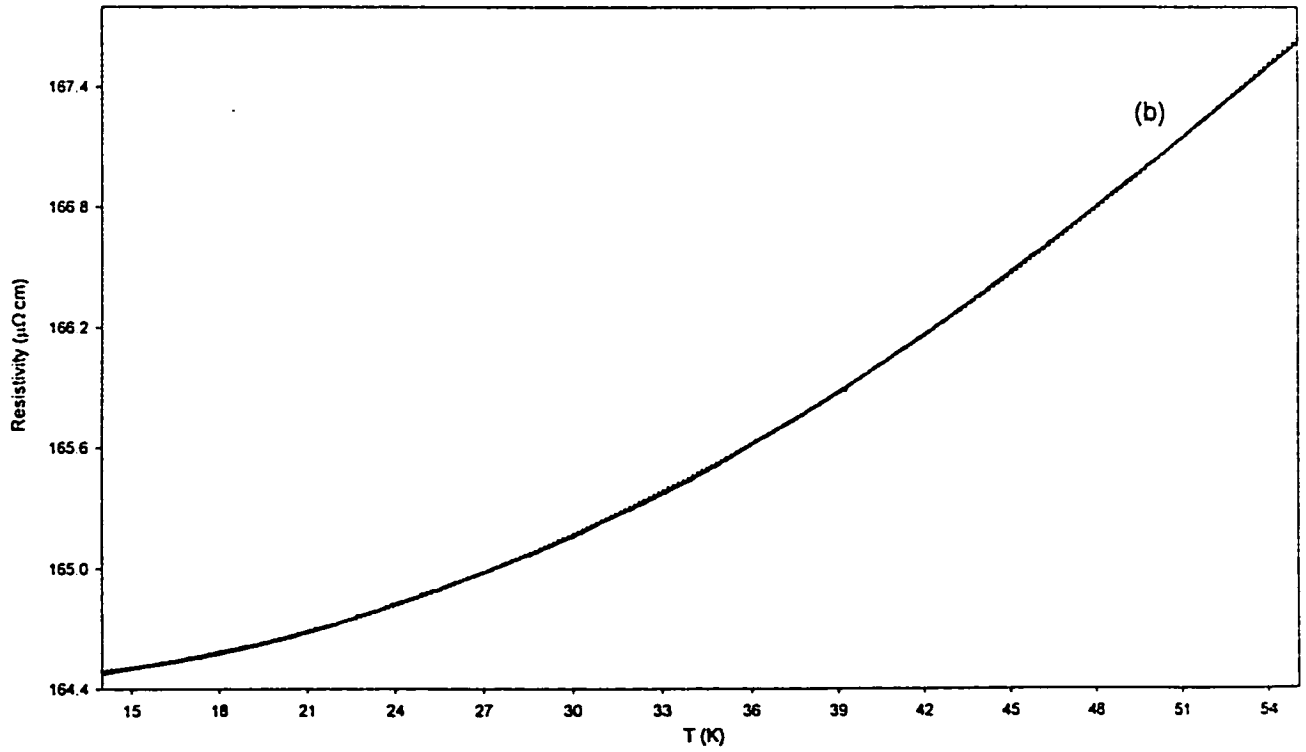

Fig. (4-21) The fit (triangles) of the temperature dependence of the electrical resistivity (solid line) of (a) sample C8 and (b) sample C9 to the sum of eq. (2-16) and the reciprocal of eq. (2-40).

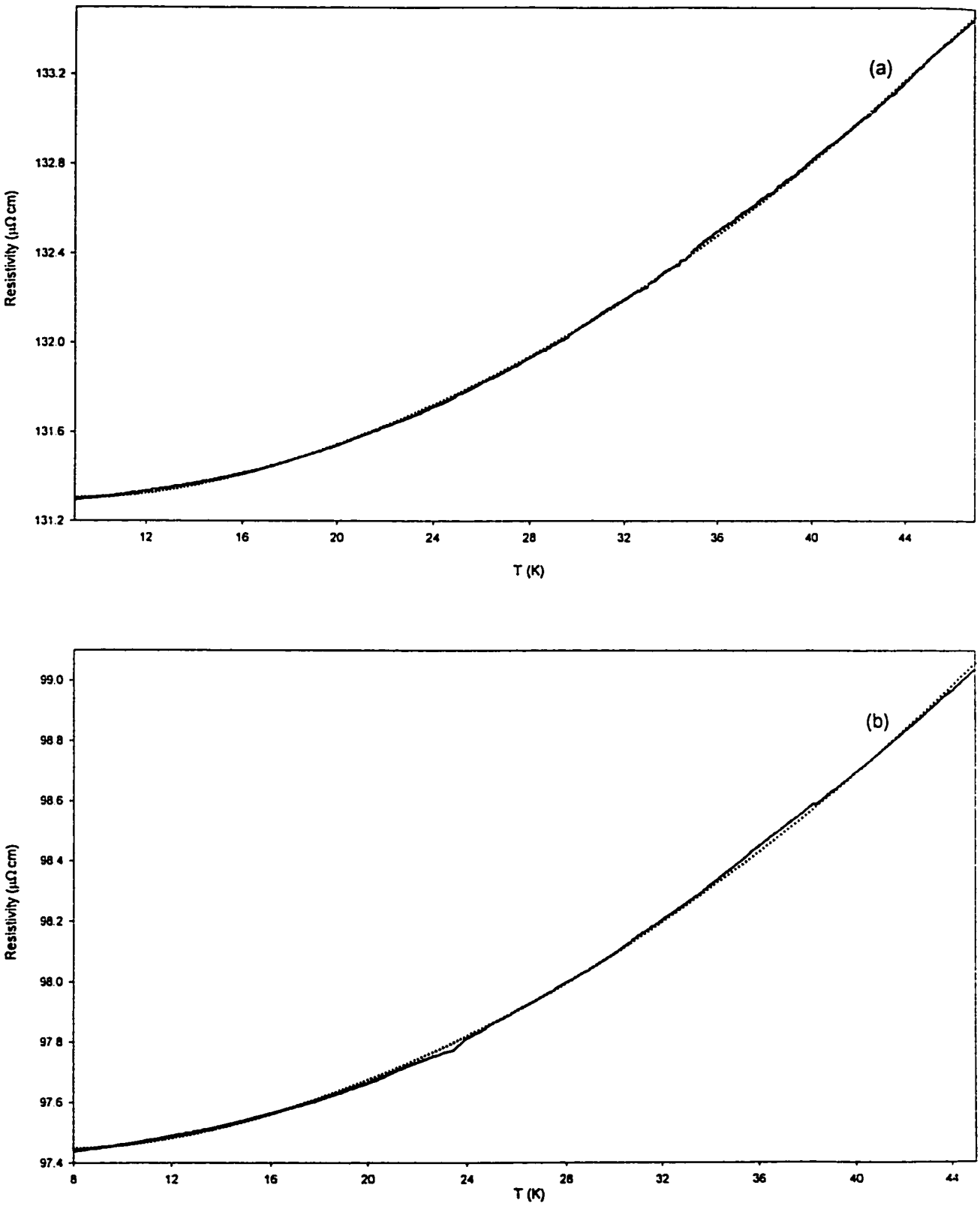

Fig. (4-22) The fit (triangles) of the temperature dependence of the electrical resistivity (solid line) of (a) sample C10 and (b) sample C11 to the sum of eq. (2-16) and the reciprocal of eq. (2-40).

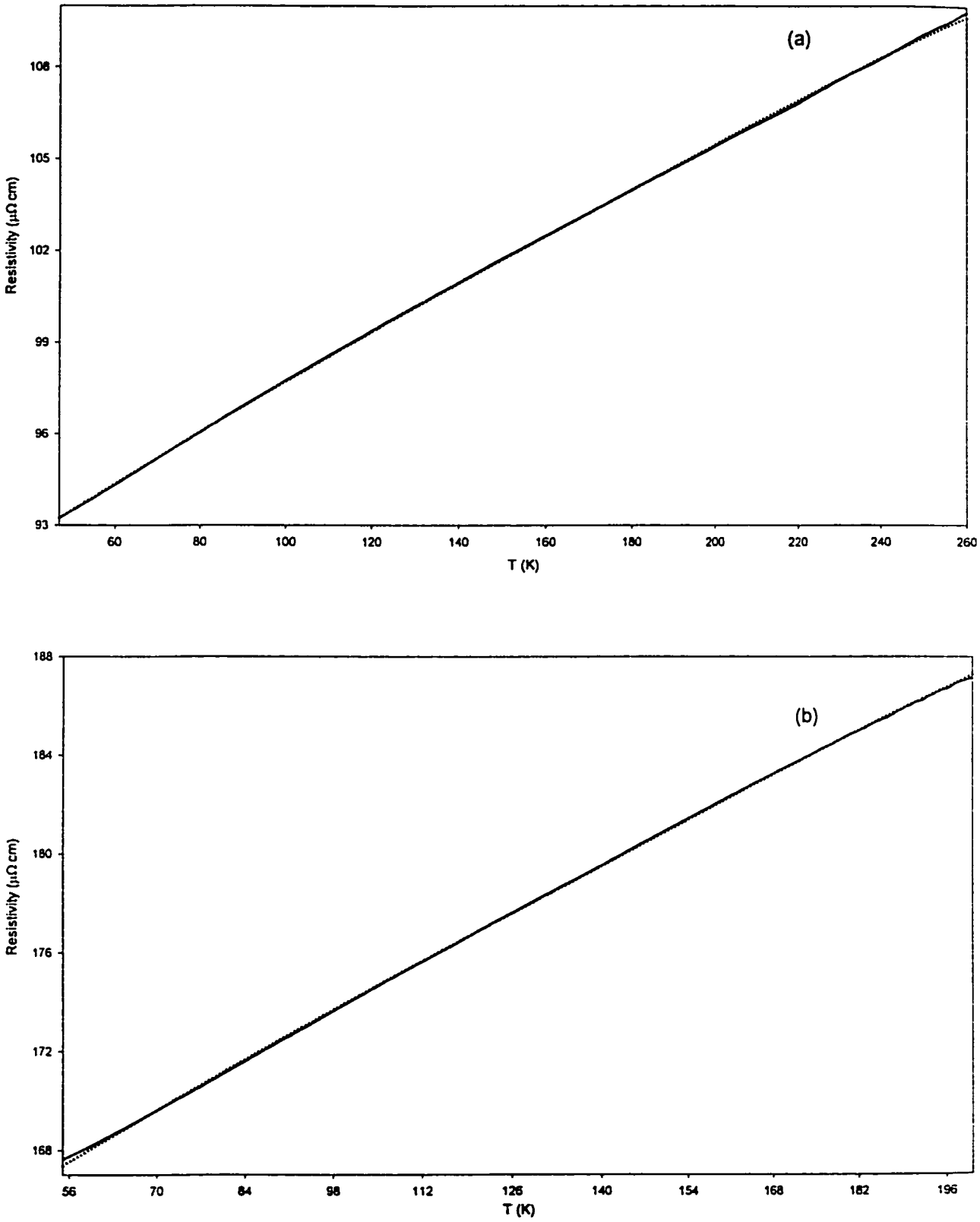

Fig. (4-23) The fit (triangles) of the temperature dependence of the electrical resistivity (solid line) of (a) sample C8 and (b) sample C9 to eq. (2-36).

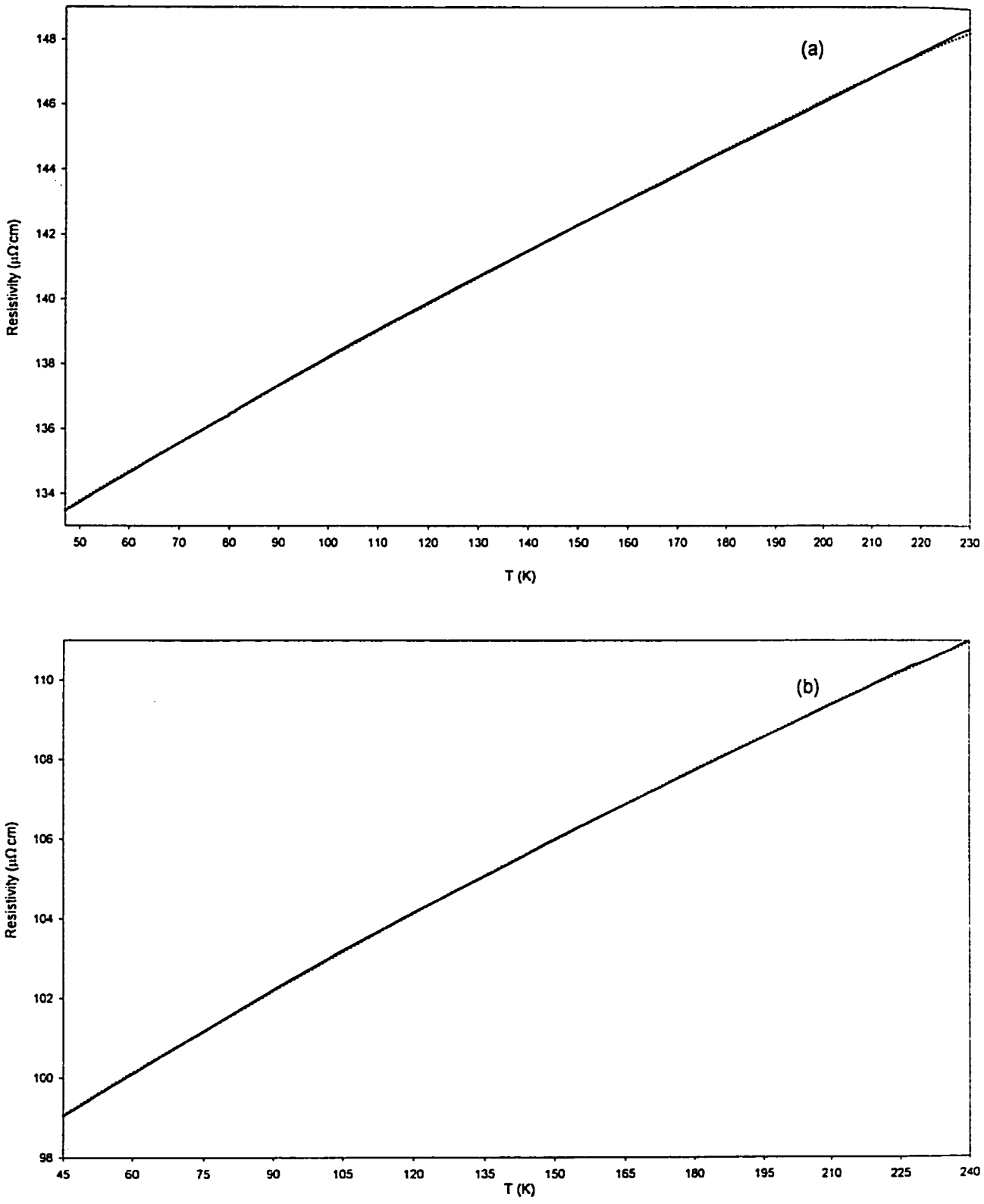

Fig. (4-24) The fit (triangles) of the temperature dependence of the electrical resistivity (solid line) of (a) sample C10 and (b) sample C11 to eq. (2-36).

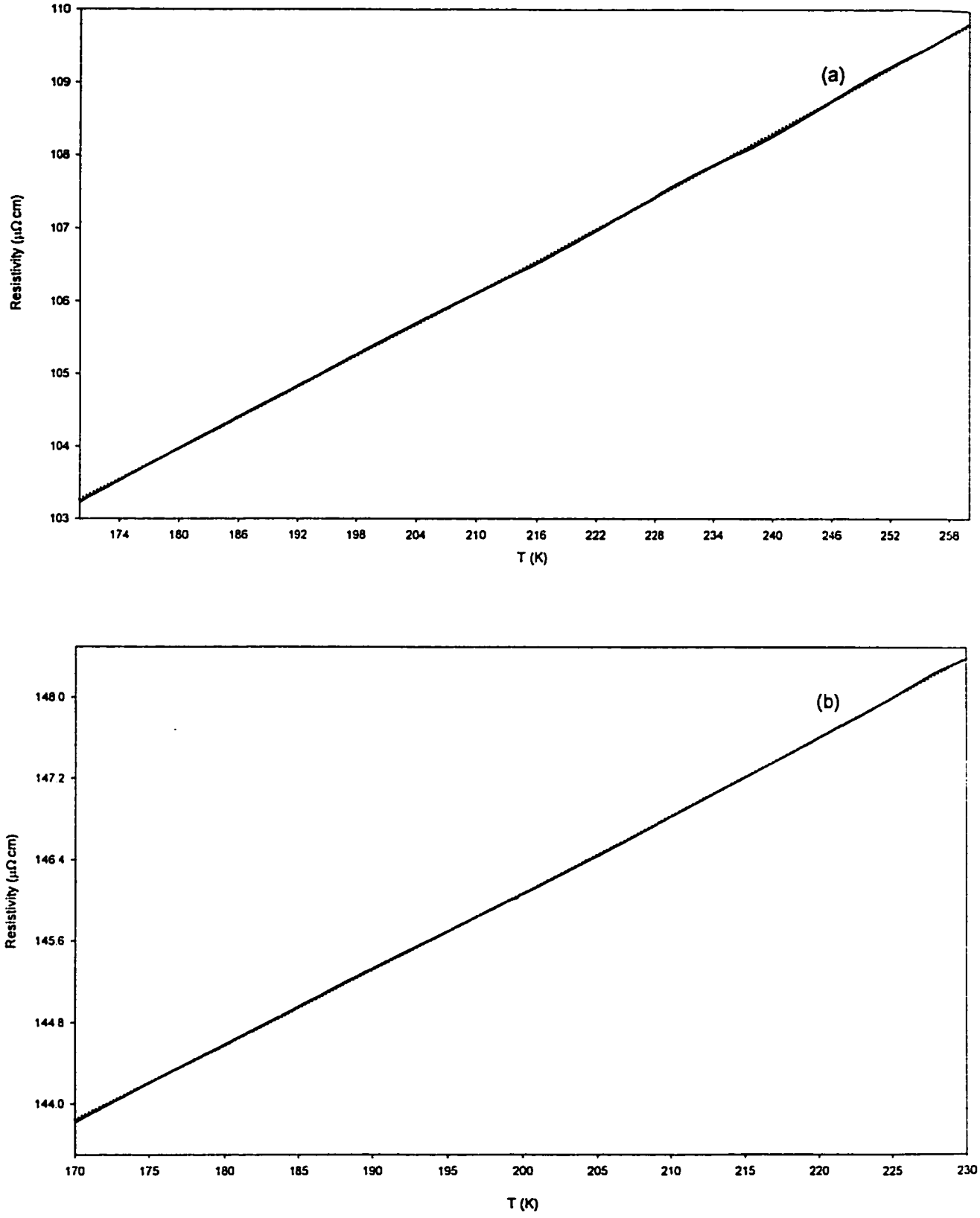

Fig. (4-25) The fit (triangles) of the temperature dependence of the electrical resistivity (solid line) of (a) sample C8 and (b) sample C10 to eq. (2-26).

5. Conclusions

The electrical resistivity measurements in a wide temperature range provided a good tool for investigating the applicability of various theories attempting to account for the temperature dependence of electrical resistivity. In the pure crystalline metals, the nearly free electron model can qualitatively and quantitatively account for the temperature dependence of the electrical resistivity of the studied metals. The values of the residual resistivity for Au and Pt indicate that the purity of the two samples is high. The two samples do not have magnetic impurities as the Kondo effect was not observed in the electrical resistivity measurements. In the low temperature range, the electron-electron scattering is the dominant scattering mechanism. Above the Debye temperature, the phonon electron scattering is the dominant scattering mechanism.

The temperature dependence of the electrical resistivity for the amorphous metallic alloy samples studied can be described qualitatively by the Ziman model, which is based on the nearly-free -electron model. The scattering mechanism of the conduction electrons of the amorphous samples can be categorized in the weak scattering limit regime. A small, but significant correction must be added to the Ziman model in order to account for the additional scattering contributions that exist in the wide temperature range.

In the low-temperature range, the WL scattering is the major correction to the temperature dependence of the electrical resistivity predicted by the Ziman model. The WL contribution is the dominant effect at the beginning of the law-temperature fitting range. This effect decays and vanishes at the end of this fitting range. The total electrical resistivity is the sum of the residual resistivity, the WL contribution, and the phonon inelastic scattering contribution. Figure (5-1) shows an example of

the individual fitting curves of eq. (2-16) and the reciprocal of eq. (2-40) and the total resulting electrical resistivity for sample C1.

In the high-temperature range, the magnetic contribution in the samples C2–C7, C8, and C10 is the major correction to the temperature dependence of the electrical resistivity. This dependence is linear. A quadratic term, which represents the magnetic contribution, should be added. Figure (5-2) shows an example of the individual linear fit, the magnetic contribution, and the resulting total electrical resistivity for sample C6. For the samples C1, C9, and C11 the phonon-phonon coupling scattering is the major correction to the temperature dependence of the electrical resistivity to the linear term predicted by the Ziman model. Figure (5-3) shows an example of the individual linear contribution, the negative phonon-phonon coupling, and the resulting total electrical resistivity for sample C11.

One of the major shortcomings of the Ziman model is its inability to provide an explanation for the resistivity minima of the temperature dependence of the electrical resistivity curve at temperatures below 20 K for some amorphous alloys. All the samples of group I have resistivity minima in their temperature dependence of the electrical resistivity. The Kondo effect could be a possible explanation for this phenomenon. Another, and perhaps more plausible explanation could be the EEI effect, the major correction to the elastic scattering predicted by the Ziman model of the temperature dependence of electrical resistivity. Figure (5-4) shows an example of the individual fitting curves of eq. (2-15) and the reciprocal of eq. (2-43) and the total resulting electrical resistivity for sample C4.

Finally, the Ziman model with the proper corrections, which may increase or decrease the predicted electrical resistivity, in considered to be an adequate and successful model in accounting for

the temperature dependence of the electrical resistivity of all of the studied amorphous metallic alloys in this study.

Magnetoresistence measurements at low temperatures are suggested for future work. This will provide experimental evidence to verify two effects. First, to find out whether the electrical resistivity minima in the temperature dependence of the electrical resistivity are due to Kondo effect or due to EEI effect. Second, to verify that the additional contribution to the electrical resistivity at low temperatures is due to WL effect.

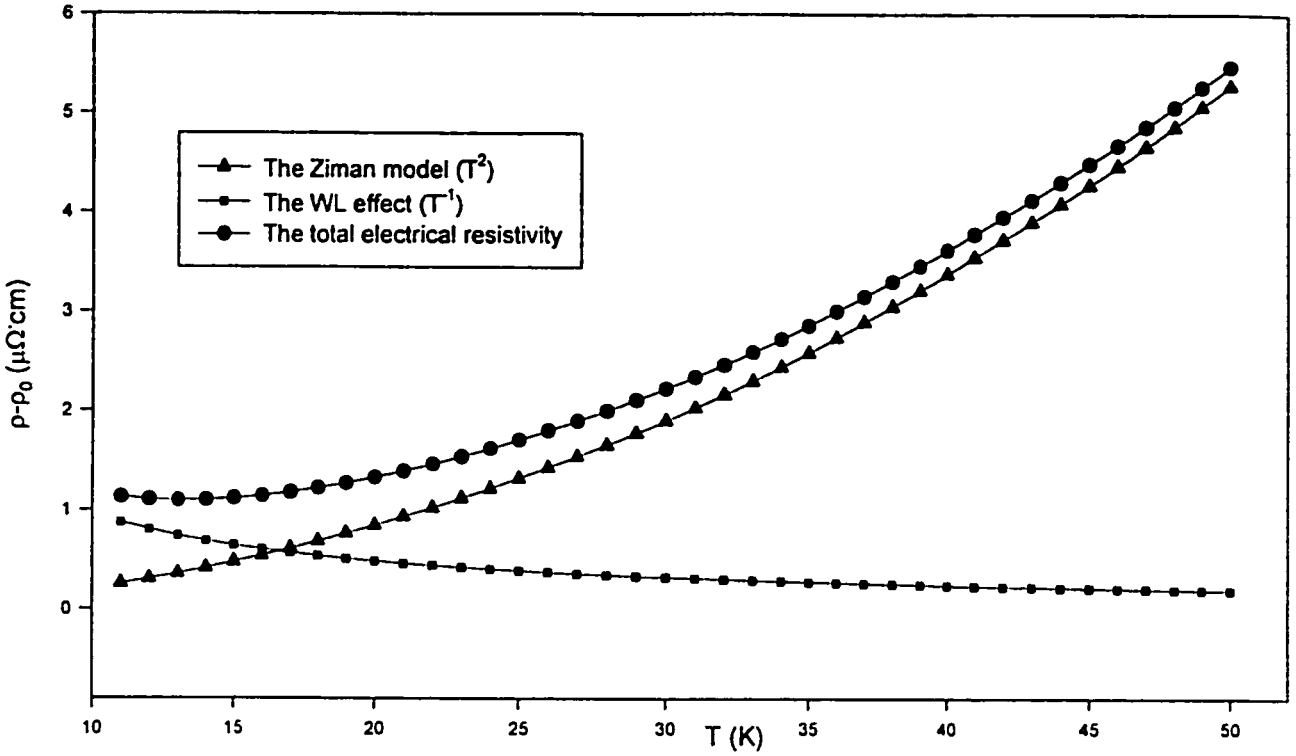

Fig. (5-1) The Ziman model fit (triangles), the WL fit (squares), and the resulting total resistivity fit (circles) of the temperature dependence of the electrical resistivity of sample C1.

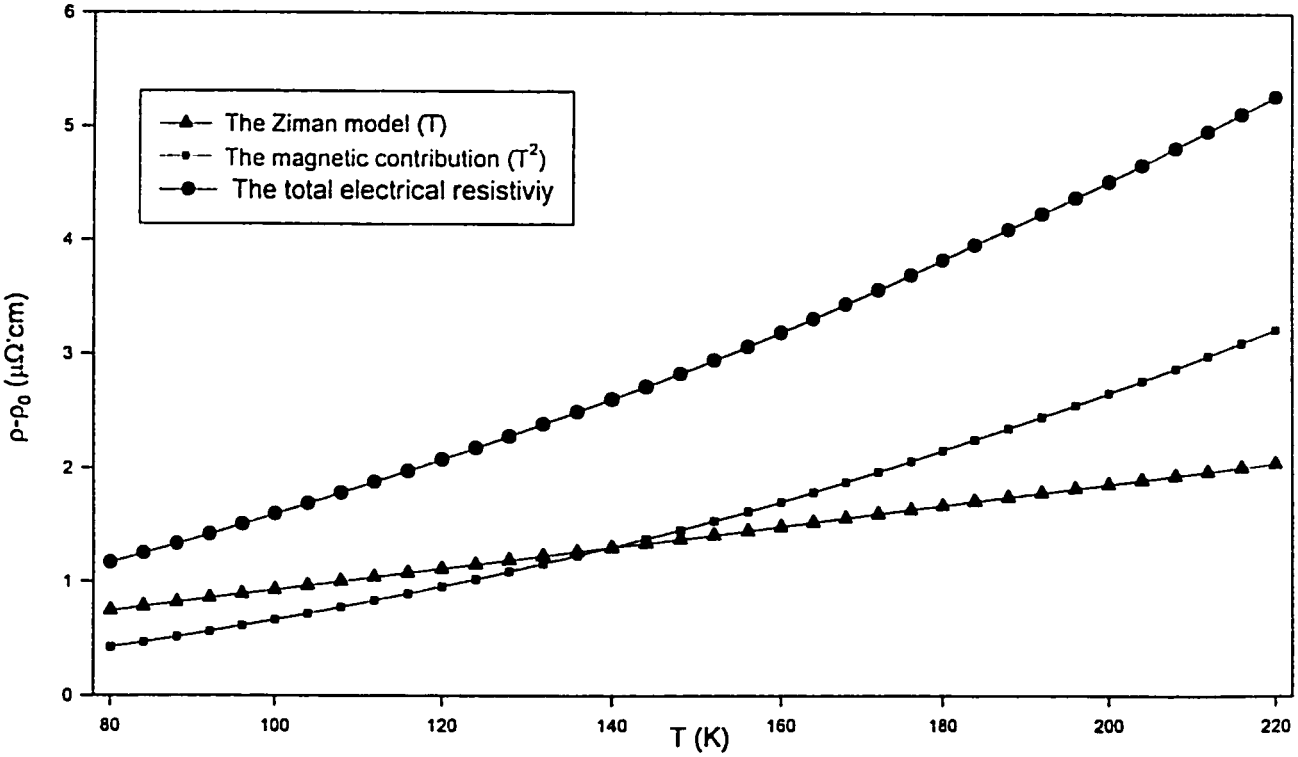

Fig. (5-2) The Ziman model fit (triangles), the magnetic contribution fit (squares), and the resulting total resistivity fit (circles) of the temperature dependence of the electrical resistivity of sample C6.

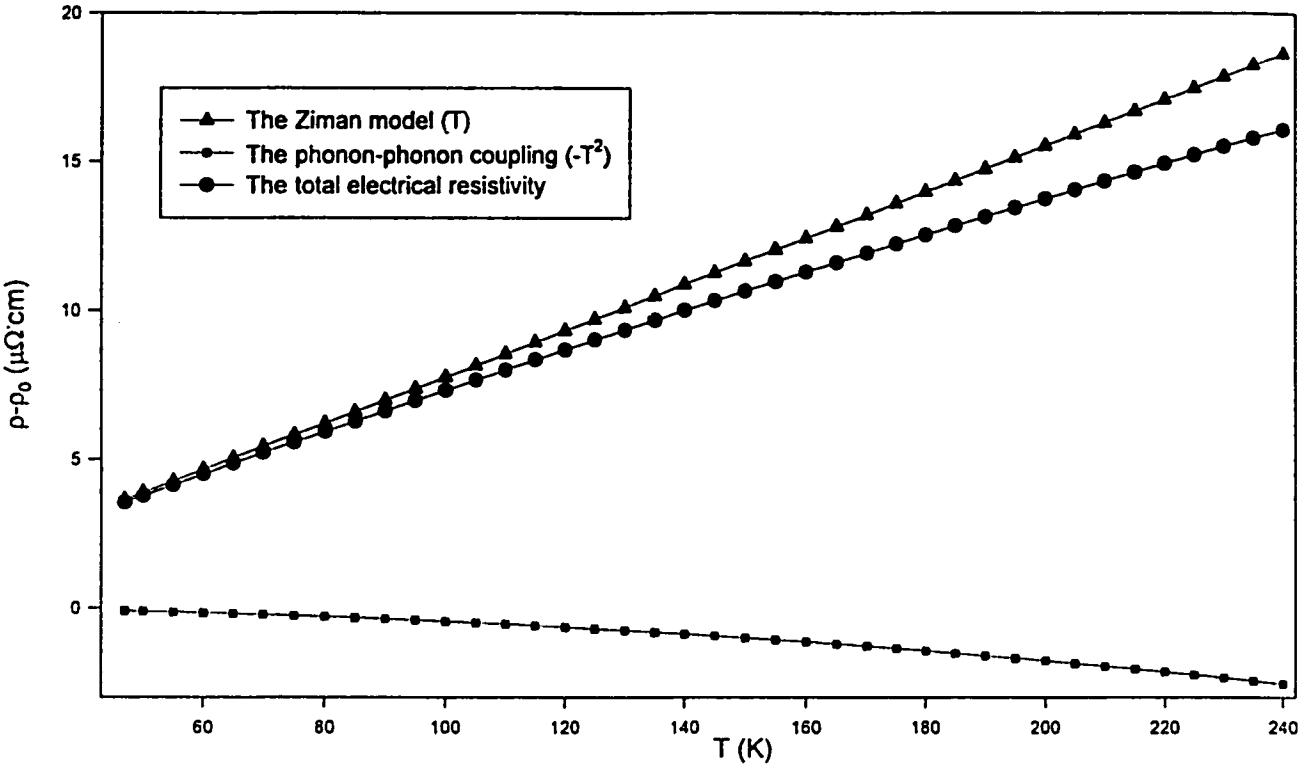

Fig. (5-3) The Ziman model fit (triangles), the phonon-phonon coupling correction fit (squares), and the resulting total resistivity fit (circles) of the temperature dependence of the electrical resistivity of sample C11.

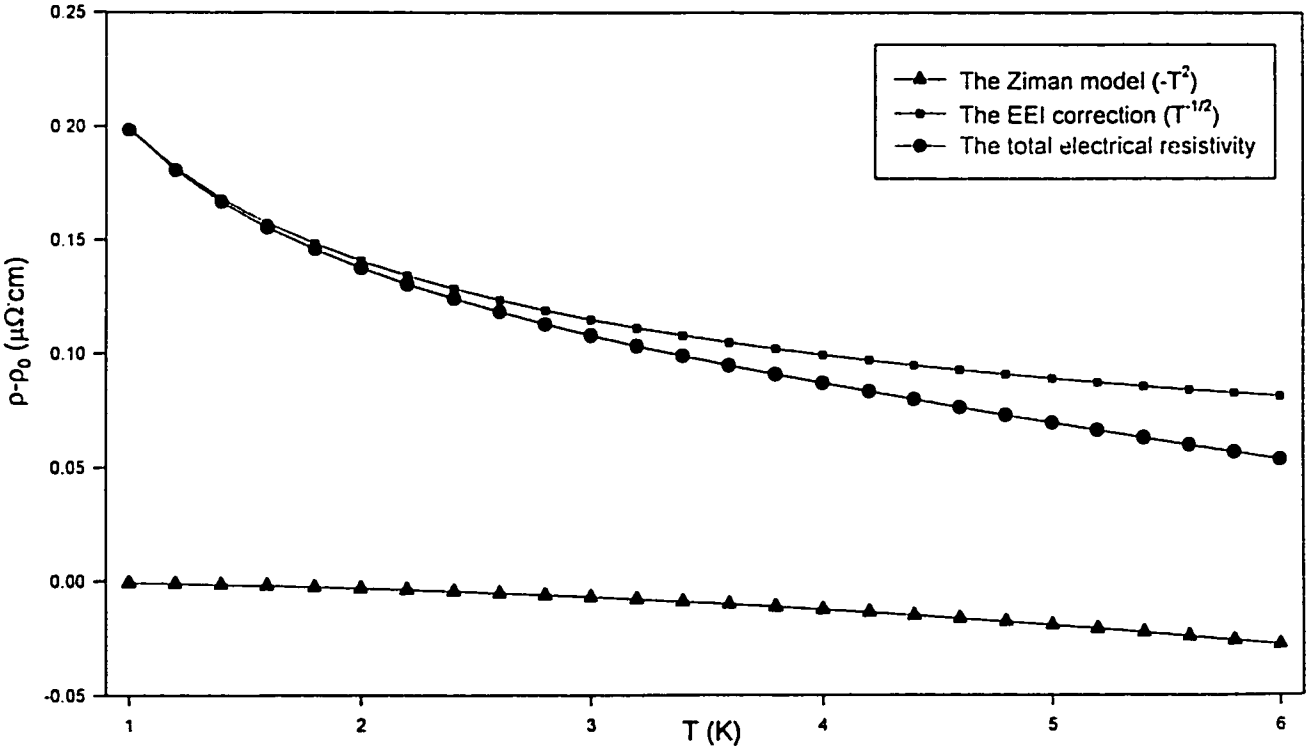

Fig. (5-4) The Ziman model fit (triangles), the EEI correction fit (squares), and the resulting total resistivity fit (circles) of the temperature dependence of the electrical resistivity of sample C4.

References:

1) K. Moorjani and J.M.D. Coey, *Methods and Phenomena 6, Magnetic Glasses* (Elsevier, New York, 1984).

2) M.A. Howson and B.L. Gallagher, Phys. Rep. **170**, 5 (1988).

3) J.S. Dugdale, Contemp. Phys. **28**, 6 (1987).

4) P. A. Lee, T.V. Ramakrishnan, Rev. Mod. Phys. **57**, 2 (1985).

5) U. Mizutani, in *Physics and Technology*, edited by Y. Sakuri, Y. Hamakawa, T. Masumoto, K. Shirae, and K. Suzuki (Elsevier Science Publishers B.V., 1993), p. 74.

6) C. Kittel, *Introduction to Solid State Physics* (John Wiley & Sons, New York, 1996).

7) P.L. Rossiter, *The Electrical Resistivity of Metals and Alloys* (Cambridge University Press, New York, 1987).

8) A.A. Abrikosov, *Introduction to the Theory of Normal Metals* (Academic Press, New York, 1972).

9) I.A. Campbell and A. Fert, in *Transport Properties of Ferromagnets*, edited by E.P. Wohlfarth (North-Holland, Amsterdam, 1982), p. 747.

10) R. W. Cochrane, J. Phys. F **8**, L39, 1540 (1978).

11) U. Mizutani, Prog. Mater. Sci., **28**, 97 (1983).

12) G. Dietz and R. Sonnberger, Z. Phys. B **46**, 213 (1982).

13) U. Mizutani, IEEE Transl. J. Magn. Jpn., **TJMJ-1**, 185(1985).

14) P.J. Cote and L.V. Meisel, Phys. Rev. Lett. **39**, 102 (1977).

15) T. Yoshida and U. Mizutani, J. Phys. F **12** , 2331 (1982).

16) U. Mizutani, Phys. Status Solidi B **176**, 9 (1993).

17) Hugh D. Young, *Fundamentals of Optics and Modern Physics* (McGraw-Hill, New York, 1968).

18) O. Oreirach, R. Evans, H-J Güntherod and H-U Künzi, J. Phys. F **2**, 709 (1972).

19) R. Harris, M. Shalmon, and M. Zuckermann, Phys. Rev. B **18**, 10 (1978).

20) S.N. Kaul, W. Ketteler, and M. Rosenberg, Phys. Rev. B **33**, 7 (1986).

21) S.N. Kaul, W. Ketteler, and M. Rosenberg, Phy. Rev. B **35**, 13 (1987).

22) U. Mizutani, Mater. Sci. Eng., **19**, 82 (1993).

23) M. Dikeakos and Z. Altounian, J. Non-Cryst. Solids **250-252**, 786 (1999).

24) W. Yun-Ping and Z. Dian, Phys. Rev. B. **49**, 13204 (1994).

25) C.C. Tsuei, Phys. Rev. Lett. **57**, 15 (1986).

26) P.D. Babu, S. N. Kaul, J. Non-Crys. Solids **220**, 147 (1997).

27) A.G. Aronov, Europhys. News 24 (1993).

28) J.C. Plenet, A. Prerez, J. Rivory, J.M. Frigerio, and O. Laborde, Phys. Lett. A **162**, 193 (1992).

29) H. Fukuyama and K. Hoshino, J. Phys. Soc. Jpn. **50**, 2131 (1981).

30) R. W. Cochrane and J.O. Strom-Ölsen, Phys. Rev. B **29**, 2 (1984).

31) J.B. Bieri, A. Fert and G. Creuzet, in *Proc. Int. Conf. Localization and Transport Phenom. Impure Met.*, edited by L. Schweitzer and B. Kramer (Physikalische-Technische Bundesanstalt, Braunsweig, 1984), p. 94.

(1984).

32) M. Olivier, J.O. Strom-Ölsen, Z. Altounian, R.W. Cochrane, and M. Traudeau, Phys. Rev. B **38**, 4 (1986).

33) T.K. Nath and A.K. Majumdar, Phys. Rev. B **55**, 9 (1997).

34) D. Greig and M.A. Howson, in *Proc. Int. Conf. Localization and Transport Phenom. Impure Met.*, edited by L. Schweitzer and B. Kramer (Physikalische-Technische Bundesanstalt, Braunsweig, 1984), p. 90.

35) J.J. Lin and C.Y. Wu, Phys. Rev. B **48**, 8 (1993).

36) Keithly low-level measurements (Keithly Instruments Inc., Cleveland, 1993).

37) Keithly application note series, 301, (Keithly Instruments Inc., Cleveland, 1995).

38) Keithly application note series, 200, (Keithly Instruments Inc., Cleveland, 1994).

39) Ind. Phys. **1**, 31 (1995).

40) R. Zallen, *The Physics of Amorphous Solids* (Wiley, New York, 1983).

41) Z. M. Stadnik, unpublished.

42) SigmaPlot manual, (SPSS Inc., New York, 1997).

43) T.S. Park and M. Sostarich, J. Appl. Phys. **53**, 8251 (1982).

44) G. Venugopal Rao and Anil K. Bhatnagar, in *AIP Con. Proc.* edited by V. Strivastara, A.K. Bahatnagar, and D. G. Naugle (American Institution of Physics, New York, 1994), p. 324.

45) R. Harris and J.O. Strom-Ölsen, in *Topics in Applied Physics*, edited by H.Beck and H.-J. Güntherodt (Springer-Verlag, Berlin, 1983), p. 325.

46) R.W. Cochrane and J.O. Strom-Ölsen, J. Phys. F, **7**, 1799 (1977).

47) W. Kettler, R. Wernhardt, and M. Rosenberg, J. Appl. Phys. **53**, 8248 (1982).

48) Z. M. Stadnik, P. Griesbach, G. Dehe, P. Gütlich, G. stroink, and T. Miyazaki, Phys. Rev. B **35**, 8740 (1987).

APPENDIX (A)

The following computer program, written in the Qbasic language, controls the devices through the GPIB cable. The program is designed to read up to $3x10^4$ data points for each sample

```
DECLARE SUB reread1 ()
DECLARE SUB reread ()
  CLS
  COLOR 12, 0
  PRINT "          ****************************************"
  PRINT "          *      program written by        *"
  COLOR 14, 0
  PRINT "          *        KHALID AL-QADI          *"
  COLOR 12, 0
  PRINT "          *  OTTAWA UNIVERSITY/PHYSICS 1997  *"
  PRINT "          ****************************************"
  PRINT
  COLOR 13, 0
  PRINT " WHERE DO YOU WANT TO STORE YOUR DATA ==> ";
  COLOR 11, 0
  INPUT file$
  BEEP
  CLS
  COLOR 13, 0
' begin variables decleration ---------------
    max = 10
    riseup = .001
    count = 0
    changetemp = 0
' end variables decleration ---------------
  OPEN "gpib0" FOR OUTPUT AS #1
  OPEN "gpib0" FOR INPUT AS #2
  PRINT #1, "ABORT"
  PRINT #1, "RESET"
  PRINT #1, "REMOTE 12"
  PRINT #1, "REMOTE 16"
  PRINT #1, "output 12; :suni k"
  PRINT #1, "output 12; :func 'temp'"
  CLOSE #1
  CLOSE #2
  OPEN "gpib0" FOR OUTPUT AS #1
  OPEN "gpib0" FOR INPUT AS #2

  PRINT #1, "output 12; :data:fres?"
```

```
   PRINT #1, "enter 12"
   INPUT #2, temp$
   firsttemp = VAL(temp$)
   CLOSE #1
   CLOSE #2

'M A I N   L O O P
OPEN "o", #3, file$
FOR MAINLOOP = 1 TO 3
     FOR i = 1 TO max
     FOR j = 1 TO max
     FOR k = 1 TO max
     FOR l = 1 TO max
     OPEN "gpib0" FOR OUTPUT AS #1
     OPEN "gpib0" FOR INPUT AS #2
10    IF char$ = "q" THEN GOTO 30
20    char$ = INKEY$
          PRINT #1, "output 12; :func 'temp'"
          PRINT #1, "output 12; :data:fres?"
          PRINT #1, "enter 12"
          INPUT #2, temp$
          n1(i, j, k, l) = VAL(temp$) + changetemp
          secondtemp = n1(i, j, k, l)
          IF secondtemp - firsttemp < riseup THEN CALL reread: GOTO 10 ELSE
          firsttemp = secondtemp
          IF changetemp = 0 THEN IF firsttemp > 199.99 THEN GOSUB ctemp
          CALL reread1
          PRINT #1, "output 16; :func 'fres'"
          PRINT #1, "output 16; :data:fres?"
          PRINT #1, "enter 16"
          INPUT #2, ohm$
          n2(i, j, k, l) = VAL(ohm$)
          count = count + 1
          PRINT "At Temp="; n1(i, j, k, l);
          PRINT "     R="; n2(i, j, k, l);
          PRINT "       No. of mea.="; count
          CLOSE #1
          CLOSE #2
       NEXT l
     NEXT k
     NEXT j
     NEXT i
```

```
30    CLOSE #1
      CLOSE #2
      IF i > 1 THEN j = max: k = max: l = max ELSE IF j > 1 THEN k = max: l = max ELSE IF k > 1
THEN l = max
      IF i > max THEN i = max
      IF j > max THEN j = max
      IF k > max THEN k = max
      IF l > max THEN l = max

      COLOR 14, 0
      PRINT
      PRINT "       I am writing the data to the file ";
      COLOR 15, 0
      PRINT file$;
      COLOR 14, 0
      PRINT " .. Wait please"

      FOR ii = 1 TO i
      FOR jj = 1 TO j
      FOR kk = 1 TO k
      FOR ll = 1 TO l

      PRINT #3, n1(ii, jj, kk, ll), ":", n2(ii, jj, kk, ll)

      NEXT ll
      NEXT kk
      NEXT jj
      NEXT ii

   BEEP
   FOR w = 1 TO 1000
   NEXT w
   BEEP
   FOR w = 1 TO 1000
   NEXT w
   BEEP
   CLS
NEXT MAINLOOP
END
ctemp:
  PRINT #1, "output 12; :suni c"
  changetemp = 273.16
  fisrttemp = 273.16 - fisttemp
  secondtemp = 273.16 - secondtemp
            PRINT #1, "output 12; :func 'temp'"
```

```
        PRINT #1, "output 12; :data:fres?"
        PRINT #1, "enter 12"
        INPUT #2, temp$
        PRINT temp$
        PRINT "I am here"
        FOR www = 1 TO 3000
        www = www
        NEXT www
RETURN


SUB reread STATIC
  CLOSE #1
  CLOSE #2
  OPEN "gpib0" FOR OUTPUT AS #1
  OPEN "gpib0" FOR INPUT AS #2
END SUB

SUB reread1 STATIC
  CLOSE #1
  CLOSE #2
  OPEN "gpib0" FOR OUTPUT AS #1
  OPEN "gpib0" FOR INPUT AS #2
END SUB
```